M. Tech (Power System)

PERFORMANCE ANALYSIS OF INDUCTION MOTOR DRIVE USING DIFFERENT CONTROL TECHNIQUES

DISSERTATION

SUBMITTED IN PARTIAL FULFILLMENT OF THE REQUIREMENTS
FOR THE AWARD OF THE DEGREE OF

MASTER OF TECHNOLOGY
IN
POWER SYSTEM

SUBMITTED BY:

AJAY KUMAR SAHU

2K17/PSY/01

UNDER THE SUPERVISION OF

PROF. DHEERAJ JOSHI

DEPARTMENT OF ELECTRICAL ENGINEERING
DELHI TECHNOLOGICAL UNIVERSITY
(Formerly Delhi College of Engineering)
Bawana Road, Delhi-110042

2019

Ajay Kumar Sahu 2019

DEPARTMENT OF ELECTRICAL ENGINEERING

DELHI TECHNOLOGICAL UNIVERSITY

(Formerly Delhi College of Engineering)

Bawana Road, Delhi-110042

CANDIDATE'S DECLARATION

I, Ajay Kumar Sahu, Roll No. 2K17/PSY/01 student of M. Tech. (Power System), hereby declare that the dissertation titled "Performance Analysis of Induction Motor Drive using Different Control Techniques" which is submitted by me to the Department of Electrical Engineering, Delhi Technological University, Delhi in partial fulfilment of the requirement for the award of the degree of Master of Technology.

Place: Delhi **AJAY KUMAR SAHU**

Date:

DEPARTMENT OF ELECTRICAL ENGINEERING

DELHI TECHNOLOGICAL UNIVERSITY

(Formerly Delhi College of Engineering)

Bawana Road, Delhi-110042

CERTIFICATE

I, Ajay Kumar Sahu, Roll No. 2K17/PSY/01 student of M. Tech. (Power System), hereby declare that the dissertation titled "Performance Analysis of Induction Motor Drive using Different Control Techniques" under the supervision of Prof. Dheeraj Joshi of Electrical Engineering Department, Delhi Technological University in partial fulfilment of the requirement for the award of the degree of Master of Technology has not been submitted elsewhere for the award of any Degree.

Place: Delhi **AJAY KUMAR SAHU**

Date:

Prof. DHEERAJ JOSHI

Professor

Department of Electrical Engineering

Delhi Technological University

DEPARTMENT OF ELECTRICAL ENGINEERING

DELHI TECHNOLOGICAL UNIVERSITY

(Formerly Delhi College of Engineering)

Bawana Road, Delhi-110042

ACKNOWLEDGEMENT

I would like take this opportunity to extend my gratitude to all the loyal hands for helping me out during my dissertation work. To begin with, I would like to be grateful to the dissertation guide **Prof. Dheeraj Joshi,** Department of electrical Engineering in my dissertation "Performance Analysis of Induction Motor Drive using Different Control Techniques" for his intensive support and supervision while preparing for the dissertation.

I would like to thank **Delhi Technological University (DTU)** for providing us with such a remarkable assignment to work on, which not only enhanced our knowledge based on visual basic application which includes events handlings and graphics. I would like to thank Power Electronics Lab and its staff members for co-operating with me and providing me with the best possible working environment for the dissertation. I would like to thank DTU library for making me available with best possible learning resources.

I would also like to thank Mr. Kailash Rana, PhD Scholar and my friend Shreyansh Upadhyaya for helping me in crucial stages, without their help this dissertation would have been incomplete. Lastly, I would like to thank all those whose names may not have appeared here but whose contribution has not gone unnoticed. I would like to thank all of them, for their help in various ways.

Thank you all making everything interesting and easy.

Ajay Kumar Sahu

(2K17/PSY/01)

ABSTRACT

In general speed control is essential in drive system. This involves variable frequency and voltage. Many pulse width modulation techniques are used for obtaining variable frequency and voltage from an inverter. The space vector pulse width modulation method with proportional integral control of induction motor drive is widely used in high performance drive system. It is due to its characteristics like good power factor and high efficiency. In this dissertation the voltage source inverter type space vector pulse width modulation using proportional integral control, ANN control and ANFIS control model design and implementation has been done through MATLAB/Simulink software for the speed control of induction motor. The performance of speed is increased by PI controller, ANN controller and ANFIS controller. The simulation results provide a smooth speed response and high performance under various dynamic operations. Space vector pulse width modulation (SVPWM) is more efficient among all other pulse width modulation (PWM) techniques due to its key characteristics like better DC voltage utilization, switching losses reduction and easiness in digital implementation. The complete mathematical model of the system is described and simulated in MATLAB/Simulink.

CONTENTS

LIST OF FIGURES

LIST OF TABLES

LIST OF SYMBOLS

Parameter	Definition
R_s, L_s	Stator resistance and leakage inductance
L_m	Magnetizing inductance
V_{qs}, i_{qs}	q axis stator voltage and current
V_{ds}, i_{ds}	d axis stator voltage and current
ϕ_{qs}, ϕ_{ds}	Stator q and d axis fluxes
ω_m	Angular velocity of the rotor
ω_r	Electrical angular velocity
T_e	Combined rotor and load inertia coefficient.
H	Combined rotor and load inertia constant.
F	Combined rotor and load viscous friction coefficient
L'_r	Total rotor inductance
R'_{r1}, L'_{r1}	Rotor resistance and leakage inductance
V'_{qr}, i'_{qr}	q axis rotor voltage and current
V'_{dr}, i'_{dr}	d axis rotor voltage and current
$\varphi'_{qr}, \varphi'_{dr}$	Rotor q and d axis fluxes
R'_{lr1}, L'_{lr1}	Rotor resistance and leakage inductance of cage 1
R'_{lr2}, L'_{lr2}	Rotor resistance and leakage inductance of cage 2
L'_{lr1}, L'_{lr2}	Total rotor inductances of cage 1 and 2
i'_{qr1}, i'_{qr2}	q axis rotor current of cage 1 and 2
i'_{dr1}, i'_{dr2}	d axis rotor current of cage 1 and 2
$\varphi'_{qr1}, \varphi'_{dr1}$	q and d axis rotor fluxes of cage 1
$\varphi'_{qr2}, \varphi'_{dr2}$	q and d axis rotor fluxes of cage 2

CHAPTER 1

INTRODUCTION AND LITERATURE REVIEW

1.1 INTRODUCTION

Induction motor are utilized in many applications for example heating, air-conditioning, ventilation, Industrial drives and powertrain (electric vehicles) etc. There has been great demand of controllable speed drives in industries in recent years. Control Techniques of Induction Motor (IM) are Variable frequency control techniques of IM. It can be divided into two major types: scalar control, vector control methods. Scalar control is also known as V/F control. The configuration is normally used with speed feedback. However, this controller does not attain a good precision in both speed and torque responses, predominantly because of the fact that stator flux and torque are not directly controlled.

1.1.1 THREE-PHASE VSI

The word inverter in the context of power electronics designates a class of power conversion (or power conditioning) circuits that operates from a dc voltage source or a dc current source and converts it into ac voltage or current. Even though input to an inverter circuit is a dc source, it is not uncommon to have this dc derived from an ac source such as utility ac supply. If the input dc is a voltage source, the inverter is called a voltage source inverter (VSI). Current source inverter (CSI), where the input to the circuit is a current source. The VSI circuit has direct control over 'output (ac) voltage' whereas the CSI directly controls 'output (ac) current'. Shape of voltage waveforms output by an ideal VSI should be independent of load connected at the output.

Some examples where voltage source inverters are used are: uninterruptible power supply (UPS) units, adjustable speed drives (ASD) for ac motors, electronic frequency changer circuits etc.

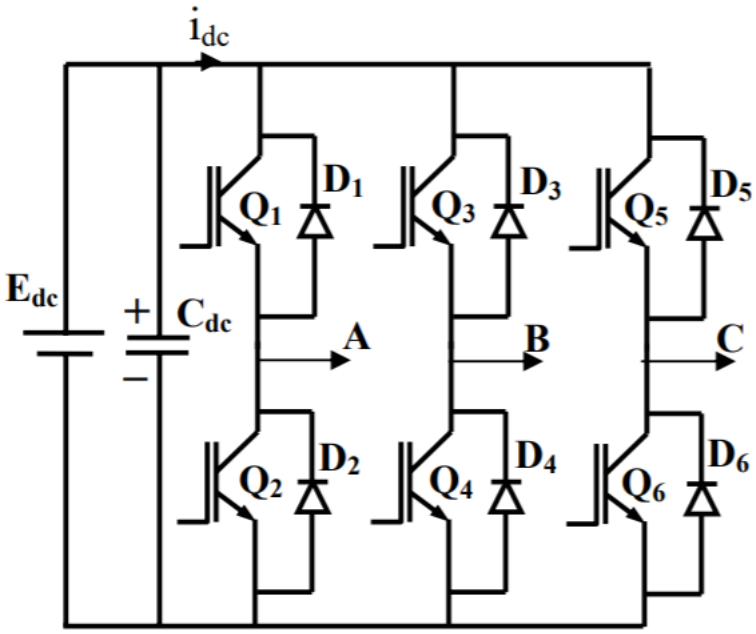

Fig.1.1 General Structure of 3-Phase VSI

It requires only a single dc source and for medium output power applications the preferred devices are n-channel IGBTs. E_{dc} is the input dc supply and a large dc link capacitor (C_{dc}) is put across the supply terminals. Capacitors and switches are connected to dc bus using short leads to minimize the stray inductance between the capacitor and the inverter switches. Q_1, Q_2, Q_3 etc. are fast and controllable switches. D_1, D_2, D_3 etc. are fast recovery diodes connected in anti-parallel with the switches. 'A', 'B' and 'C' are output terminals of the inverter that get connected to the ac load. A three-phase inverter has three load-phase terminals whereas a single-phase inverter has only one pair of load terminals.

1.1.2 PWM METHOD

Pulse width modulated (PWM) inverters are among the most used power-electronic circuits in practical applications. These inverters are capable of producing ac voltages of variable magnitude as well as variable frequency. The PWM inverters are very commonly used in adjustable speed ac motor drive loads where one needs to feed the

motor with variable voltage, variable frequency supply. There are several different PWM techniques, differing in their methods of implementation.

The Space Vector Pulse Width Modulation (SVPWM) method is an advanced, computation intensive PWM method and possibly the best among all the PWM techniques for variable frequency drive application. It exhibits the feature of good dc-bus voltage utilization and Low total harmonic distortion (THD) compared to other PWM methods. SVPWM is more suitable for digital implementation and can increase the obtainable maximum output voltage with maximum line voltage approaching 70.7% of the DC link voltage in the linear modulation range. Because of its superior performance characteristics, it has been finding widespread application in recent years.

SVPWM took place due to its easy digital implementation, better harmonics performance, high DC voltage utilization ratio, reduced switching losses and convenience for capacitor voltage balancing. Moreover, the SVPWM has 15% higher linear modulation range than that of SPWM. However, by increasing the number of levels, SVPWM faces the problem of more complex computations as compared to carrier-based PWM. Therefor many efforts have been made to achieve the SVPWM's performance by using zero sequence voltage injection in carrier-based PWM.

1.2 LITERATURE REVIEW

The Space Vector Pulse Width Modulation (SVPWM) method is an advanced, computation intensive PWM method and possibly the best among all the PWM techniques for variable frequency drive application [1]. Induction motor are used in many applications such as HVAC (heating, ventilation and air-conditioning), Industrial drives (motion control, robotics), automotive control (electric vehicles), etc. In recent years there has been a great demand in industry for adjustable speed drives.

With the development of microcontrollers, SVPWM took place due to its easy digital implementation, better harmonics performance, high DC voltage utilization ratio, reduced switching losses and convenience for capacitor voltage balancing. Moreover, the SVPWM has 15% higher linear modulation range than that of SPWM [2]. However, by increasing the number of levels, SVPWM faces the problem of more complex computations as compared to carrier-based PWM. Therefor many efforts have been

made to achieve the SVPWM's performance by using zero sequence voltage injection in carrier based PWM [3]-[7].

The Space Vector Pulse Width Modulation (SVPWM) method is an advanced, computation intensive PWM method and possibly the best among all the PWM techniques for variable frequency drive application. It exhibits the feature of good dc-bus voltage utilization and Low total harmonic distortion (THD) compared to other PWM methods. SVPWM is more suitable for digital implementation and can increase the obtainable maximum output voltage with maximum line voltage approaching 70.7% of the DC link voltage in the linear modulation range [10].

A Model Predictive Control scheme was used in [22] entitled 'Artificial Neural Network Based Controller for Speed Control of an Induction Motor using Indirect Vector Method'. In their work, the plant was first identified using the NN Toolbox. This led to the generation of training data which was used to train the network to obtain optimum value of weights and biases.

Artificial Intelligent Controller (AIC) could be the best controller for Induction Motor control. Over the last two decades researchers have been working to apply AIC for induction motor drives [23-27]. This is because that AIC possesses advantages as compared to the conventional PI, PID and their adaptive versions. The Artificial Intelligence (AI) techniques, such as Expert System (ES), Fuzzy Logic (FL), Artificial Neural Network (ANN or NNW) and Genetic Algorithm (GA) have recently been applied widely in power electronics and motor drives. The performance of inverter is compared for various switching frequencies for different architectures have been presented in [34].

Competitive NN based SVM was first proposed in [35] for under modulation region. A multi layer feed forward network based SVM proposed in [36] is shown to perform well in both regions of modulation. Theoretically it has been shown that increase in the number of layers improves the performance of the network.

A comprehensive survey of neuro fuzzy rule generation algorithms for real-time applications is examined by S. Mitra et al. [37]. Fuzzy logic has a good capability of interpretability and can also integrate expert's knowledge. The hybridization of both paradigms yields the capabilities of learning, good interpretation and incorporating prior knowledge [38].

CHAPTER 2

SPACE VECTOR PWM BASED INVERTER

2.1 SPACE VECTOR PWM:

The space vector modulation technique is somewhat similar to the Sine+3rd harmonic PWM technique but the method of implementation is different. Before going into details of this technique, it would be useful to explore the concept of voltage space-vector, in analogy with the concept of flux space-vector as used in three-phase ac machine. The stator windings of a three phase ac machine (with cylindrical rotor), when fed with a three phase balanced current produce a resultant flux space vector that rotates at synchronous speed in the space. The flux vector due to an individual phase winding is oriented along the axis of that particular winding and its magnitude alternates as the current through it is alternating. The magnitude of the resultant flux due to all three windings is, however, fixed at 1.5 times the peak magnitude due to individual phase windings. The resultant flux is commonly known as the synchronously rotating flux vector. Now, in analogy with the fluxes, if a three phase balanced voltage is applied to the windings of a three phase machine, a rotating voltage space vector may be talked of. The resultant voltage space vector will be rotating uniformly at the synchronous speed and will have a magnitude equal to 1.5 times the peak magnitude of the phase voltage. Fig.2.1 shows a set of three phase balanced sinusoidal voltages. Let these voltages be applied to the windings of a three phase ac machine as shown in Fig.2.1(b). Now, during each time period of the phase voltages six discrete time instants can be identified, as done in Fig.2.1(a), when one of the phase voltages have maximum positive or negative instantaneous magnitude. The resultants of the three space voltages at these instants have been named V_1 to V_6. The spatial positions of these resultant voltage space vectors have been shown in Fig.2.1(b). At these six discrete instants, these vectors are aligned along the phase axes having

maximum instantaneous voltage. As shown in Fig.2.1(a) the magnitude of these voltage vectors is1.5 times the peak magnitude of individual phase voltage.

The instantaneous voltage output from a 3-phase inverter, discussed in earlier lessons, cannot be made to match the three sinusoidal phase voltages of Fig.2.1(a) at all time instants. This is so because the inverter outputs are obtained from rectangular pole voltages and contain, apart from the fundamental, harmonic voltages too. However, the instantaneous magnitudes of the inverter outputs and the sinusoidal voltages can be made to match at the six discrete instants (talked above) of the output cycle. At these six discrete instants one of the phase voltages is at its positive or negative peak magnitude and the other two have half of the peak magnitude. The polarity of the peak phase-voltage is opposite to that of the other two phase-voltages. A similar pattern is seen in the instantaneous phase voltages output by a 3-phase inverter and is explained below.

Fig.2.2 shows a three-phase voltage source inverter whose output terminals are fed to the three terminal of a three-phase ac machine (in fact to any three-phase balanced load). From the knowledge of 3-phase voltage source inverters, it may be obvious that the two switches of each inverter pole conduct in a complementary manner. Thus, the six switches of the three poles will have a total of eight different switching combinations. Out of these eight combinations, two combinations wherein all the upper switches or all the lower switches of each pole are simultaneously ON result in zero output voltage from the inverter. These two combinations are referred as null states of the inverter. The remaining six switching combinations, wherein either two of the high side (upper) switches and one of the low side (lower) switch conduct, or vice versa, are active states. Accordingly, instantaneous magnitude of two of the phase voltages are 1/3rd Edc and the third phase voltage is 2/3rd Edc (where Edc is the dc link voltage). The voltage polarities of the two phases getting 1/3rd Edc are identical and opposite to the third phase having 2/3rd Edc. Fig.2.2 also shows, in a tabular form, the instantaneous magnitudes of the three load-phase voltages (normalized by the dc link voltage magnitude) during the six active states of the inverter. The switching states of the inverter have been indicated by a 3-bit switching word. The 1st (MSB) bit for leg ‘A’, 2nd bit for leg ‘B’ and 3rd bit for leg ‘C’. When a particular bit is 1, the high (upper) side switch of that leg is ON and when the bit is 0, the low side switch is ON. Thus, a switching word 101 indicates that high side switches of

legs ‘A’ and ‘C’ and low side switch of leg ‘B’ conduct. The resulting voltage pattern is identical to the voltage pattern of space voltage vector V1 of Fig.2.1 provided 2/3rd E_{dc} equals the peak magnitude of phase voltage in Fig.2.2. The table given in Fig.2.2 shows how six active states of the inverter produce space voltage vectors V1 to V6 that can be identified on one to one basis with the six voltage vectors of Fig.2.2. There are some important differences between the resultant space voltage vectors due to the sinusoidal phase voltages of Fig.2.1(a) and the space voltage vectors formed by the inverter output voltages.

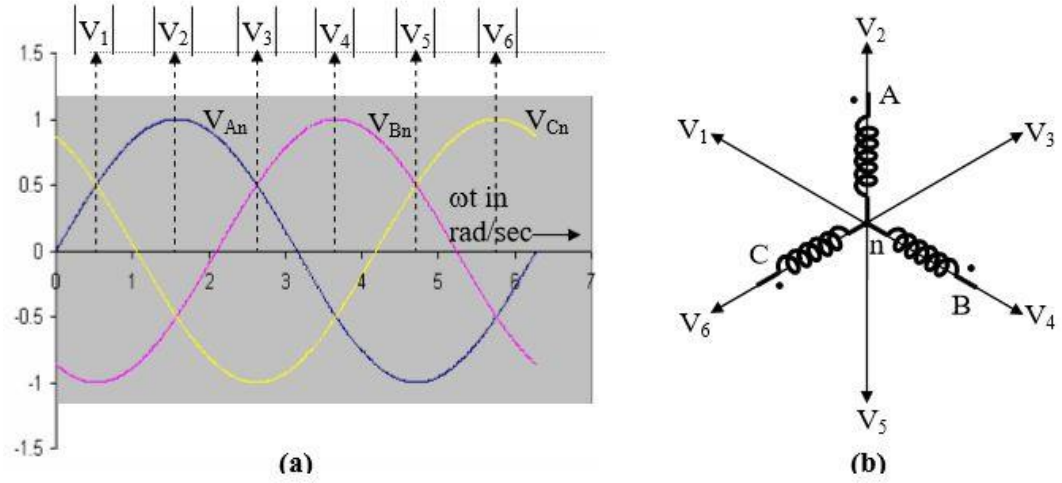

Fig.2.1 The concept of voltage space vectors: (a) 3-phase balanced voltages, (b) The voltage space vectors.

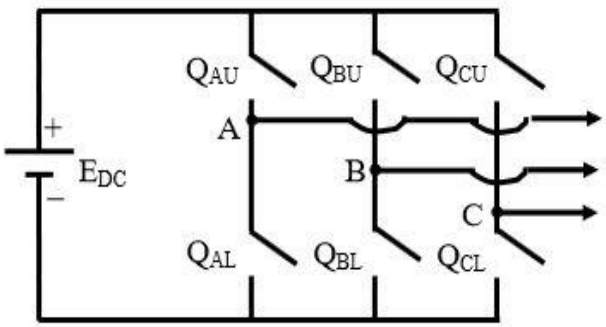

Switch states ⇨	(V1) 101	(V2) 100	(V3) 110	(V4) 010	(V5) 011	(V6) 001
V_{An} ⇨	1/3	2/3	1/3	-1/3	-2/3	-1/3
V_{Bn} ⇨	-2/3	-1/3	1/3	2/3	1/3	-1/3
V_{Cn} ⇨	1/3	-1/3	-2/3	-1/3	1/3	2/3

Fig.2.2 Space vectors output by a 3-phase voltage source inverter

2.2 SMOOTHLY ROTATING SPACE VOLTAGE VECTOR FROM INVERTER

The continuously varying sinusoidal waveforms, as shown in Fig. 2.1, result in a space voltage vector of fixed magnitude rotating at fixed (synchronous) speed in the space. If the inverter could have produced ideal sinusoidal 3-phase voltages, the resultant space voltage vector would have also moved smoothly in space with constant magnitude and constant angular speed. However, by now the reader would know that the practical power electronic inverter could never produce the perfectly ideal sinusoidal voltages. In fact, when the inverter switches from one active state to another, the space voltage vector changes its direction abruptly, the abrupt change in direction being in multiples of 60 electrical degrees. If at a time only one bit of the inverter switching word changes (i.e., only one leg of the inverter changes the switching state) the abrupt change in space vector direction is by 60 electrical degrees.Knowing that the inverter cannot produce ideal sinusoidal voltage waveforms, a good PWM inverter aims to remove low frequency harmonic components from the output voltage at the cost of increasing high frequency distortion. The high frequency ripple in the output voltage can easily be filtered by a small external filter or by the load inductance itself. In terms of voltage space vectors, the above trade-off between low and high frequency ripples means that the resultant voltage vector will have two components; (i) a slowly moving voltage vector of constant magnitude and constant speed superimposed with (ii) a high frequency ripple component whose direction and magnitude changes abruptly.

The space-vector PWM technique aims to realize this slowly rotating voltage space vector (corresponding to fundamental component of output voltage) from the six active state voltage vectors and two null state vectors. The active state voltage vectors have a magnitude equal to E_{dc} and they point along fixed directions whereas null state vectors have zero magnitude. Fig. 2.3 shows the voltage space-vector plane formed by the active state and null state voltage vectors. The null state voltage vectors V_7 and V_8 are each represented by a dot at the origin of the voltage space plane. The switching word for V_7 is 000, meaning all lower side switches are ON and for V_8 is 111, corresponding to all upper side switches ON. The active-state voltage space vectors point along directions shown previously in Fig. 2.1(b). A regular hexagon is formed

after joining the tips of the six active voltage vectors. The space plane of Fig. 2.3 can be divided in six identical zones (I to VI). The output voltage vector from the inverter (barring high frequency disturbances) should be rotating with fixed magnitude and speed in the voltage plane. Now it is possible to orient the resultant voltage space-vector along any direction in the space plane using the six active vectors of the inverter. Suppose one needs to realize a space voltage vector along a direction that lies exactly in the centre of sector-I of the space plane shown in fig.2.3. For this the inverter may be continuously switched (at high frequency) between V1 and V2 active states, with identical dwell time along these two states. The resultant vector so realized will occupy the mean angular position of V_1 and V_2 and the magnitude of the resultant vector can be found to be 0.866 times the magnitude of V1 or V2 (being the vector sum of 0.5 V_1 and 0.5 V_2). Further, the magnitude of the resultant voltage vector can be controlled by injecting suitable durations of null state.

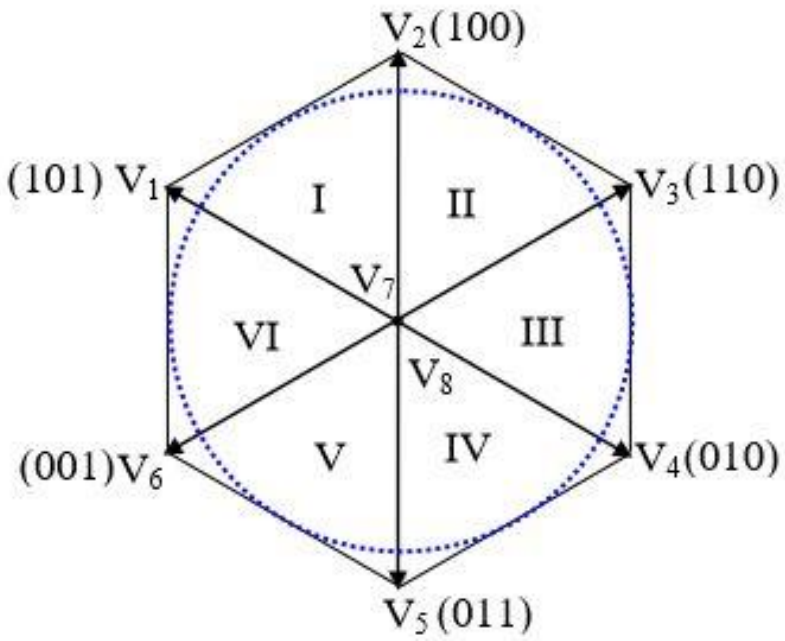

Fig.2.3 The voltage space vectors output by a 3-phase inverter

2.3 ALGORITHM FOR PRODUCING SINUSOIDAL OUTPUT VOLTAGES USING SVPWM

The SV-PWM is concerned with the control of inverter output voltages in a unified manner. It does not control the individual phase voltages separately. The instantaneous magnitude and direction of the desired resultant voltage vector is decided as per the frequency and magnitude of inverter's fundamental output voltage. The SV-PWM is best realized with the help of a digital computing device, like microprocessor or Digital Signal Processor. The algorithm to be executed is outlined below:

(1) Get the input data like; input dc link voltage (E_{dc}), desired output frequency 'f_{OP}' (this will determine the speed of the resultant voltage vector), desired phase sequence of output voltage (will determine which way, clockwise or anticlockwise, the resultant voltage vector is moving), desired magnitude of output voltage and the desired switching frequency. It will be shown later that the switching frequency (f_{SW}) and sampling time period (T_S) are related. During each sampling time period three switching take place, where one turn-on and one turn-off is taken as one switching.

(2) Calculate magnitude factor 'α' from the knowledge of input dc link voltage and the desired output voltage (αE_{dc} = 3/2 times peak of phase voltage). Also, calculate the sampling time period $T_S = 1/(3f_{SW})$.

(3) Initialize sector position = I, and angle 'θ'=0. Assume the rotating space voltage vector to remain stalled at this position for the sampling time period 'T_S'. Output the inverter switching pulses as per the calculated time durations so as to realize the space vectors in the following sequence: $V_8(111)$, $V_1(101)$, $V_2(100)$, $V_7(000)$.

(4) Calculate the next position angle $\theta = 2T_S \pi f_{OP} + \theta_{old}$ for clockwise rotation in the vector space-plane of Fig. 2.3. Recalculate the time durations as in step (3) above but this time the switching sequence will be $V_7(000)$, $V_2(100)$, $V_1(101)$, $V_8(111)$.

(5) Step(4) is to be repeated but every time the switching sequence alternates between the sequences given in steps 4 and 5. This helps in reducing the switching losses. We should note that this way there are only 3 switching per sampling period. The switching to next space vector involves change of only one bit of the switching word (i.e. only one turn-on and one turn-off). When the space vector enters sector-II (for $\theta \geq \pi/3$), the vector V_1 is replace by V_2 and V_2 is replaced by V_3. At the

same time, angular position is reset to a value within $\pi/3 \geq \theta \geq 0$ by subtracting 60^o from the old value. Every time the voltage vector enters a new sector the angle θ is readjusted so that it varies between 0^o and 60^o. The active state vectors are also reassigned as described above. The process continues to produce a continuously rotating voltage space vector of fixed magnitude and fixed speed.

2.4 THREE PHASE VOLTAGE SOURCE PWM INVERTER

The circuit model of a typical three phase voltage source PWM inverter is shown in fig.2.4 S_1 to S_6 are the six power switches that shape the output, which are controlled by the switching variables a, a′, b, b′, c and c′. When an upper transistor is switched on,i.e., when a, b or c is 1, the corresponding lower transistor is switched off, i.e. the corresponding a′, b′ or c′ is 0. Therefore, the on and off states of the upper transistors S1, S3 and S5 can be used to determine the output voltage.

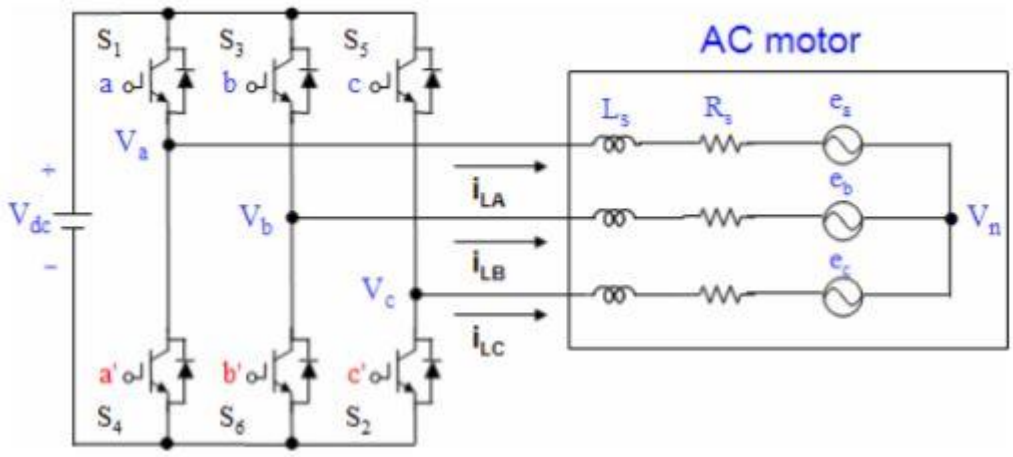

Fig.2.4 Three phase voltage source PWM inverter

Table 2.1 Switching vectors, phase voltages and output line to line voltages

Voltage Vectors	Switching Vectors			Line to neutral voltage			Line to line voltage		
	a	b	c	V_{an}	V_{bn}	V_{cn}	V_{ab}	V_{bc}	V_{ca}
V_0	0	0	0	0	0	0	0	0	0
V_1	1	0	0	2/3	-1/3	-1/3	1	0	-1
V_2	1	1	0	1/3	1/3	-2/3	0	1	-1
V_3	0	1	0	-1/3	2/3	-1/3	-1	1	0
V_4	0	1	1	-2/3	1/3	1/3	-1	0	1
V_5	0	0	1	-1/3	-1/3	2/3	0	-1	1
V_6	1	0	1	1/3	-2/3	1/3	1	-1	0
V_7	1	1	1	0	0	0	0	0	0

2.5 DETERMINATION OF SWITCHING TIME OF EACH SWITCH

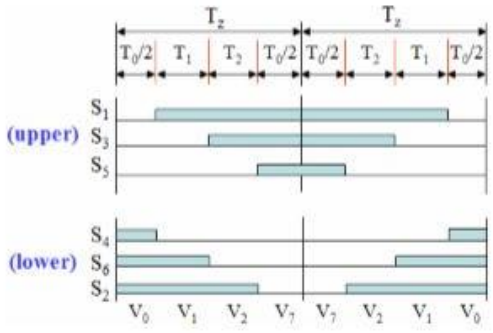

(a) Sector 1.

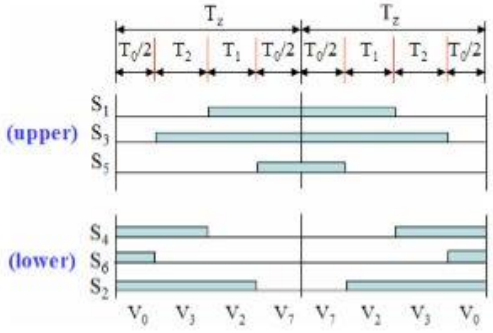

(b) Sector 2.

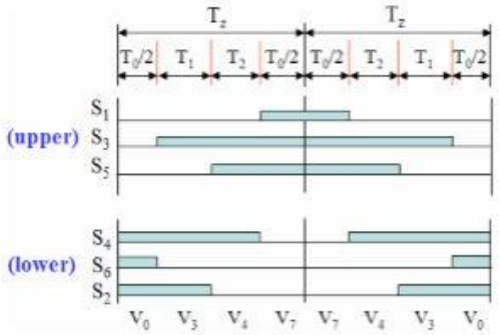

(c) Sector 3.

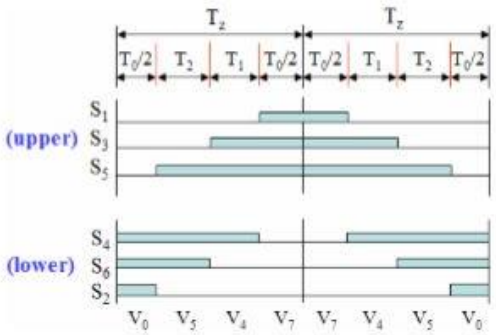

(d) Sector 4.

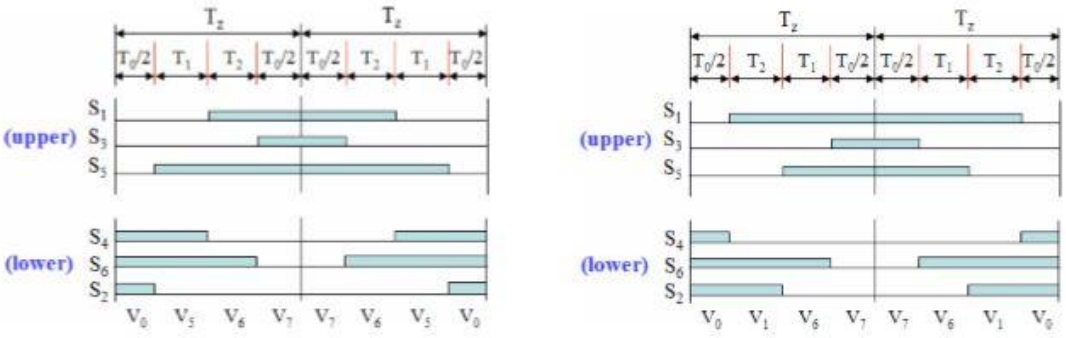

(e) Sector 5. (f) Sector 6.

Fig. 2.5 Space Vector PWM switching patterns at each sector

Based on Fig. 2.5, the switching time at each sector is summarized in Table 2, and it will be built in Simulink model to implement SVPWM.

Table 2.2 Switching Time Calculation at Each Sector

Sector	Upper Switches (S_1, S_3, S_5)	Lower Switches (S_4, S_6, S_2)
1	$S_1 = T_1 + T_2 + T_0/2$ $S_3 = T_2 + T_0/2$ $S_5 = T_0/2$	$S_1 = T_0/2$ $S_3 = T_2 + T_0/2$ $S_5 = T_1 + T_2 + T_0/2$
2	$S_1 = T_1 + T_0/2$ $S_3 = T_1 + T_2 + T_0/2$ $S_5 = T_0/2$	$S_1 = T_2 + T_0/2$ $S_3 = T_0/2$ $S_5 = T_1 + T_2 + T_0/2$
3	$S_1 = T_0/2$ $S_3 = T_1 + T_2 + T_0/2$ $S_5 = T_2 + T_0/2$	$S_1 = T_1 + T_2 + T_0/2$ $S_3 = T_0/2$ $S_5 = T_2 + T_0/2$
4	$S_1 = T_0/2$ $S_3 = T_2 + T_0/2$ $S_5 = T_1 + T_2 + T_0/2$	$S_1 = T_1 + T_2 + T_0/2$ $S_3 = T_2 + T_0/2$ $S_5 = T_0/2$

5	$S_1 = T_2 + T_0/2$ $S_3 = T_0/2$ $S_5 = T_1 + T_2 + T_0/2$	$S_1 = T_2 + T_0/2$ $S_3 = T_1 + T_2 + T_0/2$ $S_5 = T_0/2$
6	$S_1 = T_1 + T_2 + T_0/2$ $S_3 = T_0/2$ $S_5 = T_2 + T_0/2$	$S_1 = T_0/2$ $S_3 = T_1 + T_2 + T_0/2$ $S_5 = T_2 + T_0/2$

2.6 MATHEMATICAL ANALYSIS OF SVPWM

Voltage is converted from abc voltage to dqo transformation.

2.6.1 Determination of V_d, V_q. V_{ref} and Angle alpha (α)

$$V_d = V_{an} - V_{bn}cos60 - V_{cn}cos60 \quad 2.1$$

$$V_d = V_{an} - \frac{1}{2}V_{bn} - \frac{1}{2}V_{cn} \quad 2.2$$

$$V_q = 0 + V_{bn}cos30 - V_{cn}cos30 \quad 2.3$$

$$V_q = V_{an} + \frac{\sqrt{3}}{2}V_{bn} - \frac{\sqrt{3}}{2}V_{cn} \quad 2.4$$

$$\begin{bmatrix} V_d \\ V_q \end{bmatrix} = \frac{2}{3}\begin{bmatrix} 1 & -\frac{1}{2} & -\frac{1}{2} \\ 0 & \frac{\sqrt{3}}{2} & -\frac{\sqrt{3}}{2} \end{bmatrix}\begin{bmatrix} V_{an} \\ V_{bn} \\ V_{cn} \end{bmatrix} \quad 2.5$$

$$\left|\overline{V_{ref}}\right| = \sqrt{{V_d}^2 + {V_q}^2} \quad 2.6$$

$$\alpha = tan^{-1}\left(\frac{V_q}{V_d}\right) = \omega t = 2\pi f t, \quad 2.7$$

Where, f = fundamental frequency

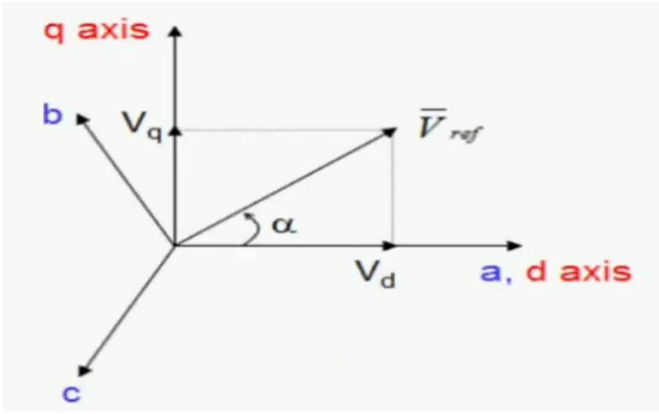

Fig.2.6 d-q transformation

2.6.2 Switching time duration at sector 1

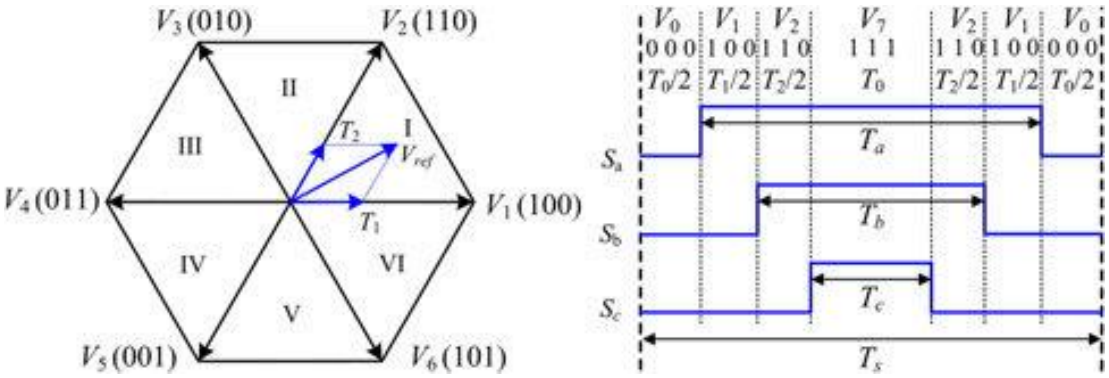

Fig.2.7 Switching Time Duration

$$\int_0^{T_z} \bar{V}_{ref} dt = \int_0^{T_1} \bar{V}_1 dt + \int_{T_1}^{T_1+T_2} \bar{V}_2 dt + \int_{T_1+T_2}^{T_z} \bar{V}_0 dt \qquad 2.8$$

$$T_z \cdot \bar{V}_{ref} = (T_1 \cdot \bar{V}_1 + T_2 \cdot \bar{V}_2) \qquad 2.9$$

$$T_z \cdot |\bar{V}_{ref}| \cdot \begin{bmatrix} cos\alpha \\ sin\alpha \end{bmatrix} = T_1 \cdot \frac{2}{3} \cdot V_{dc} \cdot \begin{bmatrix} 1 \\ 0 \end{bmatrix} + T_2 \cdot \frac{2}{3} \cdot V_{dc} \cdot \begin{bmatrix} cos\left(\frac{\pi}{3}\right) \\ sin\left(\frac{\pi}{3}\right) \end{bmatrix} \qquad 2.10$$

$(where, 0 \leq \alpha \leq 60°)$

$$T_1 = T_z \cdot a \cdot \frac{sin\left(\frac{\pi}{3} - \alpha\right)}{sin\left(\frac{\pi}{3}\right)} \quad 2.11$$

$$T_2 = T_z \cdot a \cdot \frac{sin(\alpha)}{sin\left(\frac{\pi}{3}\right)} \quad 2.12$$

$$T_0 = T_z - (T_1 + T_2), \qquad \left(where, T_z = \frac{1}{f_z} \ and \ a = \frac{\left|\bar{V}_{ref}\right|}{\frac{2}{3}V_{dc}}\right) \quad 2.13$$

2.6.3 Switching time duration for any sector

$$T_1 = \frac{\sqrt{3} \cdot T_z \cdot \left|\bar{V}_{ref}\right|}{V_{dc}}\left(sin\left(\frac{\pi}{3} - \alpha + \frac{n-1}{3}\pi\right)\right) \quad 2.12$$

$$T_1 = \frac{\sqrt{3} \cdot T_z \cdot \left|\bar{V}_{ref}\right|}{V_{dc}}\left(sin\left(\frac{n\pi}{3} - \alpha\right)\right) \quad 2.13$$

$$T_1 = \frac{\sqrt{3} \cdot T_z \cdot \left|\bar{V}_{ref}\right|}{V_{dc}}\left(sin\frac{n\pi}{3} \cdot cos\alpha - cos\frac{n\pi}{3} \cdot sin\alpha\right) \quad 2.14$$

$$T_2 = \frac{\sqrt{3} \cdot T_z \cdot \left|\bar{V}_{ref}\right|}{V_{dc}}\left(sin\left(\alpha - \frac{n-1}{3}\pi\right)\right) \quad 2.15$$

$$T_2 = \frac{\sqrt{3} \cdot T_z \cdot \left|\bar{V}_{ref}\right|}{V_{dc}}\left(-cos\alpha \cdot sin\frac{n-1}{3}\pi + sin\alpha \cdot cos\frac{n-1}{3}\pi\right) \quad 2.16$$

$$\therefore T_0 = T_z - (T_1 + T_2), \qquad \begin{pmatrix} where, n = 1 \ through \ 6 \ (i.e. sector \ 1 \ to \ 6) \\ 0 \leq \alpha \leq 60° \end{pmatrix} \quad 2.17$$

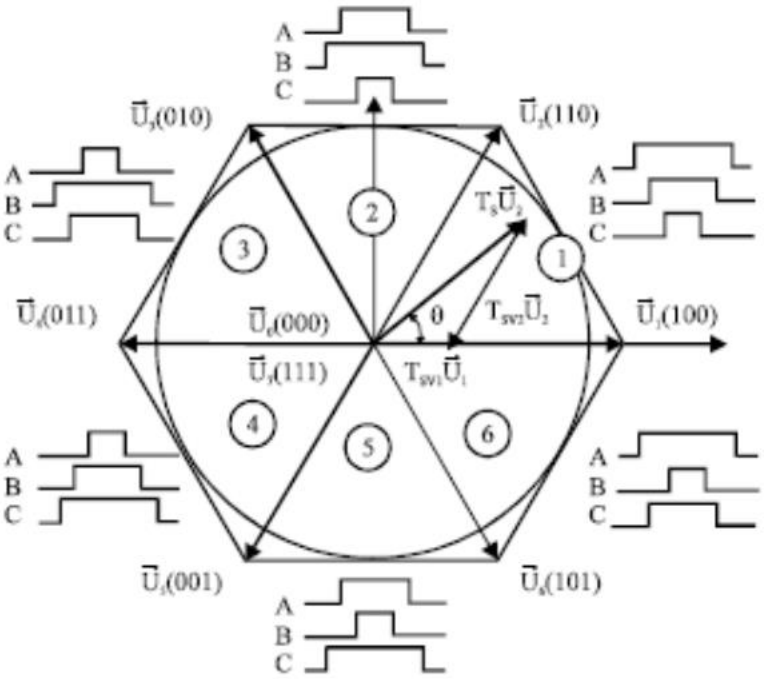

Fig.2.8 Gate Pulse of All Sectors

2.7 FLOW CHART OF SVPWM

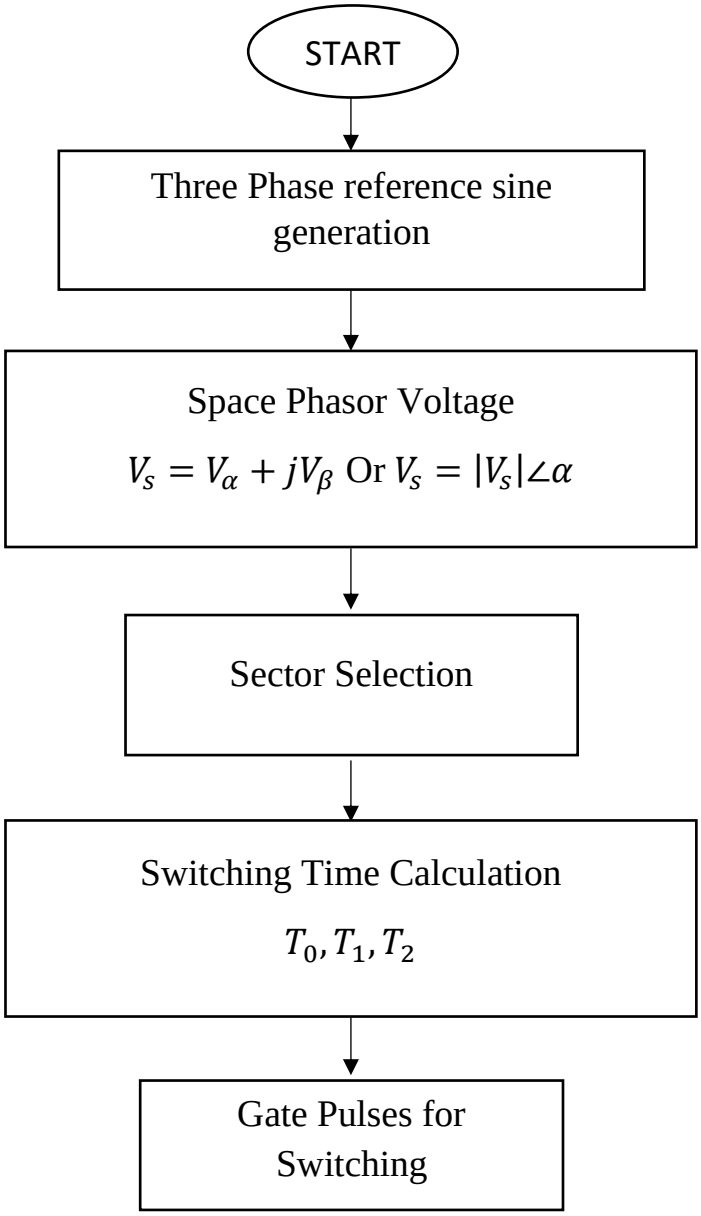

Fig.2.9 Flow Chart of SVPWM

CHAPTER 3

PI CONTROLLER

3.1 PI CONTROLLER

Because of easy design, low cost and simple structure the proportional integral controllers are most widely used in industries. As an on-off controller the proportional integral controller eliminates forced oscillation and steady state error. The overall stability and response of the speed will have negative impact due to integral mode. Therefore, the proportional integral controller will not increase the speed of the response. Because proportional controller does not have means to predict what will happen with the error in near future. So, by introducing derivative mode this problem will be solved. So now the proportional controller now gets the ability to predict error in future and then decreases reaction time. In industries speed of the response is not an issue then proportional integral controller is most widely used. Actually, proportional integral controller is an integral error compensation scheme.

The integral of the actuating signal is the reason for the response of the output. The output produced by this type of controller consists of two terms. In those two terms one is the proportional to the actuating signal and other is proportional to its integral. Therefore, in general this type of controller is known as PI controller or proportional plus integral controller.

A PID controller has proportional, integral and derivative terms that can be represented in transfer function form as,

$$K(s) = K_p + \frac{K_i}{s} + K_d s \qquad 3.1$$

where K_p represents the proportional gain, K_i represents the integral gain, and K_d represents the derivative gain, respectively.

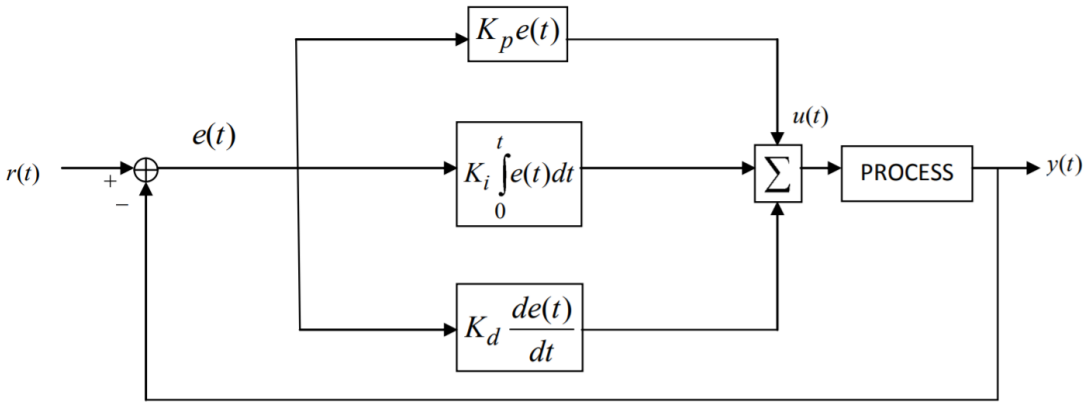

Fig.3.1 PID Controller

Output of PI controller can be written as,

$$Output(t) = K_P e(t) + K_I \int_0^t e(t)dt \qquad 3.2$$

Where, e(t) = set reference value - actual calculated value

$$e(t) = \omega ref - \omega m(t) \qquad 3.3$$

$$T_{ref}(t) = T_{ref}(t-1) + K_P\,[e(t) - e(t-1)] + K_I\, e(t) \qquad 3.4$$

Where, K_P and K_I – speed controllers gain

3.2 IMPLEMENTATION OF CONSTANT V/f STRATEGY

Implementation of the constant Volt/Hz control strategy for the inverter fed induction motor in close loop is shown in Figure 4.2. The frequency command f_s^* is enforced in the inverter and the corresponding dc link voltage i controlled through the front-end converter.

The output of PI regulator is machine slip and it is added to the machine speed to get reference frequency of the inverter. To keep the machine V/f ratio constant, the reference frequency also generates the reference voltage of the inverter.

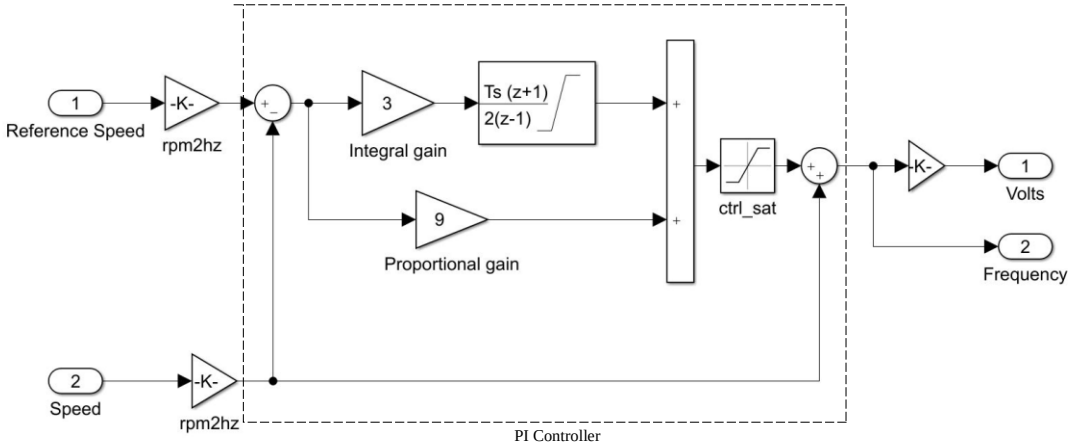

Fig.3.2 Implementation of the constant V/f control strategy for the inverter-fed induction motor in close loop

An outer speed PI control loop in the induction motor drive, shown in Figure 3.2 computes the frequency and voltage set points for the inverter. The limiter ensures that the slip-speed command is within the maximum allowable slip speed of the induction motor. The slip-speed command is added to electrical rotor speed to obtain the stator frequency command.

The equation for the induced emf in the induction machine,

$$V = 4.44N\varphi_m f \qquad 3.5$$

where N is the number of the turns per phase, φ_m is the maximum flux in the air gap and f is the frequency. The above equation is valid under the condition where stator voltage drop negligible compared to the applied voltage.

In order to reduce the speed, frequency needs to be reduced. If frequency is reduced keeping the voltage constant, thereby requiring the amplitude of the EMF to remain same, flux has to increase. This is not advisable since the machine is likely to enter in deep saturation. To avoid this, the flux must be kept constant which means voltage must be reduced with frequency. This ratio is held constant in order to maintain the flux level for maximum torque capability.

Essentially, it is the voltage across the magnetizing branch of exact equivalent circuit which is to be kept constant and it is determined by induced EMF. In this mode of operation, the voltage across the magnetizing inductance in the exact equivalent circuit reduces in amplitude with reduction in frequency and so does the inductive reactance.

This implies that the current through the inductance and the flux in the machine remains constant.

If E is the voltage across the magnetizing branch and f is frequency of excitation, then $E = kf$, where k is constant of proportionality and the torque developed can be given by

$$T_{E/f} = \frac{k^2 f^2}{\left(\frac{R_r'}{s}\right)^2 + (\omega L_{lr}')^2} \frac{R_r'}{s\omega} \tag{3.6}$$

If this equation is differentiated with respect to s and equated to zero to find slip at maximum torque, we get

$$s_m = \pm \frac{R_r'}{\omega L_{lr}'} \tag{3.7}$$

The maximum torque can be obtained by substituting this value in torque equation,

$$T_{E/f\,max} = \frac{k^2}{8\pi^2 L_{lr}'} \tag{3.8}$$

Above equation shows that this maximum value is independent of the frequency and $s\omega$ is independent of frequency, which means that maximum torque always occurs at a speed lower than synchronous speed by a fixed difference, independent of frequency and resultant torque-speed curve for constant E/f can be shown in figure 3.3

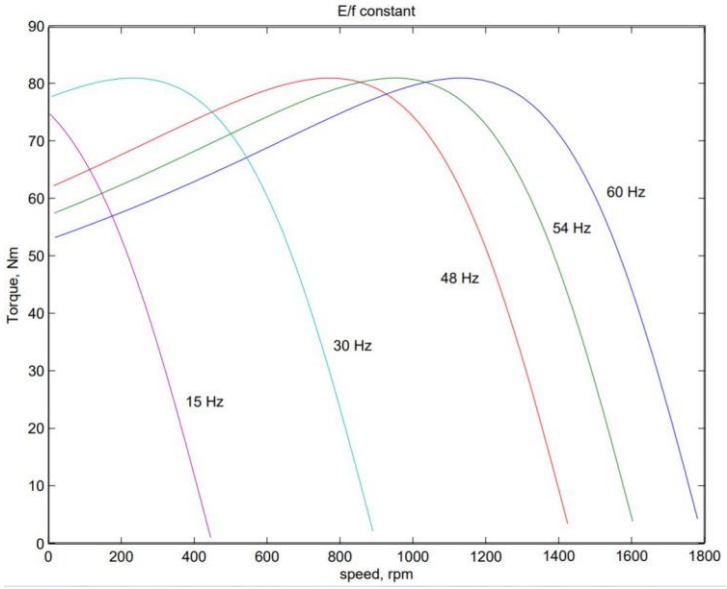

Fig.3.3 Torque-speed curve for constant E/f

E is an internal voltage which is not accessible. It is only the terminal voltage V which we have access to and can control. For a fixed V, E changes with operating slip (rotor branch impedance changes) and further due to the stator impedance drop. Thus, approximated E/f as V/f and resulting torque-speed characteristics can be seen in figure 3.4, which is far from the desired speed-torque curve.

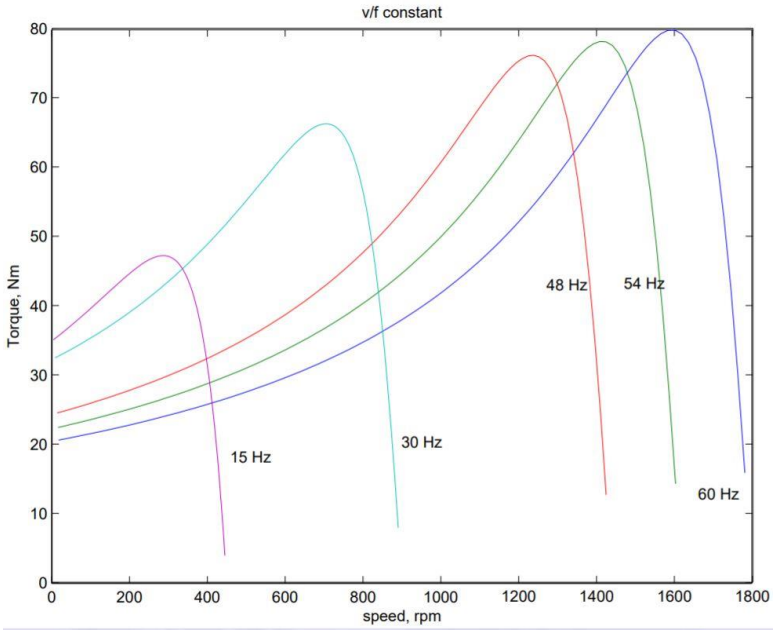

Fig. 3.4 Torque-Speed Curve for constant V/f

At low frequencies and hence low voltages the curves show a considerable reduction in peak torque. At low frequencies (and hence at low voltages) the drop across the stato impedance prevents sufficient voltage availability. Therefore, in order to maintain sufficient torque at low frequencies, a voltage more than proportional needs to be given at low speeds. With this kind of control, it is possible to get a good starting torque and steady state performance.

The adjustment of parameters is implemented by trial and error. In the end $K_p = 3$, and $K_i = 9$. So, the actual transfer function of PI controller is shown in equation 3.9

$$G(s) = \frac{3s + 9}{s} \qquad 3.9$$

CHAPTER 4

ARTIFICIAL NEURAL NETWORK

4.1 Introduction to ANN

The ability to learn, memorize and still generalize, prompted research in algorithmic modelling of biological neural system is Artificial Neural Network. ANN are foundations of Artificial Intelligence and have self-learning abilities and produce better results as more data become available. ANNs are built like human brains, with neuron nodes interconnected like a web. ANN has hundreds of thousands of artificial neurons called processing units and they are interconnected by nodes. These processing units are made up of input and output units. The input units receive various forms and structures of information based on an internal weighting system, and the neural network attempts to learn about the information presented to produce one output report. ANNs use a set of learning rules called backpropagation, an abbreviation for backwards propagation, to perfect their output results. An ANN initially goes through a training phase where it learns to recognize patterns in data, during this phase, the network compares its actual output produced with what it was meant to produce, i.e. the desired output.

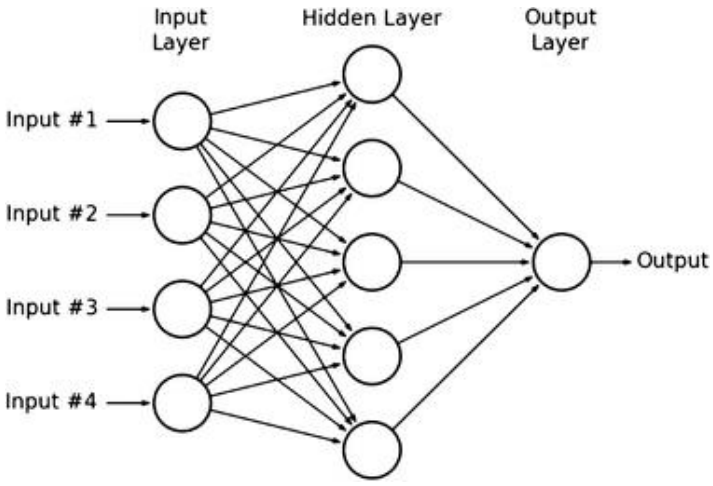

Fig.4.1 Structure of ANN

The difference between both outcomes is adjusted using backpropagation. This means that the network works backward going from the output unit to the input units to adjust the weight of its connections between the units until the difference between the actual and desired outcome produces the lowest possible error. Neural networks are typically organized in layers. Layers are made up of a number of interconnected 'nodes' which contain an 'activation function'. Patterns are presented to the network via the 'input layer', which communicates to one or more 'hidden layers' where the actual processing is done via a system of weighted connections. The hidden layers then link to output layer where the answer is output as shown in the graphic below. ANNs contain some form of 'learning rule' which modifies the weights of the connections according to the input patterns that it is presented with.

4.2 Artificial Neural Network Model

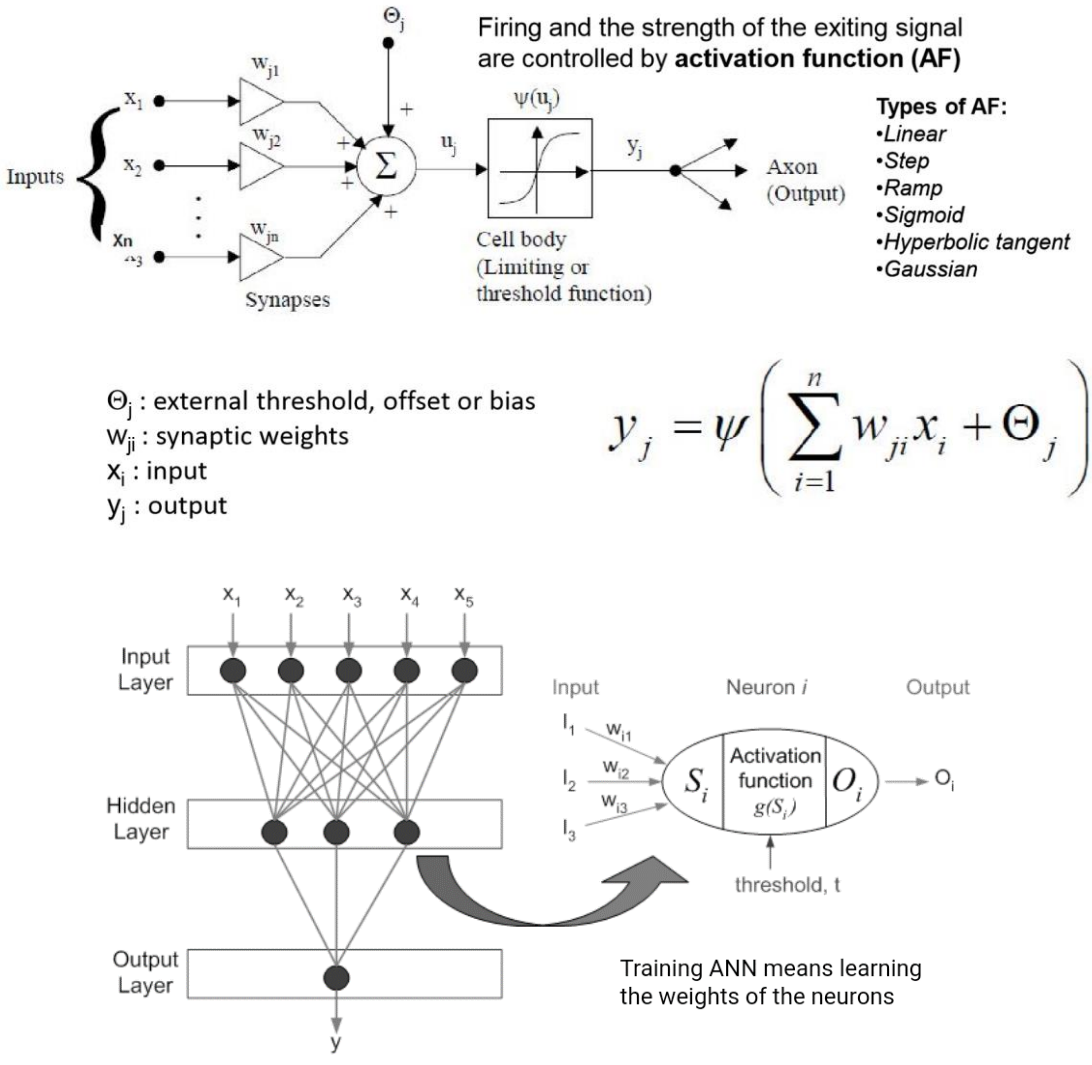

Fig.4.2 Model of ANN

An ANN as a computing system is made up of a number of simple, and highly interconnected processing elements, which processes information by its dynamic state response to externali inputs. Artificial neural Networks (ANNs) are made up of a number of simple and highly interconnected Processing Elements (PE) called neurons. The basic computational element (model neuron) is often called a node or unit. It receives input from some other units, or perhaps from an external source. Each input has an associated weight w, which can be modified so as to model synaptic learning. The unit computes some function of the weighted sum of its inputs which are shown in figure 4.2.

4.3 Performance Plot of ANN

This is plot between error vs epoch for the training, validation, and test performances of the training record returned by the function train.

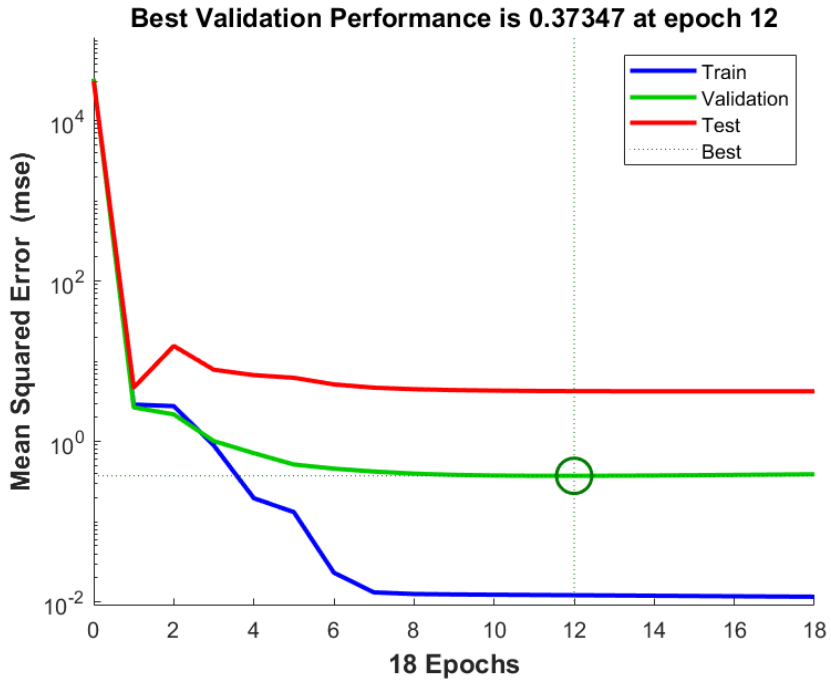

Fig.4.3 Performance Plot

Generally, the error reduces after more epochs of training, but might start to increase on the validation data set as the network starts overfitting the training data. In the default setup, the training stops after six consecutive increases in validation error, and the best performance is taken from the epoch with the lowest validation error.

4.4 Training State Plot

It is plot of the training state from a training record returned by train.

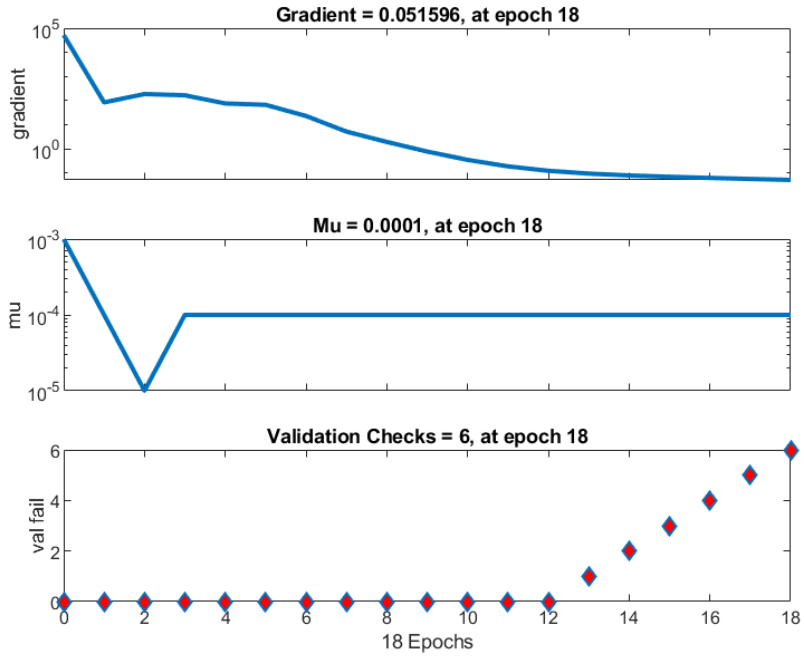

Fig.4.4 Training State Plot

4.5 Error Histogram Plot

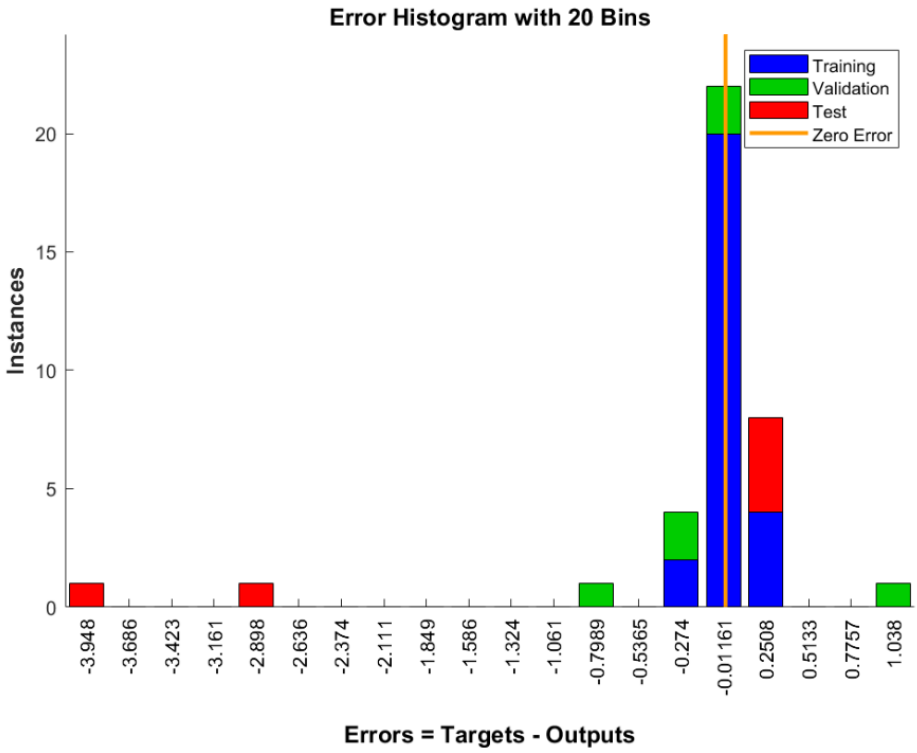

Fig.4.5 Error Histogram Plot

The total error from neural network ranges from -3.948 (leftmost bin) to 1.038 (rightmost bin). This error range is divided into 20 smaller bins, so each bin has a width of,

$$\frac{1.038 - (-3.948)}{20} = 0.2493$$

Each vertical bar represents the number of samples from dataset, which lies in a particular bin.

4.6 Regression Plot

This shows how accurately the trained model fits the dataset. If the value of coefficient of regression(R^2) is close to 1 then it shows that the model prediction is very close to the actual dataset. If it is zero then it shows that the model completely fails in making a correct prediction.

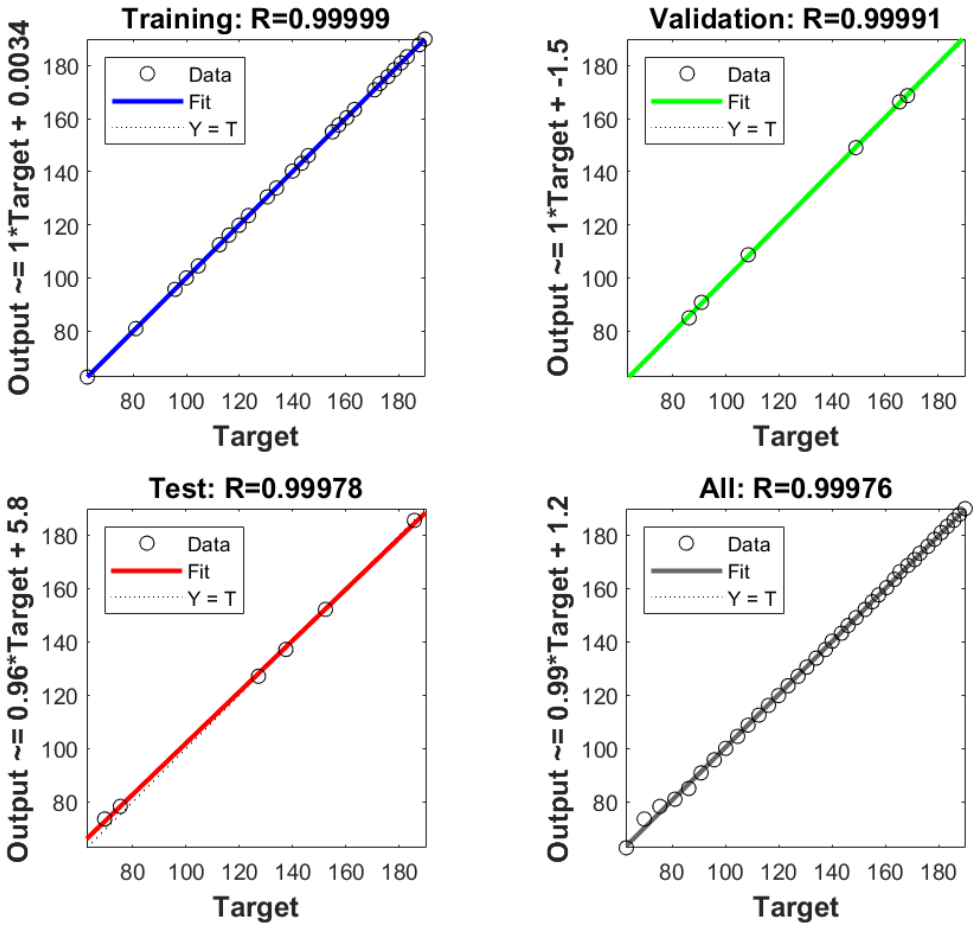

Fig.4.6 Regression Plot

4.7 Different Types of Architecture

4.7.1 Single Layer Perceptron Network

Perceptron is the simplest single layer network, considered as a linear classifier. The principal weakness of the perceptron model is that it can only solve problems that are linearly separable. However, most of the real-world problems are non-linear in nature. These type of feed forward networks contain only one layer i.e. the input layer. Moreover, it is called feed forward network because of the direction of flow of information i.e. input to output.

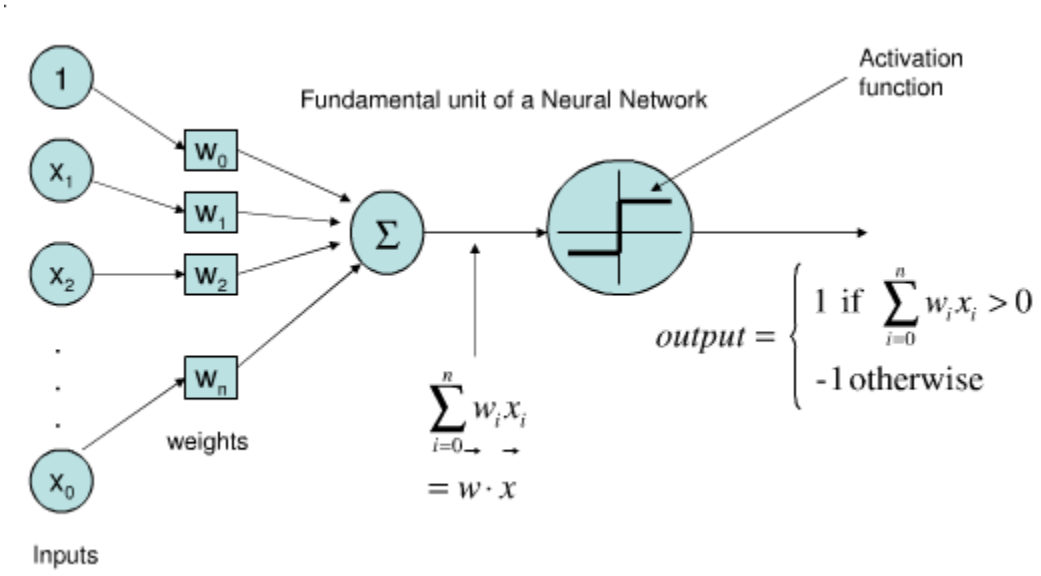

Fig.4.7 Single Layer Perceptron Network

4.7.2 Multilayer Perceptron Network

A Multilayer Perceptron (MLP) is a feed forward neural network model that maps sets of input data onto a set of appropriate output. It is a modification of the standard linear perceptron using three or more layers of neurons (nodes) with nonlinear Activation functions. Hence, it is more powerful than the perceptron as it can distinguish data that is nonlinearly Separable.

The Network consists of an input and an output layer with one hidden layer of nonlinearly-activating nodes. Each node in one layer connects with a certain weight w_{ij} to every other node in the following layer.

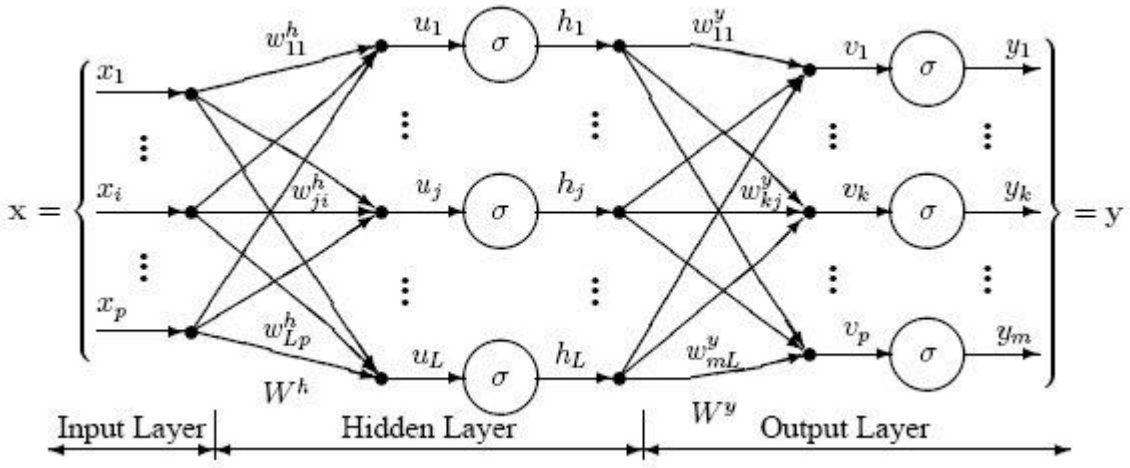

Fig.4.8 Multilayer Perceptron Network

The network is trained with back propagation algorithm. These type of feed forward networks consist of three different layers namely input layer, hidden layer and output layer.

4.7.3 Radial Basis Function Network

These types of feed forward networks work on Radial basis function. These functions are used in multidimensional space for the purpose of interpolation. Here the hidden weights formulate the output with the help of some linear function.

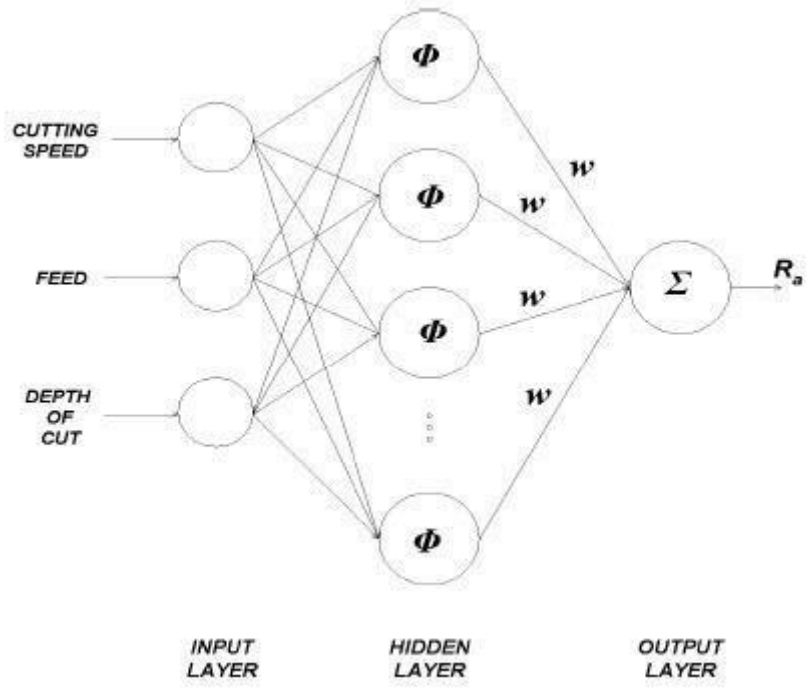

Fig.4.9 Radial Basis Function Network

4.7.4 Hopfield Network

Hopfield networks are single layer feedback networks. It is an auto associative fully interconnected network, moreover it is also symmetrically weighted network. Hopfield networks are constructed from artificial neurons. These artificial neurons have N inputs. With each input there is a weight associated. They also have an output. The state of the output is maintained, until the neuron is updated. Updating the neuron entails the following operations:

1 The value of each input, x_i is determined and the weighted sum of all the Inputs, $w_i x_i$ is calculated.

2 The output state of the neuron is set to +1 if the weighted input sum is larger or equal to 0. It is set to -1 if the weighted input sum is smaller than 0.

3 A neuron retains its output state until it is updated again.

A Hopfield network is a network of N such artificial neurons, which are fully connected. The connection weight from neuron to neuron is given by a number w. The collection of all such numbers is represented by the weight matrix W, whose components are wij.

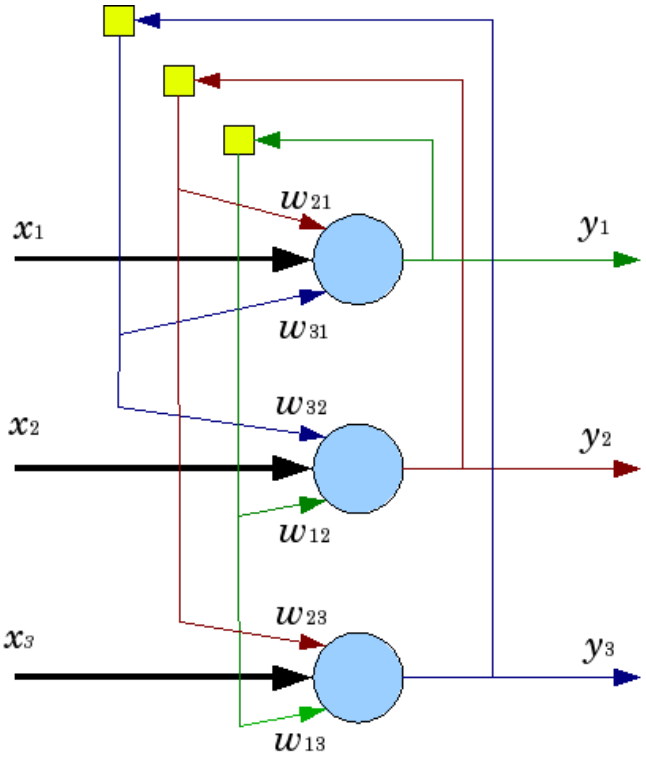

Fig.4.10 Hopfield Network

CHAPTER 5

ADAPTIVE NEURO-FUZZY INFERENCE SYSTEM

5.1 INTRODUCTION

Control of nonlinear systems based on conventional mathematical tools is a difficult problem because no systematic tools are available to deal with ill-defined and uncertain systems. By contrast, a fuzzy inference system employing fuzzy if-then rules can model the qualitative aspects of human knowledge and reasoning processes but lacks standard design procedure to employ precise quantitative analyzes. Neural networks work by detecting patterns in data, learning from the relationships and adapting to them. This knowledge is then used to predict the outcome for new combinations of data.

Adaptive systems can be described by constructing a set of fuzzy if-then rules that represent local linear input output relations of the system. The ANFIS combines both fuzzy logic principle and the concept of the neural networks. The ANFIS has advantages such as smoothness property from the fuzzy principle and adaptability property from the neural networks training structure.

5.2 FUZZY LOGIC

Fuzzy set theory is a powerful tool to deal with the imprecision characteristics in decision-making problems involving uncertainty and vagueness of real-world applications. Fuzzy inference is a process of mapping from a given input to an output dataset using the theory of fuzzy sets. Knowledge is encoded as using a set of explicit linguistic rules. Fuzzy systems implement nonlinear systems using linguistic variables in a straightforward when adequate knowledge about the system is available. Unlike Boolean logic or classical logic, which assumes that every fact is either entirely true or false, fuzzy logic extends Boolean logic to handle vague and imprecise expressions. A

fuzzy system consists of a set of fuzzy IF-THEN rules that describe the input-output mapping relationship of the networks.

Hybrid systems utilize methodologies of soft computing (fuzzy logic, neural computing, genetic computing etc) provide a perspective method to build fuzzy inference system when information about object system incomplete. Main components of fuzzy logic are fuzzification, which translates crisp (real-valued) inputs into fuzzy values; rule base reasoning, an inference engine that applies a fuzzy reasoning mechanism to obtain a fuzzy output using rules; and defuzzification, which translates this latter output into a crisp value, as shown in figure 5.1.

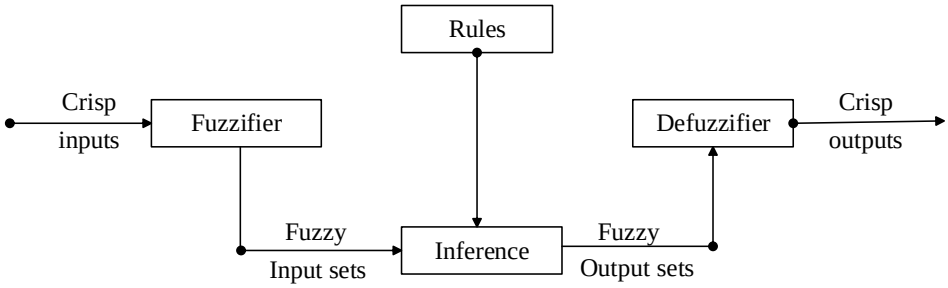

Fig.5.1 Framework of fuzzy logic system

The purpose of fuzzification is to map system input values from 0 to 1 via defined input membership functions. In rule based reasoning, the fuzzy input values membership values are mapped to classify fuzzy output through a table containing if-then rules. Rules are expressed as a logic implication p→q where p is called the antecedent of the rule and q is called the consequence of the rule. Defuzzification is a process which produces single system output (crisp) values by using a defuzzification formula and fuzzy output membership outputs. The fuzzy inference system is a popular computing framework based on the concepts of fuzzy set theory, fuzzy if-then rules, and fuzzy reasoning.

5.3 RULE BASED REASONING

Fuzzy sets are an aid in providing symbolic knowledge information in a more human understandable or natural form, and can hold uncertainties at various levels.

Manipulating a fuzzy rule based system involves the derivation of the desired “If-Then” fuzzy rules, partitioning of universes, and addressing of the membership functions.
Fuzzy rule-based systems use linguistic variables to rationale using a series of logical rules that contain IF-THEN rules which connect antecedents and consequents, respectively. An antecedent is a fuzzy clause with a certain degree of membership (between 0 and 1). Fuzzy rules can have multiple antecedents connected with AND or OR operators, where all parts are considered simultaneously and resolved into a single number. Consequents can also be comprised of multiple parts, which are then aggregated into a single output of a fuzzy set.

5.4 DEFUZZIFICATION

Defuzzification is mapping process produces a non-fuzzy control action that best represents the possibility distribution of an inferred fuzzy control action. The defuzzification has the capability to reduce fuzzy set into a single-valued quantity or into a crisp set. there is no unique defuzzification method and each defuzzification method has advantages and disadvantages.
Defuzzification is the process of producing a quantifiable result in Crisp logic, given fuzzy sets and corresponding membership degrees. It is the process that maps a fuzzy set to a crisp set. It is typically needed in fuzzy control systems. These will have a number of rules that transform a number of variables into a fuzzy result, that is, the result is described in terms of membership in fuzzy sets.

5.5 ARCHITECTURE OF ANFIS

An adaptive network is a multilayer feed-forward network composed of nodes connected by directed links, in which each node performs a particular function on its incoming signals to generate a single node output. Each link in an adaptive network specifies the direction of signal flow from one node to another; no weights is associated with the link. More specifically, the configuration of an adaptive network performs a static node function on its incoming signals to generate a single node output and each node function is a parameterized function with modifiable parameters; by changing these parameters, the node functions as well as the overall behavior of the adaptive network, are changed. Figure 5.2 shows entire system architecture consists of five

layers, namely fuzzy layer, product layer, normalized layer, de-fuzzy layer and total output layer.

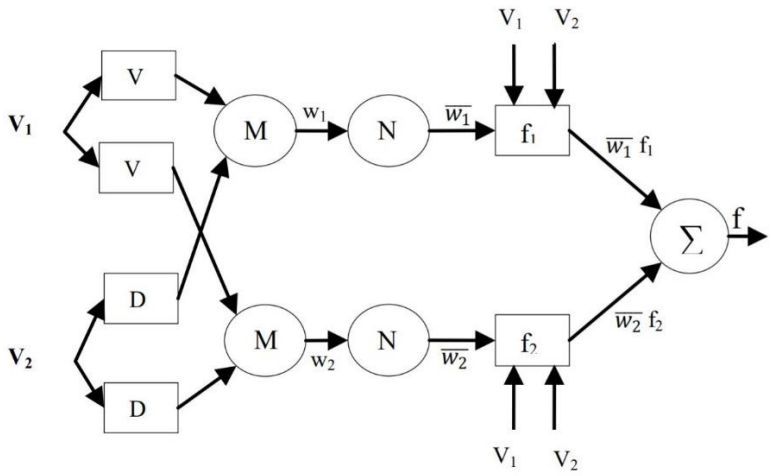

Fig.5.2 Architecture of ANFIS

With input/output data for given set of parameters, the ANFIS method models a fuzzy inference system (FIS) whose membership function parameters are tuned. The main objective of the ANFIS is to determine the optimum values of the equivalent fuzzy inference system parameters by applying a learning algorithm. The parameter optimization is done in such a way during the training session that the error between the target and the actual output is minimized.

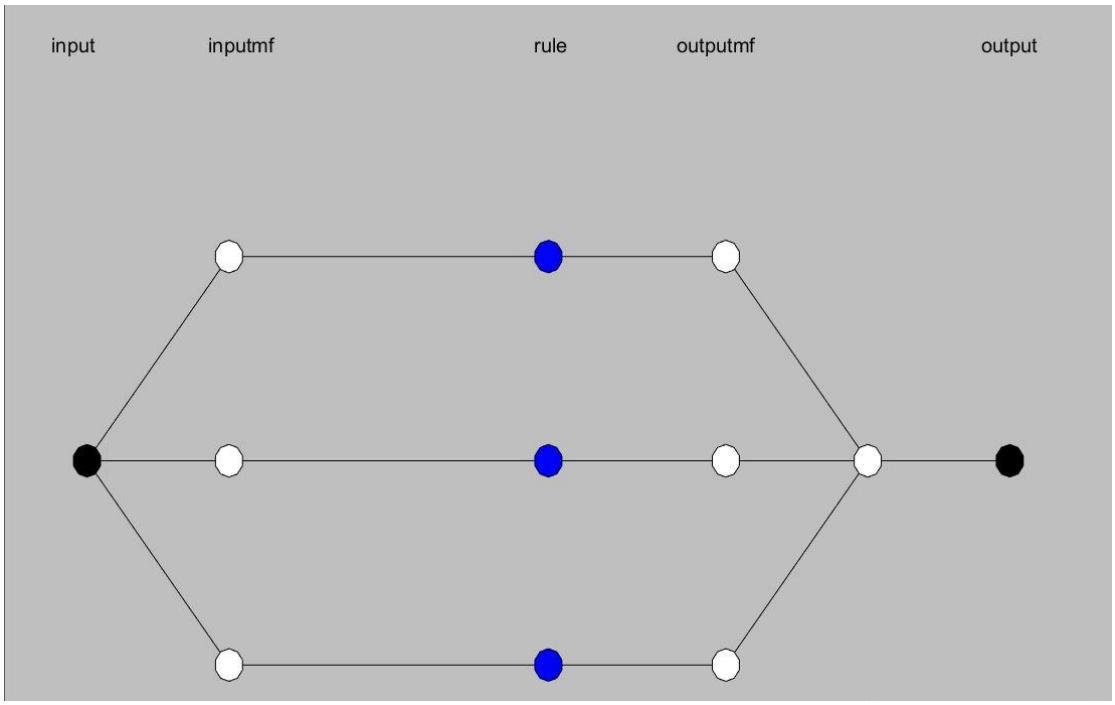

Fig.5.3 ANFIS Model Structure

ANFIS network is five layer architecture, where the first layer contains membership functions that determine membership degree of each input according to the shape of membership function. The second layer is for inference between IF and THEN part of the rule-base. Second layer performs product operation on the membership degrees in order to calculate the firing strength of each rule. Third layer normalizes the firing strength of each rule against all the rules. Fourth layer is a linear polynomial equation. The last layer is simply summation of the outputs of rules calculated in previous layer.

5.6 LAYERS OF ANFIS

A brief summary of five layers of the ANFIS algorithm is shown below.

5.6.1 Layer-1

Each input node i in this layer is an adaptive node which produce membership grade of linguistic label. It is a fuzzy layer, in which v and d are input of system. $O_{1,i}$ is the output of the i^{th} node of layer l. Each adaptive node is a square node with square function represented using equation,

$$O_{1,i} = \mu_{v,i}(v) \text{ for i=1,2} \quad \& \quad O_{1,j} = \mu_{d,j}(v) \quad \text{for i=1,2} \tag{5.1}$$

Where $O_{1,i}$ and $O_{1,j}$ denote output function and $\mu_{v,i}$ and $\mu_{d,j}$ denote membership function. For example if triangular membership function is selected then, $\mu_{v,i}(v)$ is given by:

$$\mu_{vi}(v) = max\left[min\left(\frac{v-a_i}{b_i-a_i}, \frac{c_i-v}{c_i-b_i}\right), 0\right] \tag{5.2}$$

Where a_i, b_i and c_i are the parameter of triangular membership function. Parameters in this layer are referred to as "Premise Parameter".

5.6.2 Layer-2

This layer checks weights of each membership function, it receives input values vi from first layer and acts as a membership function to represent fuzzy sets of respective input variables. Every node in this layer is fixed node labeled with M and output is calculated via product of all incoming signals. The output in this layer can be represented using equation,

$$O_{2,i} = w_i = \mu_{v,i}(v).\mu_{d,i}(d) \text{ for i=1,2} \tag{5.3}$$

Which are the firing strengths of the rules.

5.6.3 Layer-3

Every node in this layer is fixed marked with circle labeled with N, indicating normalization to the firing strength from previous layer. This layer performs pre-condition matching of fuzzy rules, i.e. they compute activation level of each rule, the number of layers being equal to number of fuzzy rules. The i^{th} node in this layer calculate ratio of i^{th} rule's strength to the sum of all rules firing strength. The output of this layer can be expressed as w_i using Eq.

$$O_{3,i} = \overline{w_i} = \frac{w_i}{w_1+w_2}, \text{ i=1,2} \qquad 5.4$$

For convenience, outputs of this layer will be called as normalized firing strengths.

5.6.4 Layer-4

This layer provides output values y, resulting from the inference of rules. The resultant output is simply a product of normalized firing rule strength and first order polynomial. Weighted output of rule represented by node function as:

$$O_{4,i} = \overline{w_i} f_i = \overline{w_i}(p_i v + q_i d + r_i), \text{ i=1,2} \qquad 5.5$$

Where $O_{4,i}$ represents layer 4 output. In this layer, p_i, q_i and r_i are linear parameter or consequent parameter.

5.6.5 Layer-5

This layer is called output layer which sums up all the inputs coming from layer 4 and transforms fuzzy classification results into crisp values. This layer consists of single fixed node labeled as $\sum$. This node computes summation of all incoming signals calculated using Eq.

$$O_{5,i} = \sum_i \overline{w_i} f_i = \frac{\sum_i w_i f_i}{w_1+w_2}, \text{ i=1,2} \qquad 5.6$$

Thus, it is observed that when the values of premise parameter are fixed, the overall output of the adaptive network can be expressed as linear combination of a consequent parameter. Overall output of a system (z) can be expressed as in Eq. 11. It can be observed that ANFIS architecture consists of two adaptive layers, namely the first layer and the fourth layer. The three modifiable parameters {ai ,bi ,ci} are so-called premise parameter in first layer and in the fourth layer, there are also three modifiable

parameters p_i, q_i and r_i pertaining to the first order polynomial. These parameters are so-called consequent parameters

$$z = \frac{w_1}{w_1 + w_2} f_1 + \frac{w_2}{w_1 + w_2} f_2 + \cdots + \frac{w_n}{w_1 + w_2} f_n \qquad 5.7$$

5.7 Neuro-Fuzzy Designer

Neuro-fuzzy designer is used to design, train and test ANFIS using input/output training data.

Neuro-Fuzzy Designer has been used to train a fuzzy inference system that:

1. Has a single output.
2. Uses weighted average defuzzification.
3. Has output membership functions all of the same type, for example linear or constant.
4. Has complete rule coverage with no rule sharing; that is, the number of rules must match the number of output membership functions, and every rule must have a different consequent.
5. Has unity weight for each rule.
6. Does not use custom membership functions.

Fig.5.4 Neuro-Fuzzy Designer

5.8 Membership Function Editor

In fuzzy set theory, a membership function defines the degree of truth, of a crisp value. Membership function is a function which returns membership degree of how crisp value is mapped to an input space referred to as universe of disclosure. Each membership function contains a curve which represents each point in a specified input partition.

Fig.5.5 Membership Function Editor

CHAPTER 6

MODELING OF PROPOSED SYSTEM IN MATLAB/SIMULINK

In this chapter simulation of all the components of project is shown. The first part of the project is three-phase inverter, simulation of this is shown in section 6.1. Switching of this three-phase inverter is given by using space vector pulse width modulation (SVPWM) technique and its simulation is shown in section 6.2. All the parts of SVPWM is also shown in this section. Three types of controllers are used in this project. First PI controller is used to control the speed of induction motor; simulation of PI controller is shown in section 6.3. In section 6.4, all the parameters of induction motor and mathematical analysis are shown. Then induction motor is run with artificial neural network (ANN), therefore simulation for ANN is shown in section 6.5 and various plots are plotted while training the ANN is also shown. Then simulation of ANFIS controller for speed control of induction motor is shown in section 6.6.

6.1 THREE PHASE VOLTAGE SOURCE INVERTER

Figure 6.1 shows the simulated model of three-phase voltage source inverter. The switches used are IGBT with anti-parallel diode. It has DC supply of 400V and gives three phase output. Gate pulses to switches are given by space vector pulse width modulation technique.

The three-phase output of inverter is given to three-phase induction motor and operation of induction motor is seen without speed controller, with PI controller, ANN based speed control method and ANFIS controller based speed controller.

Inverter has three legs with three upper switches and three lower switches. Switching is done such that when upper switch is turned on, lower switches remains off and when lower switch is turned on, upper switch remains off.

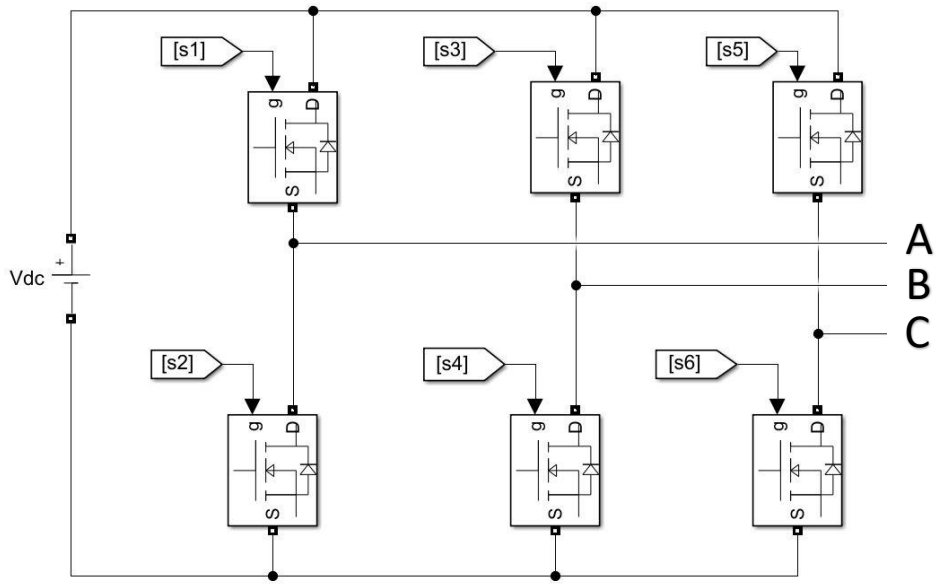

Fig.6.1 Three-Phase VSI Simulation

6.2 SVPWM

SVPWM generates pulses for three phase inverter switches. Simulation of SVPWM is divided into seven steps for the generation of gate pulse, these are

1. Three-phase reference sine generation
2. Low pass filter
3. α-β transformation
4. Sector selection
5. Ramp generation
6. Switching time calculation
7. Gate pulse logic

Each step is explained in this section. These switching pulses are given to the upper and lower switches of three-phase inverter.

6.2.1 Three-phase reference sine generation

The three-phase generator produces three sine waves with variable frequency and amplitude. The three signals are out of phase with each other by 120 degrees. The inverter-requested frequency and voltage are two of the block inputs.

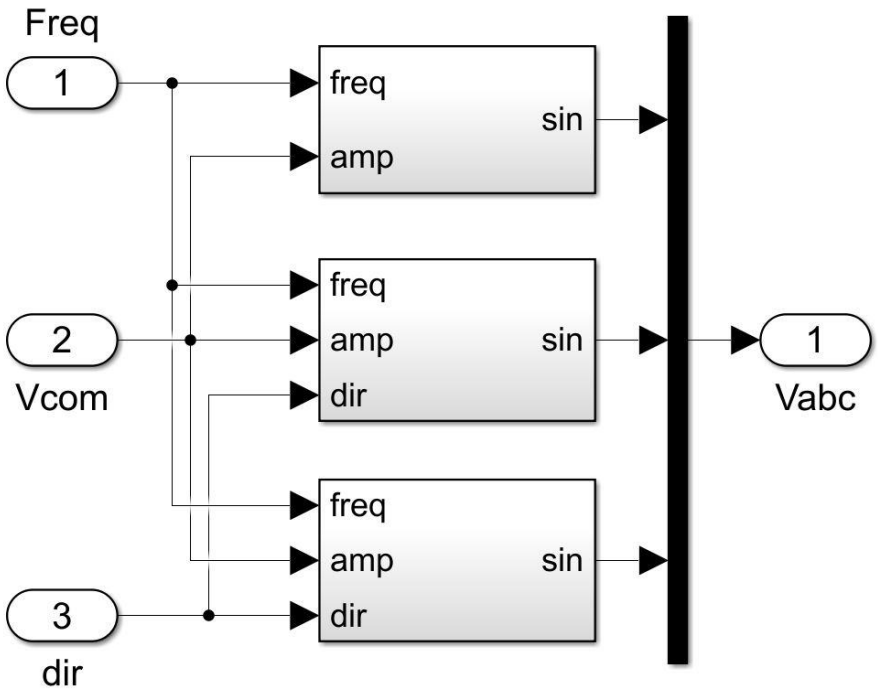

Fig.6.2 Three-phase reference sine generation

For the generation of three-phase sine wave magnitude is given in terms of volt and frequency of operation of induction motor, these three sine waves are made 120 apart.

6.2.2 Low Pass Filter

The low pass bus filter removes fast transients from the DC bus voltage measurement. This filtered voltage computes the voltage vector applied to the motor.

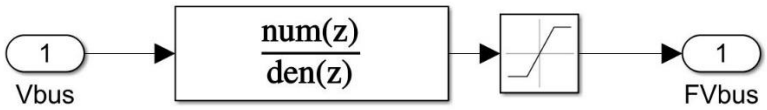

Fig.6.3 Low Pass Filter

6.2.3 α-β transformation

In alpha-beta transformation, variables are converted from the three-phase system to the two-phase αβ system. This three-phase input is given from three-phase reference sine generator and output is magnitude of V_α, V_β and angle between them. Angle is given to sector selector and magnitudes are given to switching time calculator.

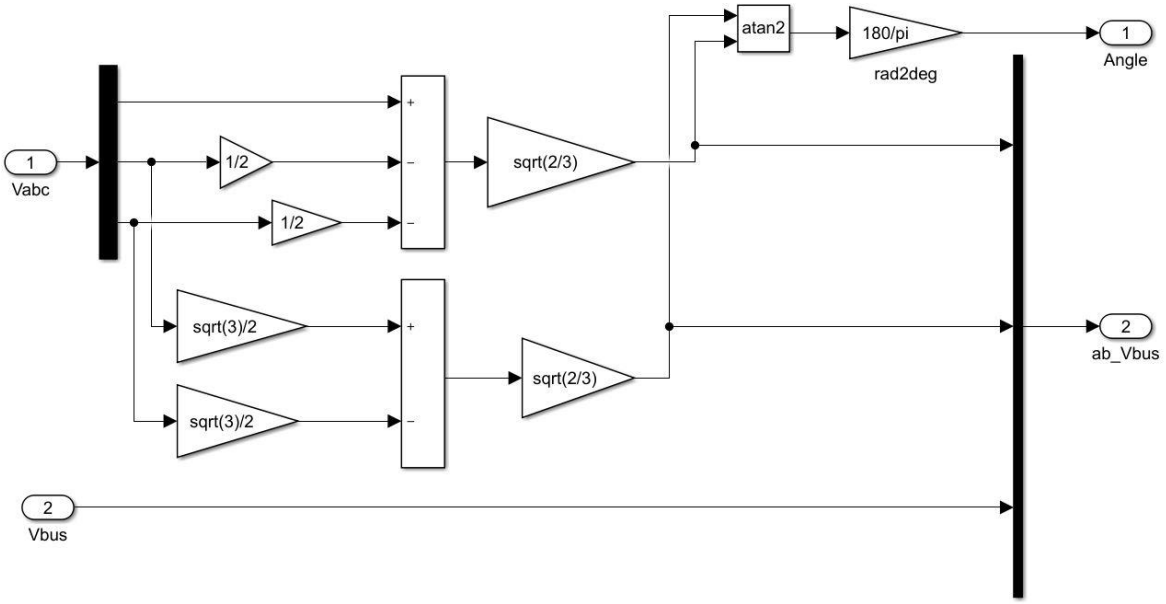

Fig.6.4 α-β transformation

6.2.4 Sector selection

The αβ vector sector finds the sector of the αβ plane in which the voltage vector lies. The αβ plane is divided into six different sectors spaced by 60º.

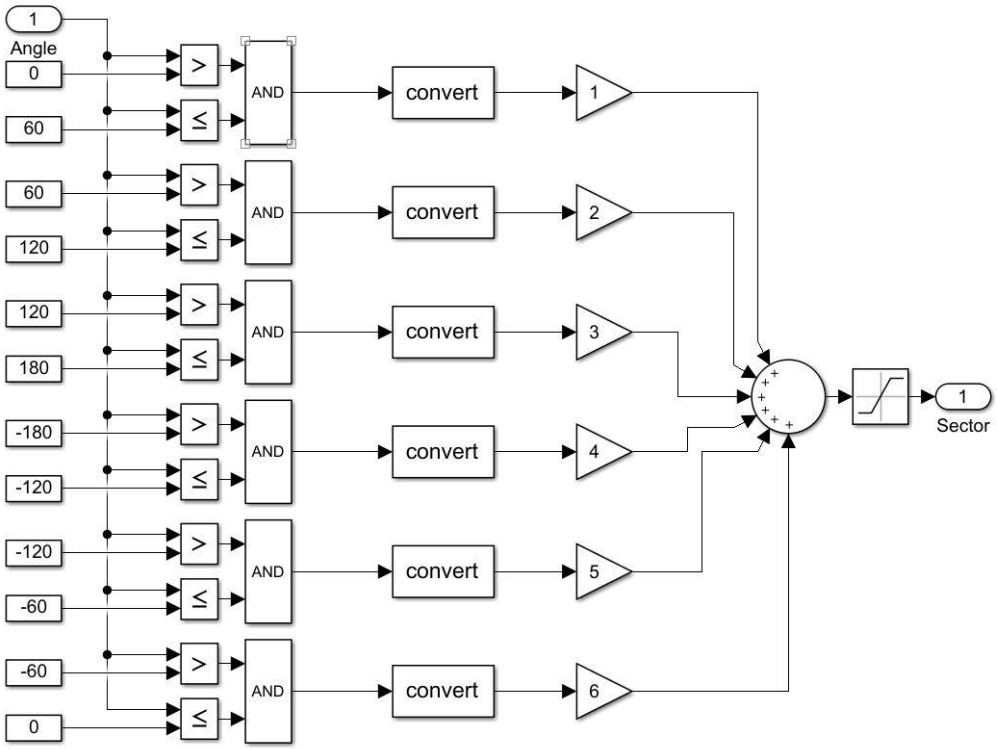

Fig.6.5 Sector Selection

Figure 6.5 is the Simulink diagram of sector selection and figure 6.6 shows the flow chart of sector determination. In flow chart it can see that first step is to read V_α and V_β. First, V_β is checked, whether it is positive or negative, in both case it is compare if $|V_\alpha| > \left|{V_\beta}/{\sqrt{3}}\right|$ and $V_\alpha \geq 0$.

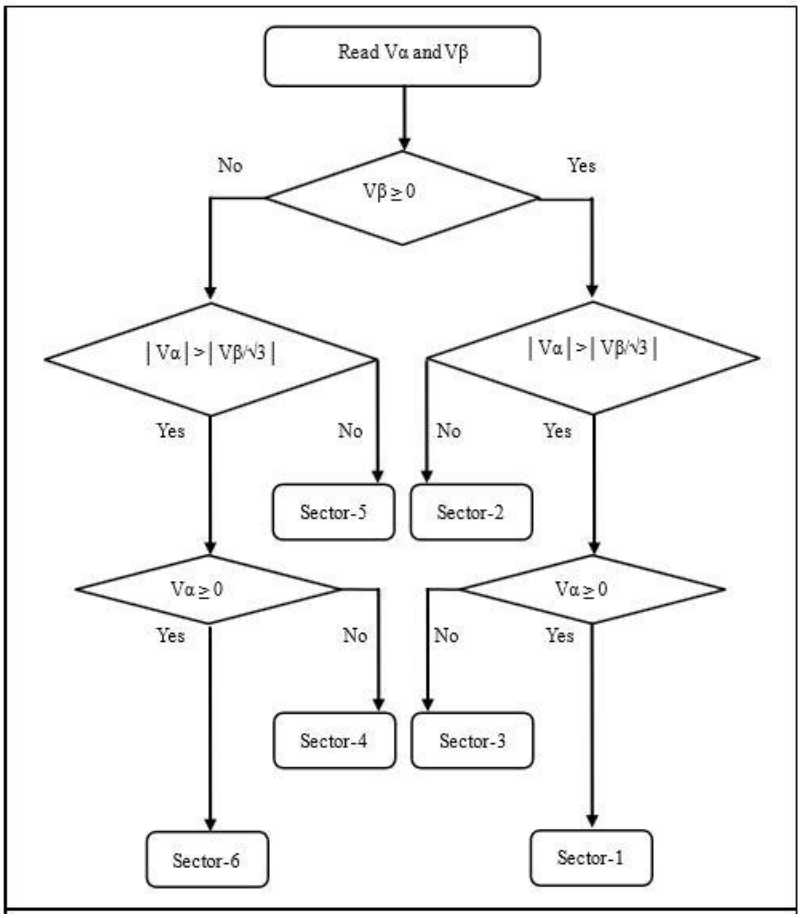

Fig.6.6 Flow Chart for Sector Determination

1. If V_β is positive and $|V_\alpha| > \left|{V_\beta}/{\sqrt{3}}\right|$ and also $V_\alpha \geq 0$, then sector-1 is selected.
2. If V_β is positive and $|V_\alpha| \leq \left|{V_\beta}/{\sqrt{3}}\right|$, then sector-2 is selected.
3. If V_β is positive and $|V_\alpha| > \left|{V_\beta}/{\sqrt{3}}\right|$ and $V_\alpha < 0$, then sector-3 is selected.
4. If V_β is negative and $|V_\alpha| > \left|{V_\beta}/{\sqrt{3}}\right|$ and $V_\alpha < 0$, then sector-4 is selected.
5. If V_β is negative and $|V_\alpha| \leq \left|{V_\beta}/{\sqrt{3}}\right|$, then sector-5 is selected.
6. If V_β is negative and $|V_\alpha| > \left|{V_\beta}/{\sqrt{3}}\right|$ and also $V_\alpha \geq 0$, then sector-6 is selected.

6.2.5 Ramp generation

The ramp generator produces a unitary ramp at the PWM switching frequency. This ramp is a time base for the switching sequence.

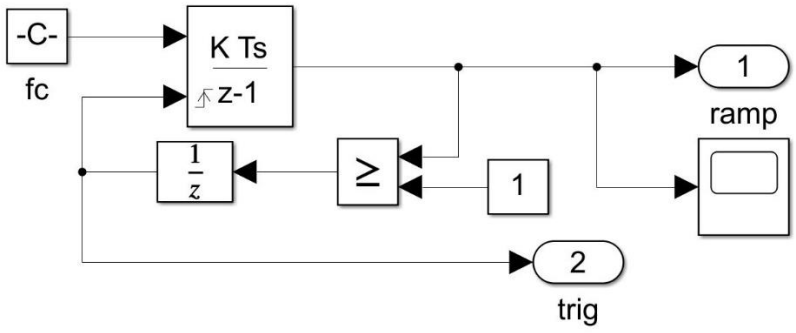

Fig.6.7 Ramp Generation

This ramp signal is given to gate pulse logic block for comparison with switching time calculated and then it gives gate pulses for switching the switches of inverter.

6.2.6 Switching time calculation

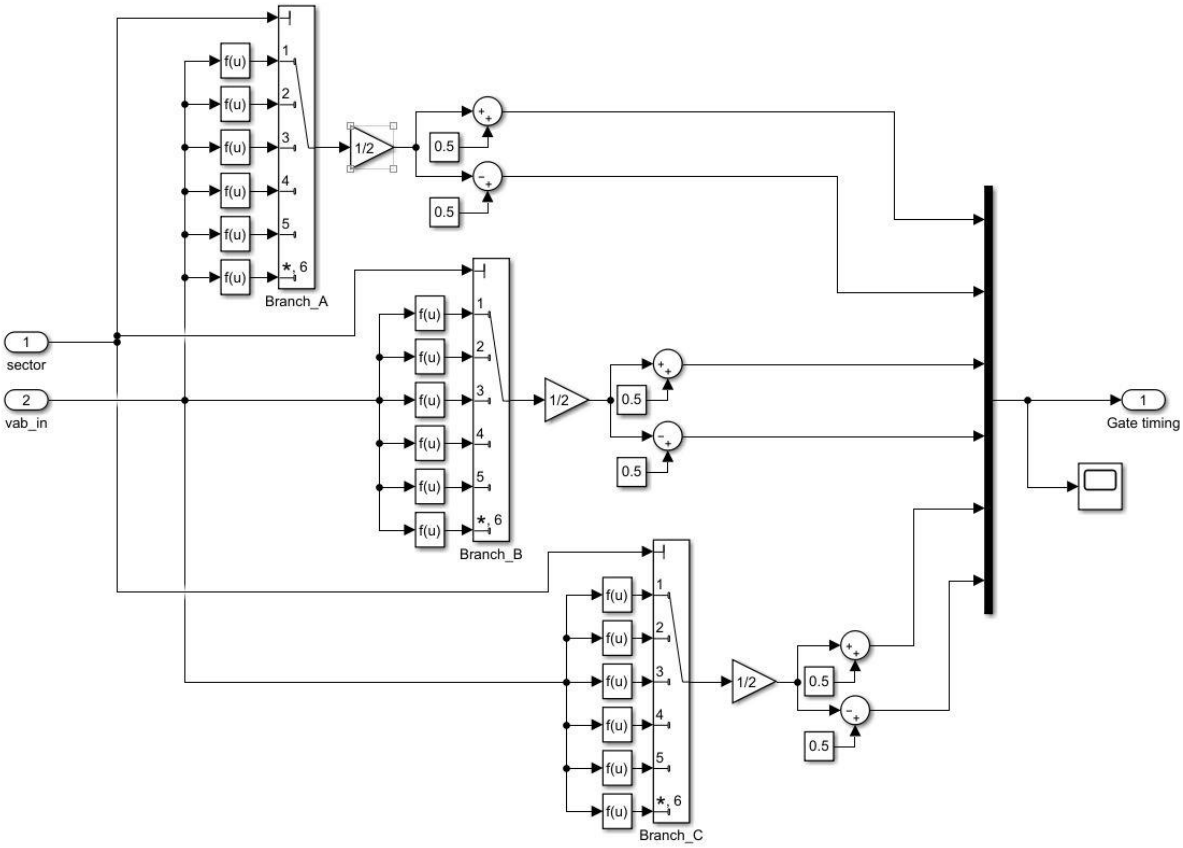

Fig.6.8 Switching time calculation

The switching time calculator calculates the timing of the voltage vector applied to the motor. The block input is the sector in which the voltage vector lies. This sector number decides the function which will be used for calculation of switching time by using multiport switch, there are three such multiport switches each for one leg and ensures that when upper switch is on lower switch remains off and when lower is on upper switch remains off.

6.2.7 Gate pulse logic

The gates logic receives the timing sequence from the switching time calculator and the ramp from the ramp generator. In this process ramp signal generated and switching sequence is compared. The first and second switching sequence is then multiplied using AND operator and output is given to upper switch. This output is inverted using NOT operator and sent to lower switch.

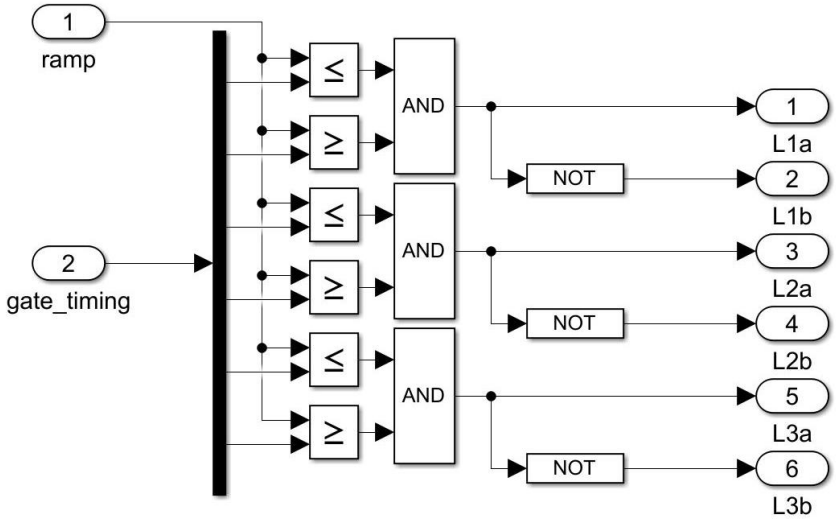

Fig.6.9 Gate pulse logic

6.3 INDUCTION MOTOR

6.3.1 Electrical system of the Double Squirrel-Cage Machine

A simple steady state equivalent circuit model of an induction motor is a very important tool for analysis and performance prediction under steady-state conditions. Figure 6.10 shows the steady-state equivalent circuit for the analysis and design of induction motor. In the equivalent circuit, all rotor parameters are referred to the stator.

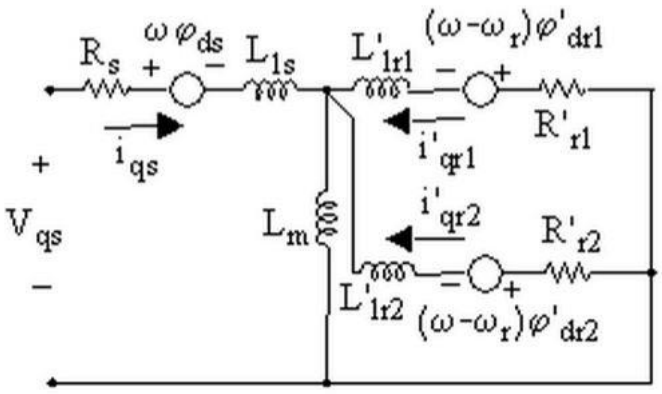

Fig.6.10 q-axis model

From KVL in fig.6.10 and fig.6.11, q-axis voltage and d-axis voltage are given by equation 6.1 and 6.2 respectively as,

$$V_{qs} = R_s i_{qs} + \frac{d\varphi_{qs}}{dt} + \omega\varphi_{ds} \qquad 6.1$$

$$V_{ds} = R_s i_{ds} + \frac{d\varphi_{ds}}{dt} - \omega\varphi_{qs} \qquad 6.2$$

Applying KVL in equivalent model of cage 1 in q-axis and d-axis model will give equations 6.3 and 6.4 respectively,

$$0 = R_{r1}{}' i'_{qr1} + \frac{d\varphi_{qr1}{}'}{dt} + (\omega - \omega_r)\varphi_{dr1}{}' \qquad 6.3$$

$$0 = R_{r1}{}' i'_{dr1} + \frac{d\varphi_{dr1}{}'}{dt} + (\omega - \omega_r)\varphi_{qr1}{}' \qquad 6.4$$

Applying KVL in equivalent model of cage 2 in q-axis and d-axis model will give equations 6.6 and 6.6 respectively,

$$0 = R_{r2}{}' i'_{qr2} + \frac{d\varphi_{qr2}{}'}{dt} + (\omega - \omega_r)\varphi_{dr2}{}' \qquad 6.5$$

$$0 = R_{r2}{}' i'_{dr2} + \frac{d\varphi_{dr2}{}'}{dt} - (\omega - \omega_r)\varphi_{qr2}{}' \qquad 6.6$$

Electromagnetic torque in double cage rotor is given by equation 6.7,

$$T_e = 1.5p(\varphi_{ds} i_{qs} - \varphi_{qs} i_{ds}) \qquad 6.7$$

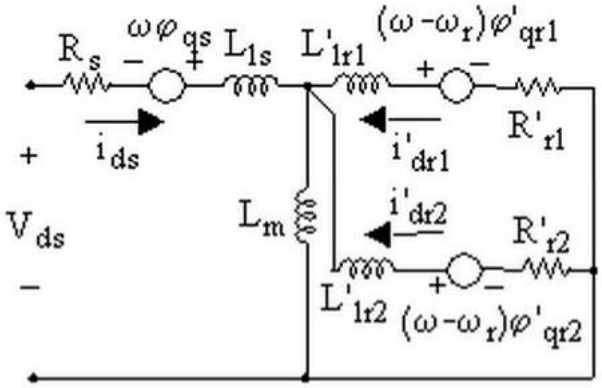

Fig.6.11 d-axis model

Stator q and d-axis fluxes are given by the equations 6.8 and 6.9 respectively,

$$\varphi_{qs} = L_s i_{qs} + L_m(i'_{qr1} + i'_{qr2}) \quad 6.8$$

$$\varphi_{ds} = L_s i_{ds} + L_m(i'_{dr1} + i'_{dr2}) \quad 6.9$$

Rotor q and d-axis fluxes of cage 1 are given by equations 6.10 and 6.11 respectively,

$$\varphi'_{qr1} = L'_{r1} i'_{qr1} + L_m i_{qs} \quad 6.10$$

$$\varphi'_{dr1} = L'_{r1} i'_{dr1} + L_m i_{ds} \quad 6.11$$

Rotor q and d-axis fluxes of cage 2 are given by equations 6.12 and 6.13 respectively,

$$\varphi'_{qr2} = L'_{r2} i'_{qr2} + L_m i_{qs} \quad 6.12$$

$$\varphi'_{dr2} = L'_{r2} i'_{qr2} + L_m i_{ds} \quad 6.13$$

Three additional quantities, stator and rotor inductances for cage 1 and cage 2, are now defined as:

$$L_s = L_{1s} + L_m \quad 6.14$$

$$L'_{r1} = L'_{1r1} + L_m \quad 6.15$$

$$L'_{r2} = L'_{1r2} + L_m \quad 6.16$$

6.3.2 Mechanical System

$$\frac{d\omega_m}{dt} = \frac{1}{2H}(T_e - F\omega_m - T_m) \quad 6.17$$

$$\frac{d\theta_m}{dt} = \omega_m \quad 6.18$$

6.4 PI CONTROLLER

The speed controller models a PI speed regulator for induction motor. The output of PI regulator is the machine slip, which is added to the machine speed to get the reference frequency of the inverter, the reference frequency also generates the reference voltage of the inverter by using a multiplying factor, this multiplying factor has been decided using trial and error method.

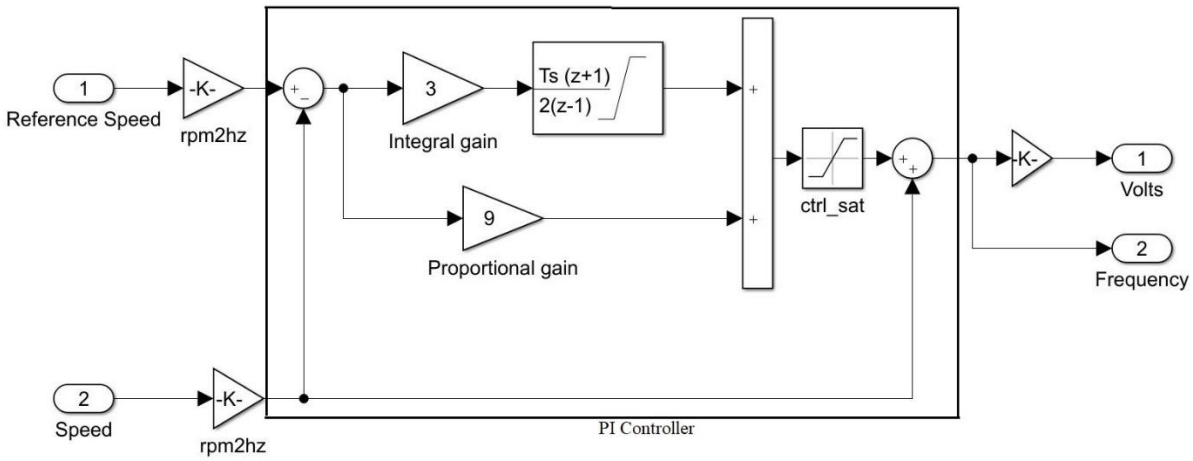

Fig.6.12 PI Controller

The input reference speed input given is a constant desired speed. This speed is converted to frequency and then this frequency is compared with the frequency of actual speed of the motor. Difference in frequency is given to PI controller and output of PI controller is then subtracted to the actual frequency to get new controlled operating frequency. This frequency is then multiplied to a constant to get new operating voltage and these voltage and frequency are given at the input of SVPWM.

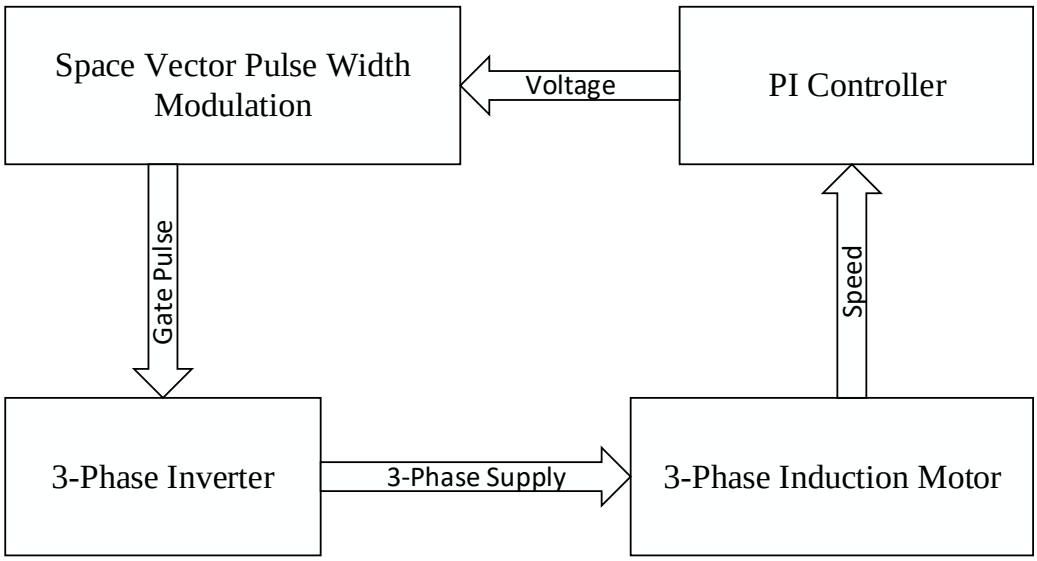

Fig.6.13 Block Diagram of simulation with PI controller

The block diagram of operation of induction motor is shown in figure 6.13. The simulation consists of four parts that is Inverter, SVPWM, Induction motor and controller. Three phase inverter gives three phase supply to induction motor. The speed of induction motor is given to PI controller which gives voltage as output. This voltage is given at the input of SVPWM, it generates gate pulses for the inverter according to reference speed.

6.5 ARTIFICIAL NEURAL NETWORK

ANN is used as speed controller in place of PI controller. ANN is trained for a speed of 1440 rpm and for mechanical torques 0 N-m to 3.7 N-m. Neural network can be started in MATLAB using command "nnstart". In this window 'fitting app' is started, here the inputs and target data defining desired network output from workspace is selected. Then network is trained and a Simulink block 'Function Fitting Neural Network' as shown in figure 6.15 is generated and deployed in simulation.

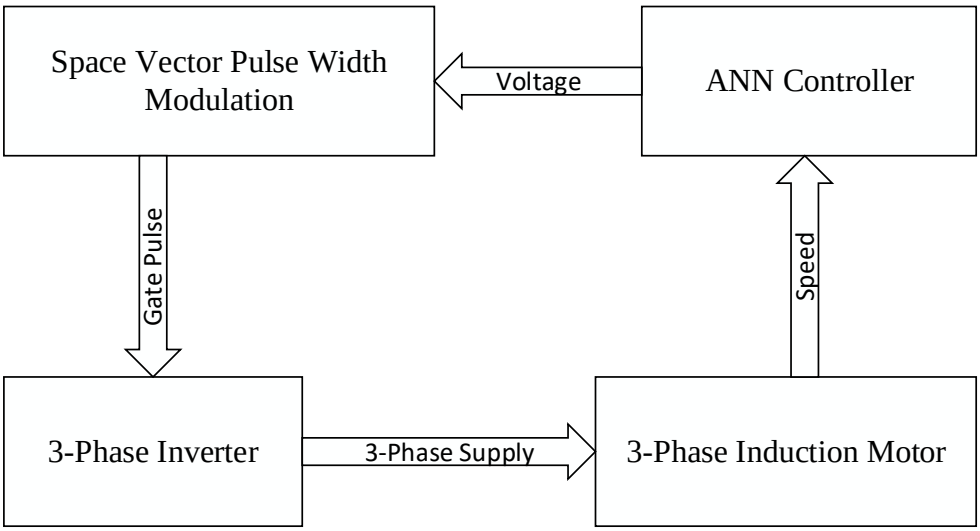

Fig.6.14 Block Diagram of Simulation with ANN Controller

6.5.1 Simulink Diagram of ANN

Neural network is deployed in Simulink and Simulink diagram is generated as shown in the figure 6.16.

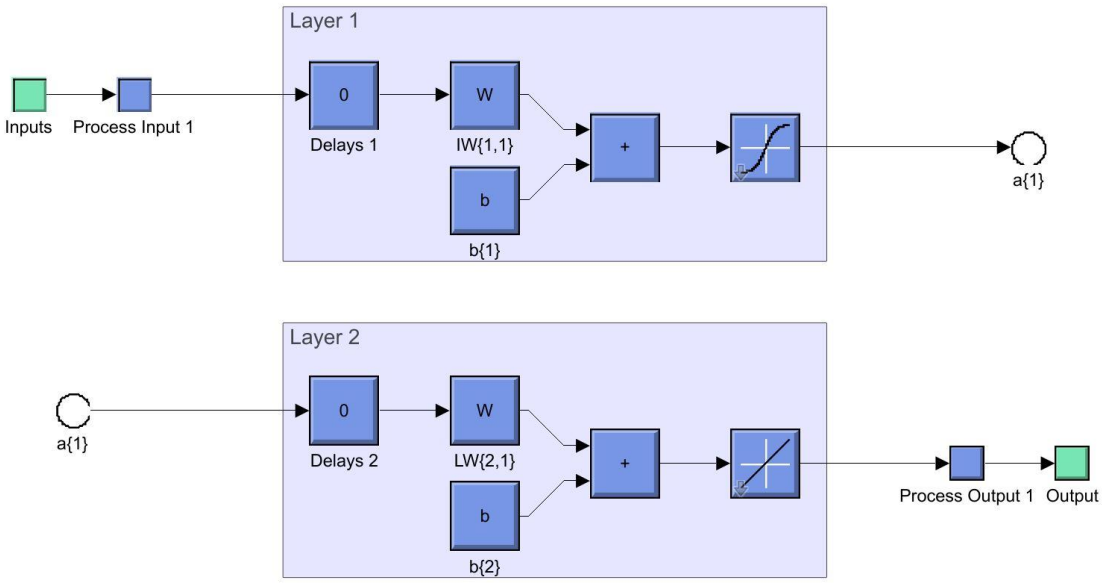

Fig.6.15 Simulink diagram of ANN

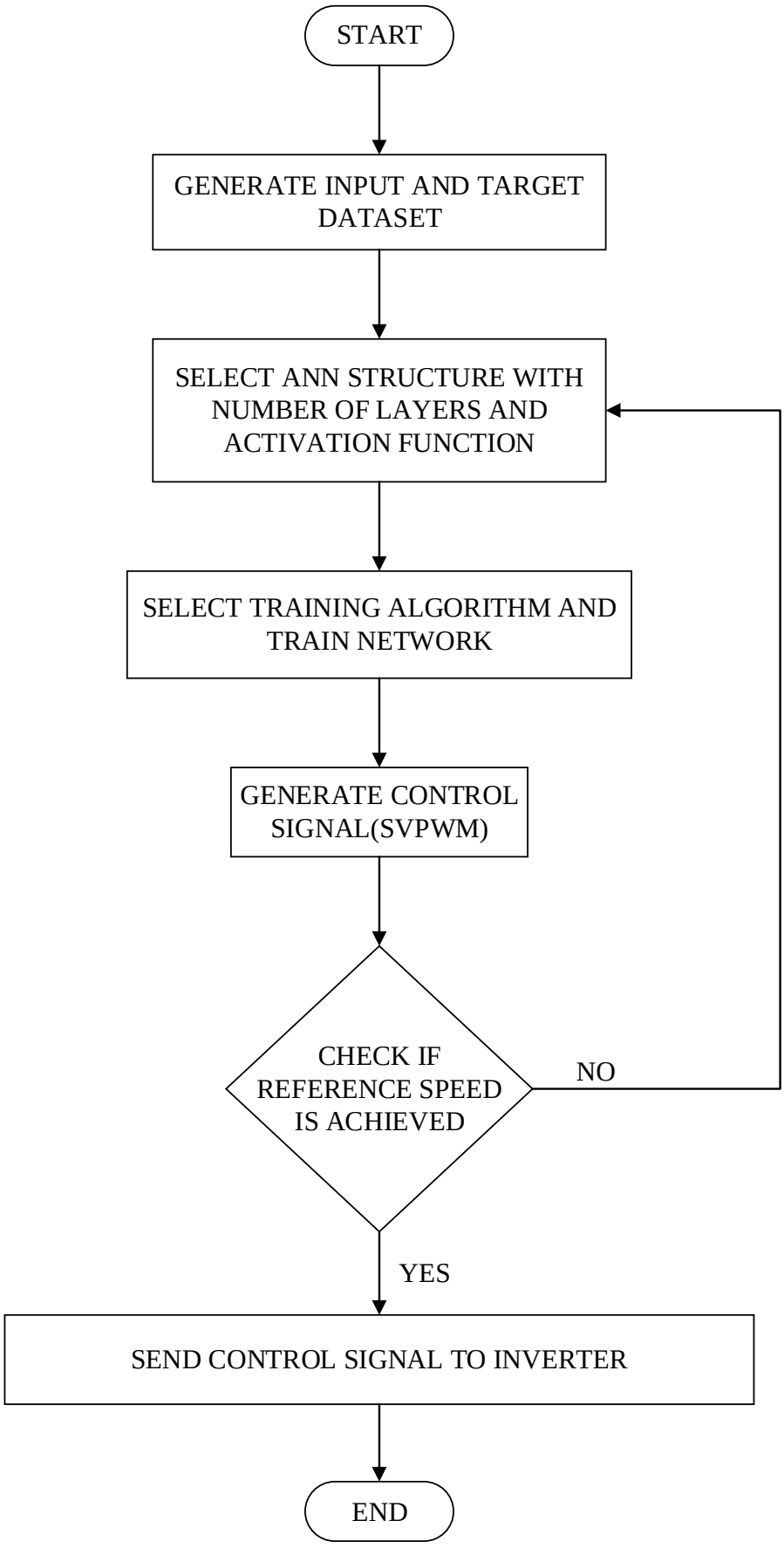

Fig.6.16 Flowchart of ANN Control Implementation

6.6 ANFIS CONTROLLER

ANFIS controller can be implemented using 'Fuzzy Logic Controller with Ruleviewer' block in simulation, for this .fis file is created and deployed in this block by training the ANFIS. To train ANFIS, Neuro-Fuzzy designer has been used which can be opened using command "anfisedit" in MATLAB. In Neuro-Fuzzy designer window, data is loaded from workspace, generate FIS and then FIS is trained. After training this trained data is tested. Then this FIS file is exported to workspace from where it is deployed in 'Fuzzy Logic Controller with Ruleviewer' block in simulation.

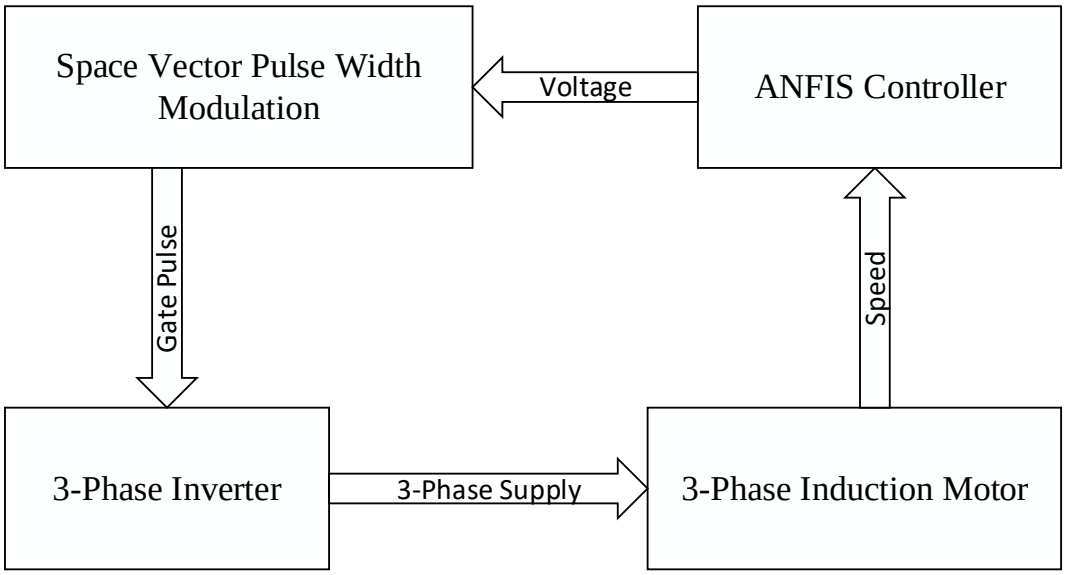

Fig.6.17 Block Diagram of Simulation with ANFIS Controller

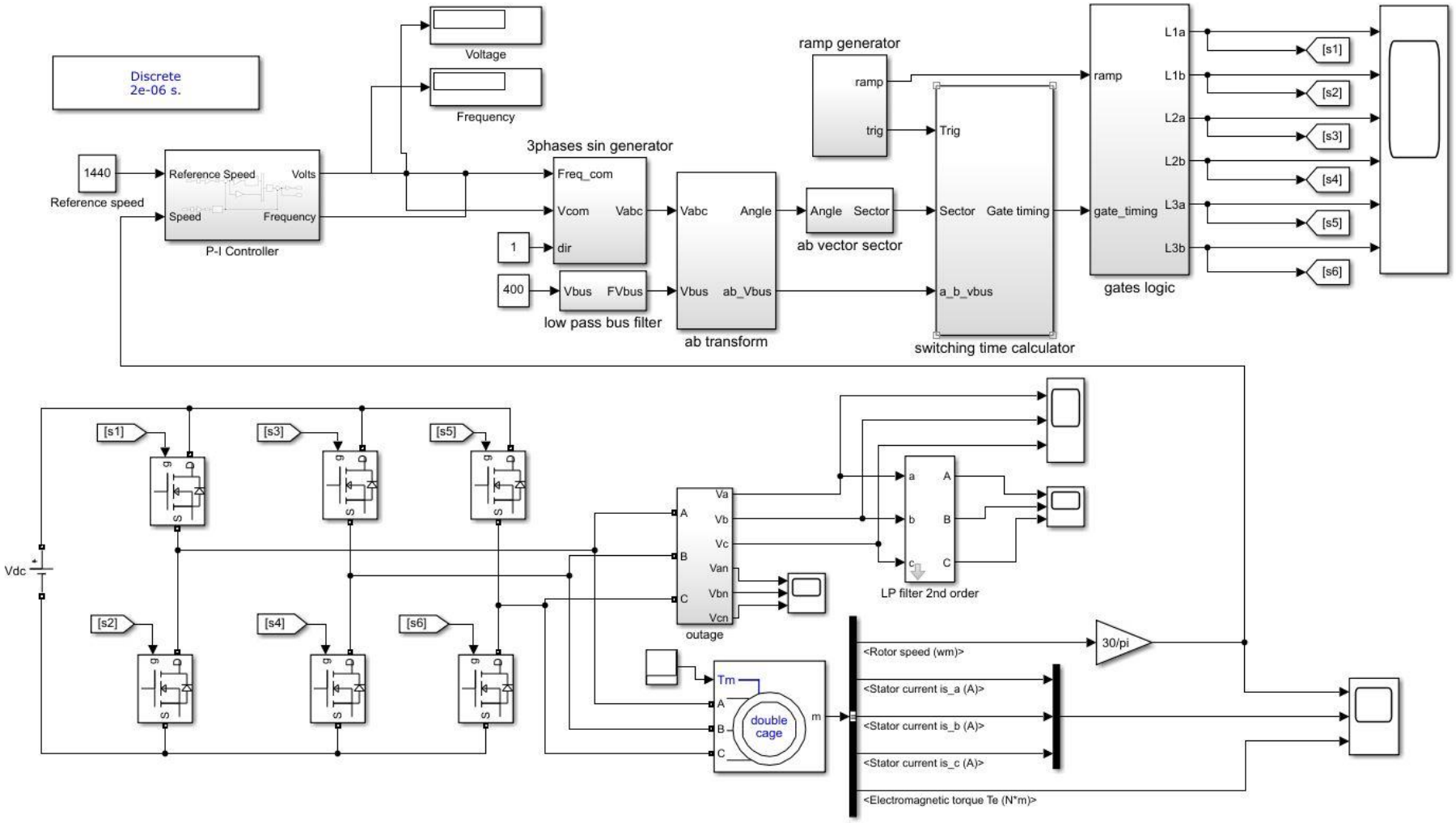

Fig.6.18 SimulinkidiagramiofimodeliwithiPIibasediV/fispeedicontroller

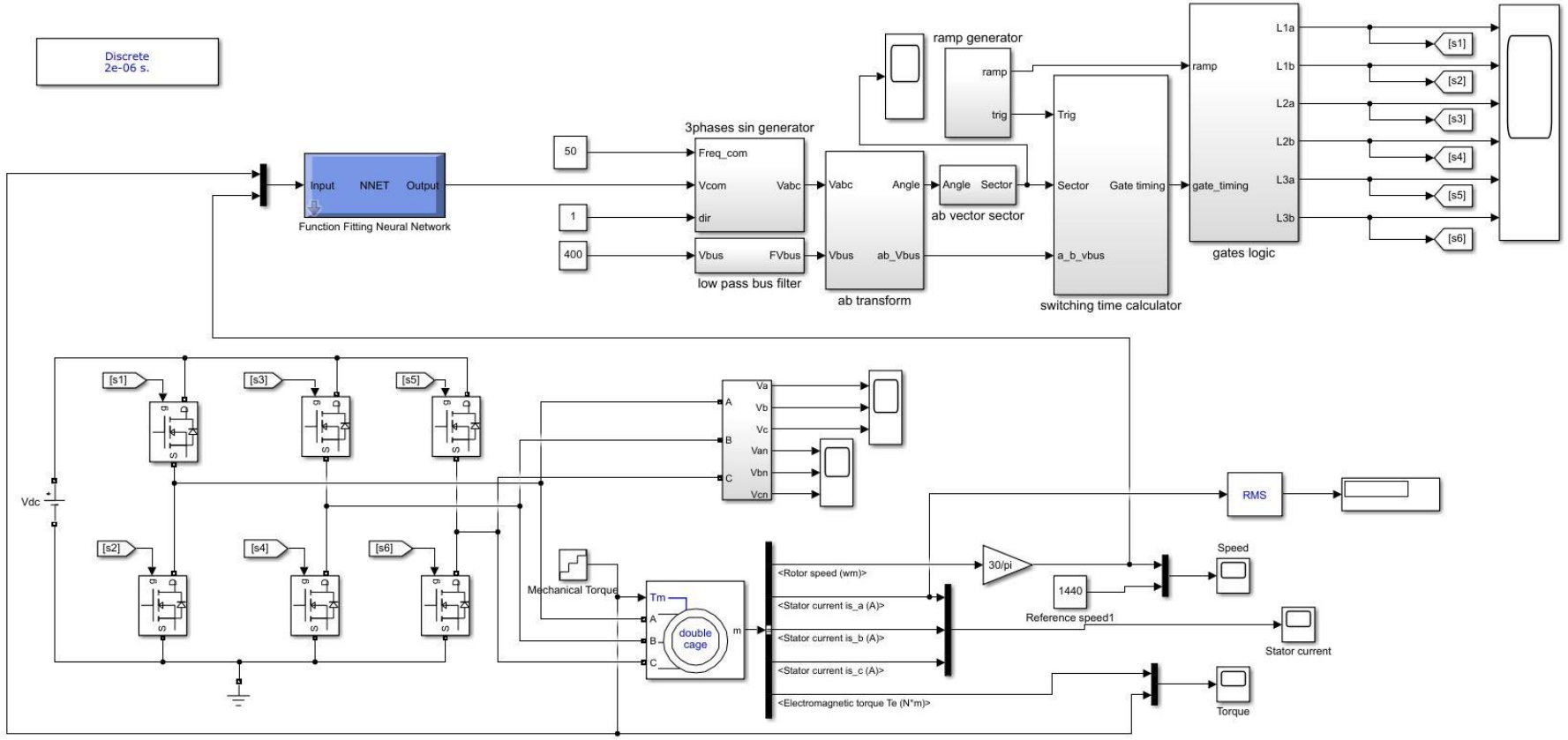

Fig.6.19 Simulink diagram of model with ANN based speed controller

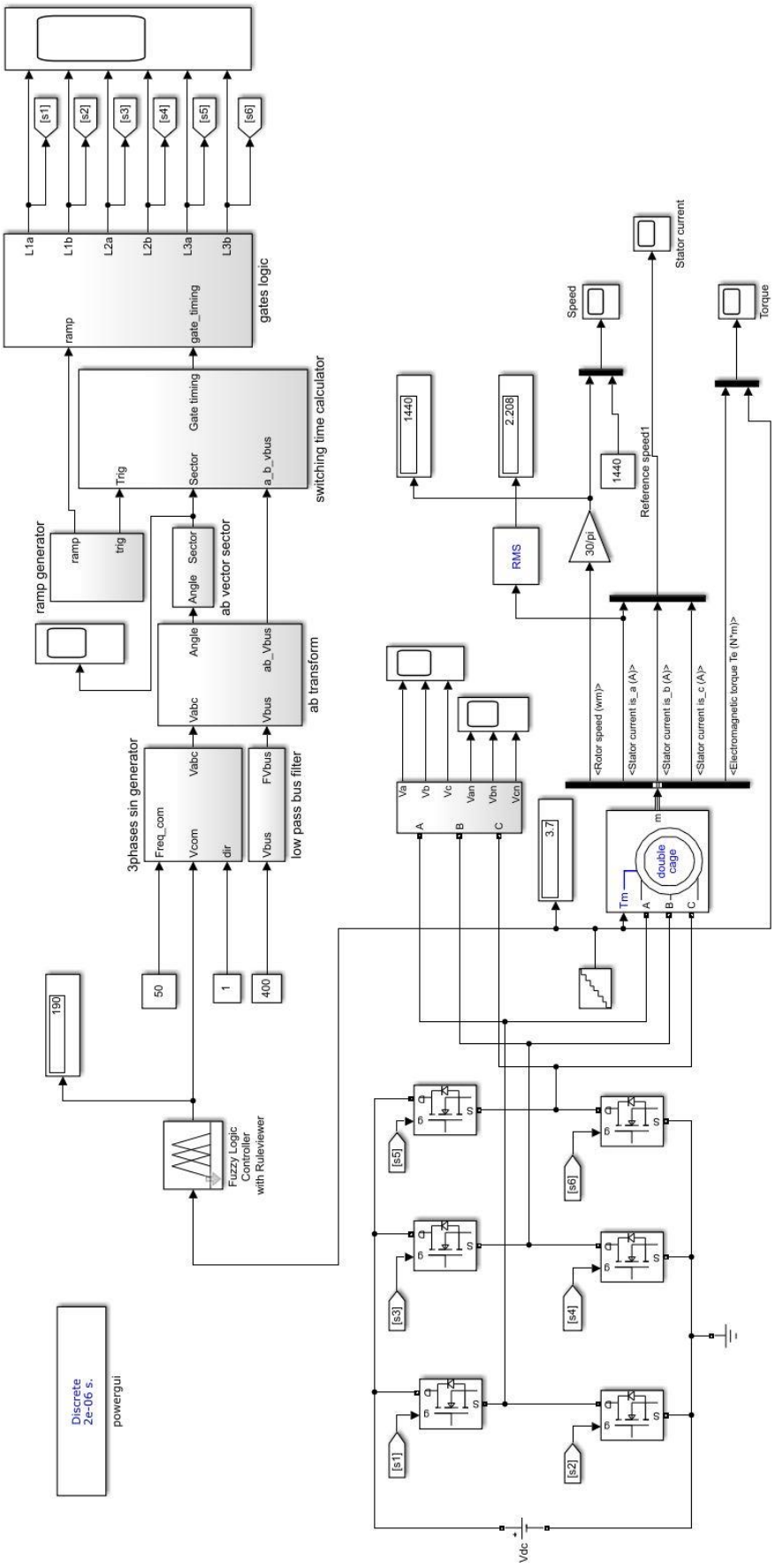

Fig.6.20 Simulink diagram of model with ANFIS based speed controller

CHAPTER 7

RESULTS AND DISCUSSION

In this chapter, results of simulation are presented. Initially the induction is run without any speed controller and its response with load change is observed and it is seen that there is drop in speed with increase in load, this observation is taken in table-1 and in simulink waveforms. Then same induction motor is run with speed controllers. First speed controller used is PI controller; this controller is tuned using hit and trial method and it is found that for K_p=9 and K_i=3, this controller is giving good results. Then response of induction motor with load change is observed and it is found that this controller is giving good speed control with vey less error in speed. The rise time and settling time using this controller can be seen in table-2.

Induction motor is also run with artificial neural network (ANN) based controller. In this controller neural network is trained with data for reference speed 1440 rpm and a simulink model of neural network is created and it is placed in place of PI controller and induction motor operation is observed with load changes and it is found that error in speed variation is even lesser using this controller as compared to PI controller. Rise time and settling time after every load change can be seen in table-3.

Then adaptive neural-fuzzy inference system (ANFIS) is used as speed controller and its response with induction motor is observed. ANFIS is also trained using dataset for same speed as ANN that is 1440 rpm. After training, a .fis file is created and is called in fuzzy logic controller block in simulink, this block is placed in place of PI controller. The error in speed, rise time and settling time are found to be even better with ANFIS controller. Error in speed is negligible, rise time and settling time can be seen in table-4 with respective change in load.

7.1 SVPWM OUTPUT

Parts of SVPWM are sector selection, gate switching time and gate pulses. There are six sectors with 60 degrees of interval each. The position of reference vector decides the sector number to be selected for switching as shown in figure 7.1 and switches to be turned on and accordingly gate switching time is obtained as shown in figure 7.2. Gate pulses decide which switch is to be turned on according to the gate switching time, these gate pulses are shown on in figure 7.3 for all the switches.

7.1.1 Sector selection:

The figure 7.1 shows the sector number in which the inverter is operating. The interval of each sector is 60 degrees. It can see that minimum value of waveform is 1 and maximum value is 6, it gives the complete control on all the six sectors.

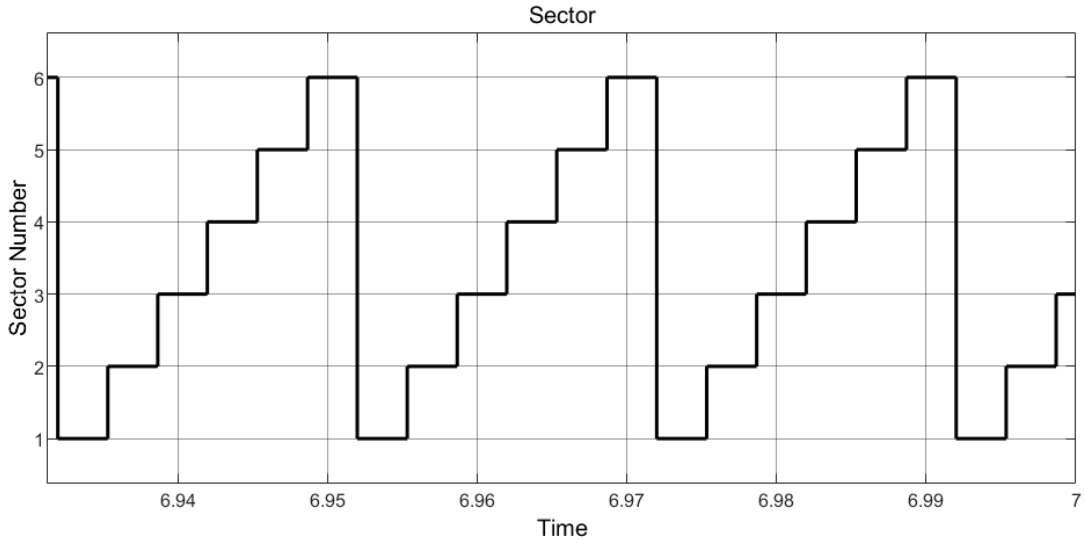

Fig.7.1 Sector Selection

In this waveform 1 represents sector 1, 2 represents sector 2 and so on. The time period is 20 m-sec therefore frequency 50 Hz, from this It can be veried that each sector is of 60 degrees.

7.1.2 Gate Switching Time

The figure 7.2 shows the M-W type of gate pulse switching time as required for switching of inverter switches in space vector pulse width modulation technique. The upper waveform is for upper switches and lower waveform is for lower switches. According to these switching time, gate pulses are obtained.

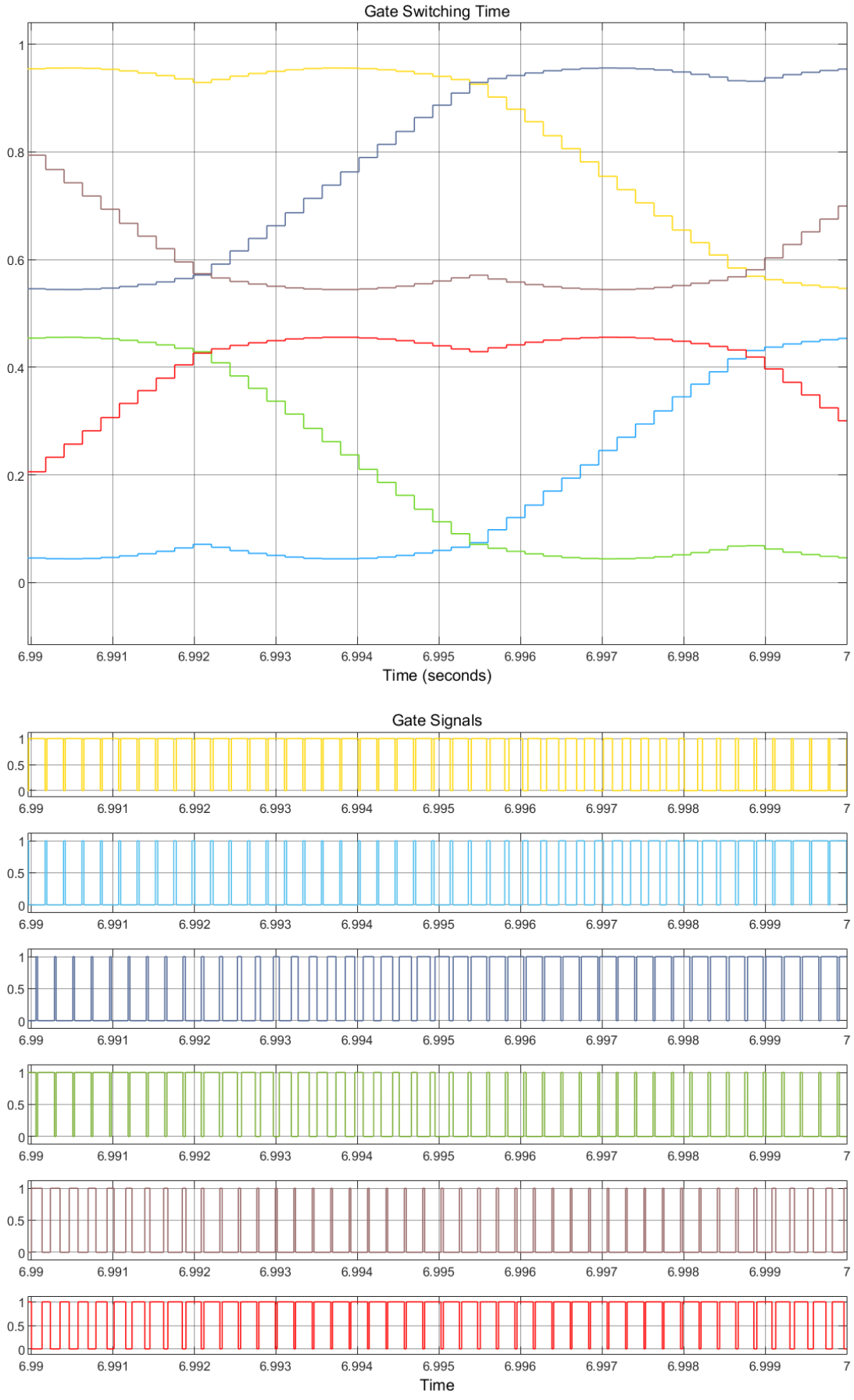

Fig.7.2 Gate Switching Time and Gate Waveforms

7.1.3 Gate Pulse

Figure 7.3 shows the gate pulses of all the switches. The switches are switched according to the switching time provided by M-W type of waveform shown in fig.7.2. First, third and fifth waveforms are of upper switches and second, fourth and sixth waveforms are for lower switches. The width of gate pulses changes according to the changes in load, because of change in speed.

7.1.4 Inverter Output Line and Phase Voltages

The developed gate pulses are extended for vector controlled drive and given to inverter switches and corresponding line and phase voltages waveforms are shown in figure 7.3 and figure 7.4 respectively. These waveforms are same throughout the time for operation of induction motor without speed controller because frequency is constant, but for the operation of induction motor with speed controllers the waveforms change its frequency according to the changes in load to maintain the speed of induction motor constant at the reference speed.

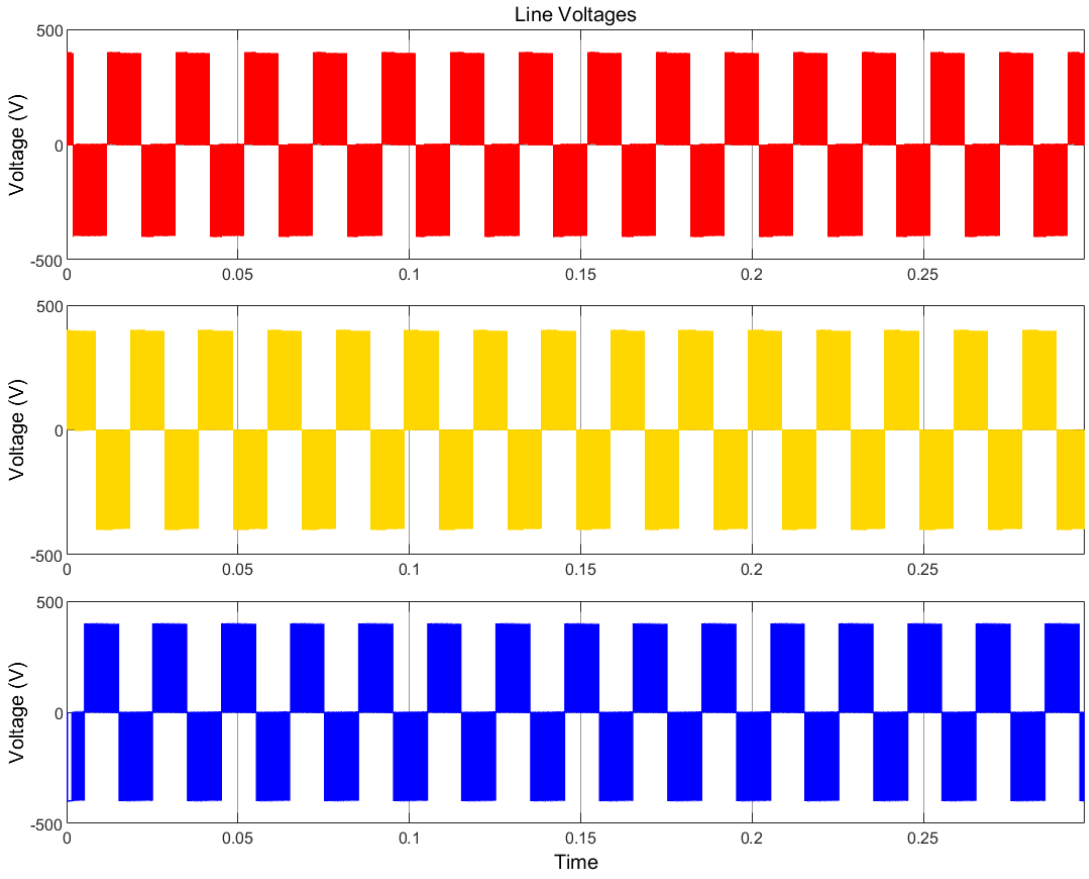

Fig.7.3 Line Voltages

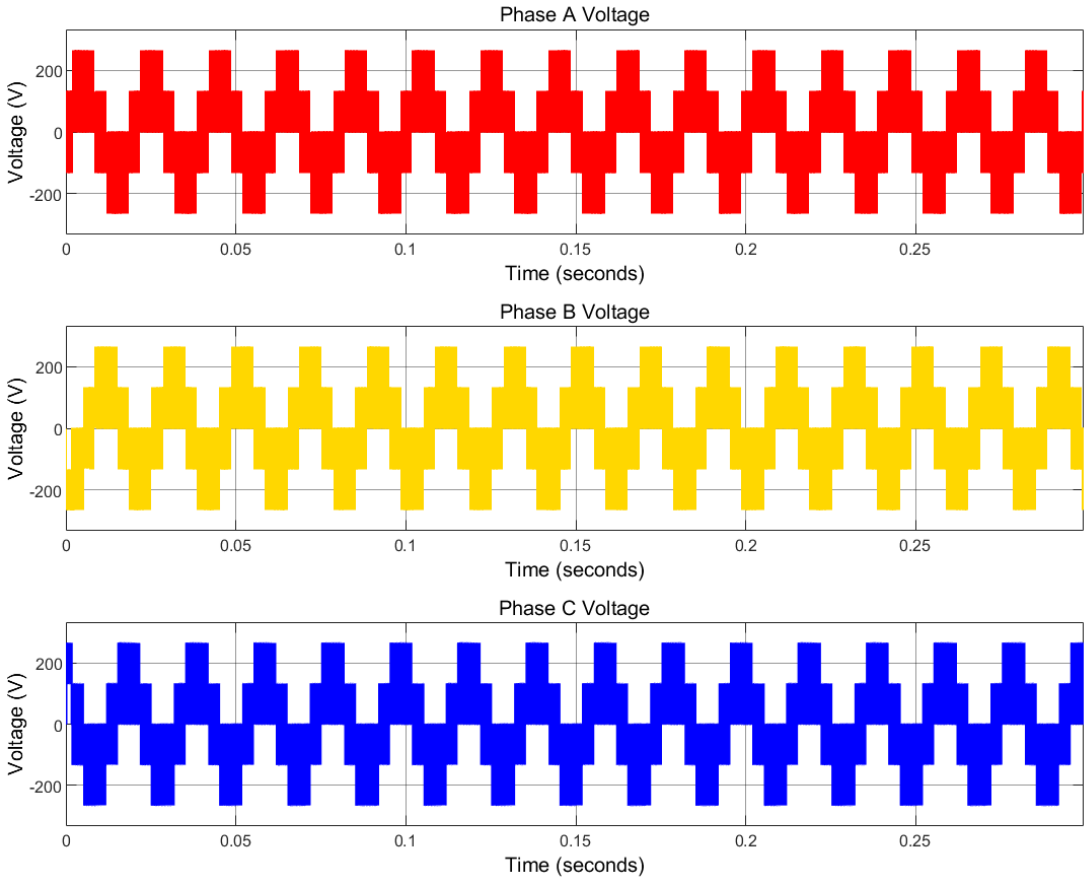

Fig.7.4 Phase Voltages

7.2 INDUCTION MOTOR OPERATION WITHOUT SPEED CONTROLLER

The induction motor is operated without any speed controller, switching to the inverter is given by SVPWM. Here the response of induction motor with changes in load has been observed. The table below shows the variation in stator current (i_a), speed with respect to change in mechanical torque. This stator current is rms value of phase a, therefore phase current. The rise time and settling time are noted by starting induction motor on the respective mechanical torque.

When high load is applied to induction motor, it ran in opposite direction gradually increasing in simulation indicating the pull-out of rotor and therefore no observation could be taken.

Table-7.1 Induction Motor Operation without Speed Controller

S. No.	Mechanical Torque (N-m)	Stator Current (A)	Speed (rpm)	Rise Time (sec)	Settling Time (sec)
1.	0	0.77	1476	0.35	0.95
2.	0.5	1	1451	0.43	1.1
3.	1	1.39	1423	0.48	1.2
4.	1.5	1.81	1392	0.6	1.45
5.	2	2.27	1354	0.835	1.9
6.	2.5	2.82	1308	1.13	2.5
7.	3	3.44	1251	1.963	4.1
8.	3.5	4.27	1163	-	-
9.	3.7	4.71	1106	-	-

Figure 7.5 is the waveform of mechanical and electromagnetic torque; here the load change done in a particular time can be seen. For this load is 0 N-m till 2 second and then load is changed to 1.5 N-m for 1.5 second, after that load is again changed at 3.5 second to 2.5 N-m and in the end ran the motor at full load of 3.7 N-m at 5 second. It has been made sure that motor reaches steady state before applying any load change. This simulation has been done for 7 seconds.

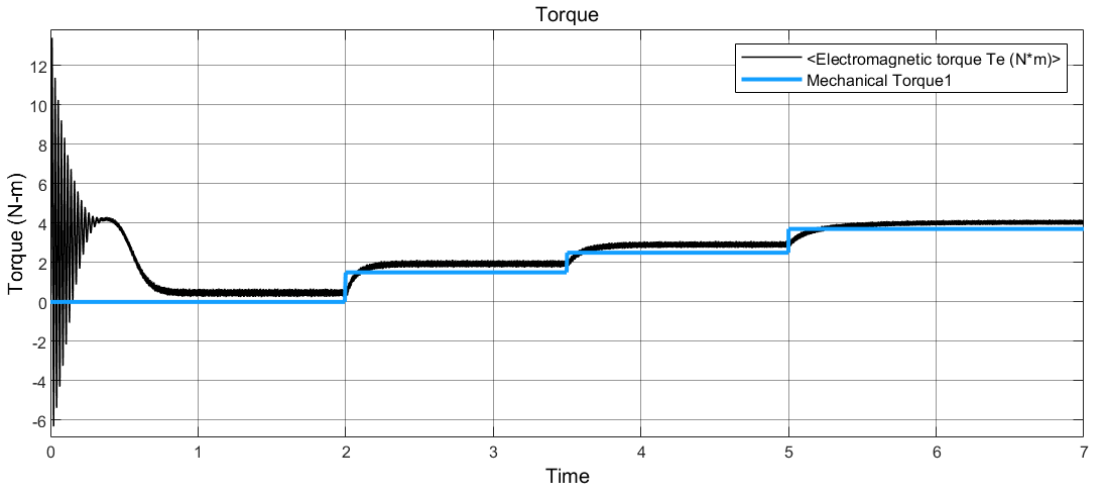

Fig.7.5 Mechanical and Electromagnetic Torque

Figures 7.6 and 7.7 shows the stator current and speed of induction motor respectively. The variation in stator current is according to mechanical torque variations shown in

figure 7.5. It can be seen that as the mechanical torque is increasing, there is an increase in stator currents and there is drop in speed.

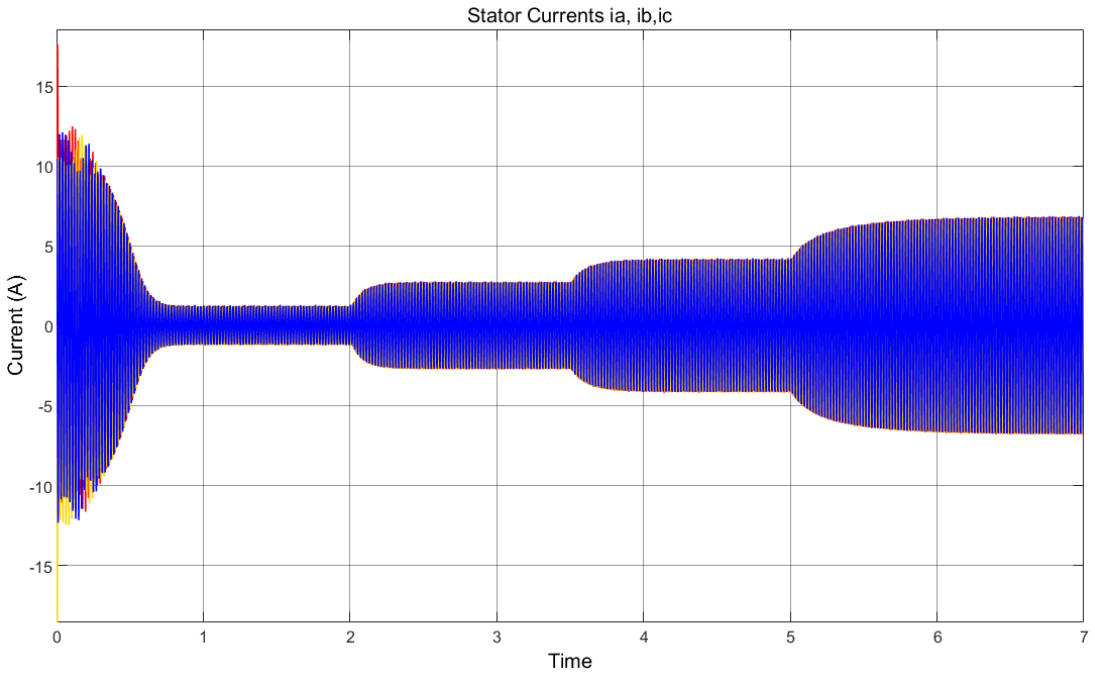

Fig.7.6 Stator Current

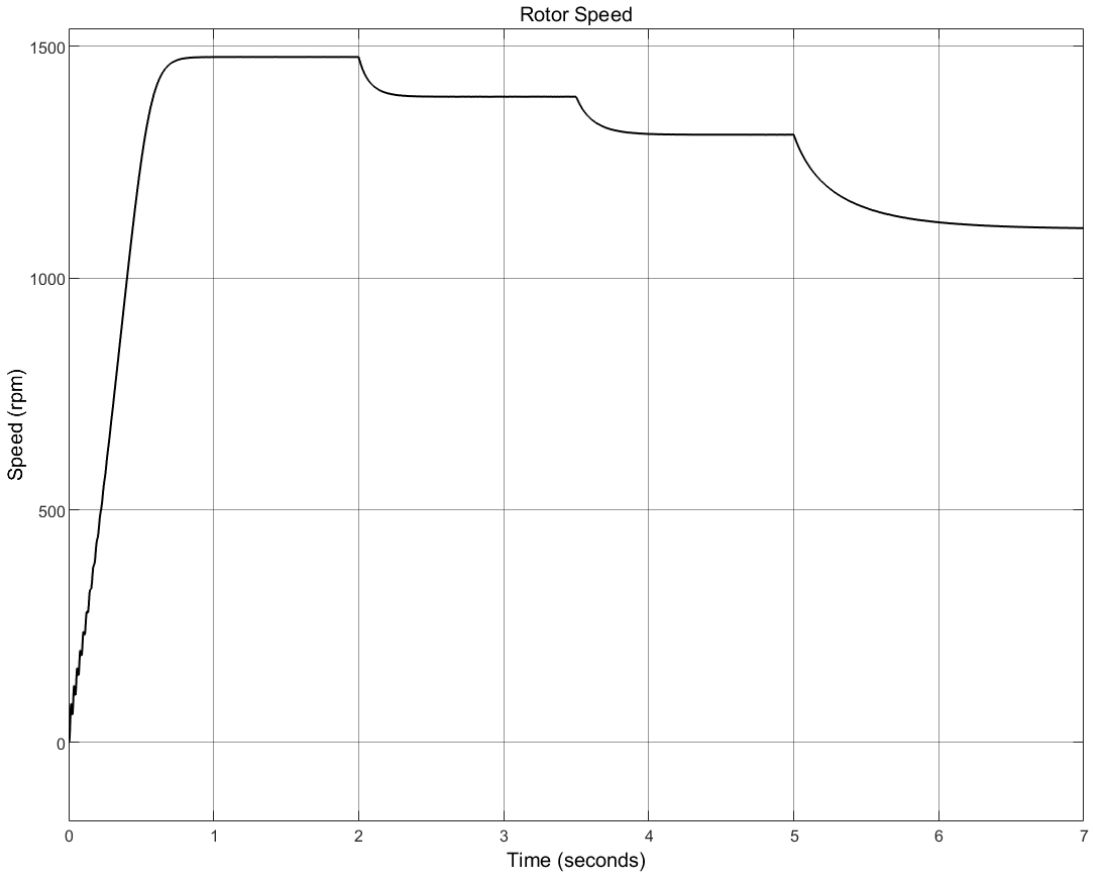

Fig.7.7 Speed

The change in speed can clearly be seen in the waveform. As the load torque is increased, it causes the motor to slow down and increases the slip and this increased slip causes rotor current to increase. To keep the speed of induction motor constant even with load changes, speed controllers have been used. In an AC machine speed is governed by the equation $N = \frac{120f}{P}$. Thus, it is evident that to change the speed it is needed to change the frequency of system because number of poles are fixed during the design of machine and hence cannot be changed.

The induction motor's torque depends on the air gap flux; therefore, it needs to be kept constant in order to achieve good torque performance. This air gap flux depends on V/f ratio hence to have good torque at all speeds it is important to vary voltage in accordance with frequency.

7.3 INDUCTION MOTOR OPERATION WITH PI CONTROLLER

The table 7.2 shows the variation in stator current (i_a) and speed with respect to change in mechanical torque. This stator current is rms value of phase current of phase a. Settling time is the time required by the motor to settle to a reference speed and it is noted for different loads in induction motor, rise time is also observed similarly.

Table-7.2 Induction Motor Operation without Speed Controller

S. No.	Mechanical Torque (N-m)	Stator Current (A)	Speed (rpm)	Rise Time (sec)	Settling Time (sec)
1.	0	1.1	1441	0.761	1.2
2.	0.5	1.18	1442	0.762	1.1
3.	1	1.29	1439	0.766	1.3
4.	1.5	1.45	1443	0.768	1.18
5.	2	1.6	1438	0.736	1.15
6.	2.5	1.87	1442	0.476	10
7.	3	2.1	1437	0.606	3
8.	3.5	2.3	1441	0.498	8
9.	3.7	2.4	1442	0.515	9

Figure 7.8 is waveform of torque with respect to time, in this waveform load changes of induction motor in the form of mechanical torque is shown. From this figure it can be observed that first induction motor is run at no load till 3 seconds and then load of 1.5 N-m is applied to induction motor for another 1.5 seconds and then load is increased to 2.5 N-m for another 1.5 seconds and then induction motor is run at full load of 3.7 N-m.

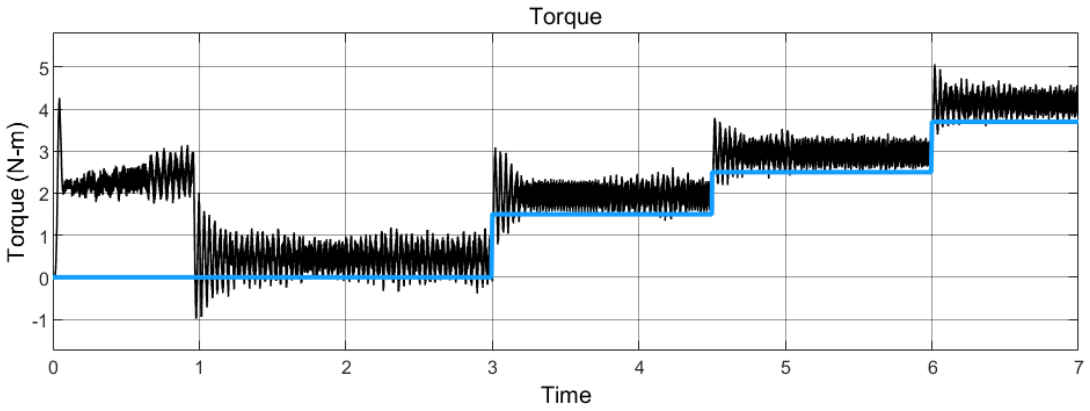

Fig.7.8 Mechanical and Electromagnetic Torque

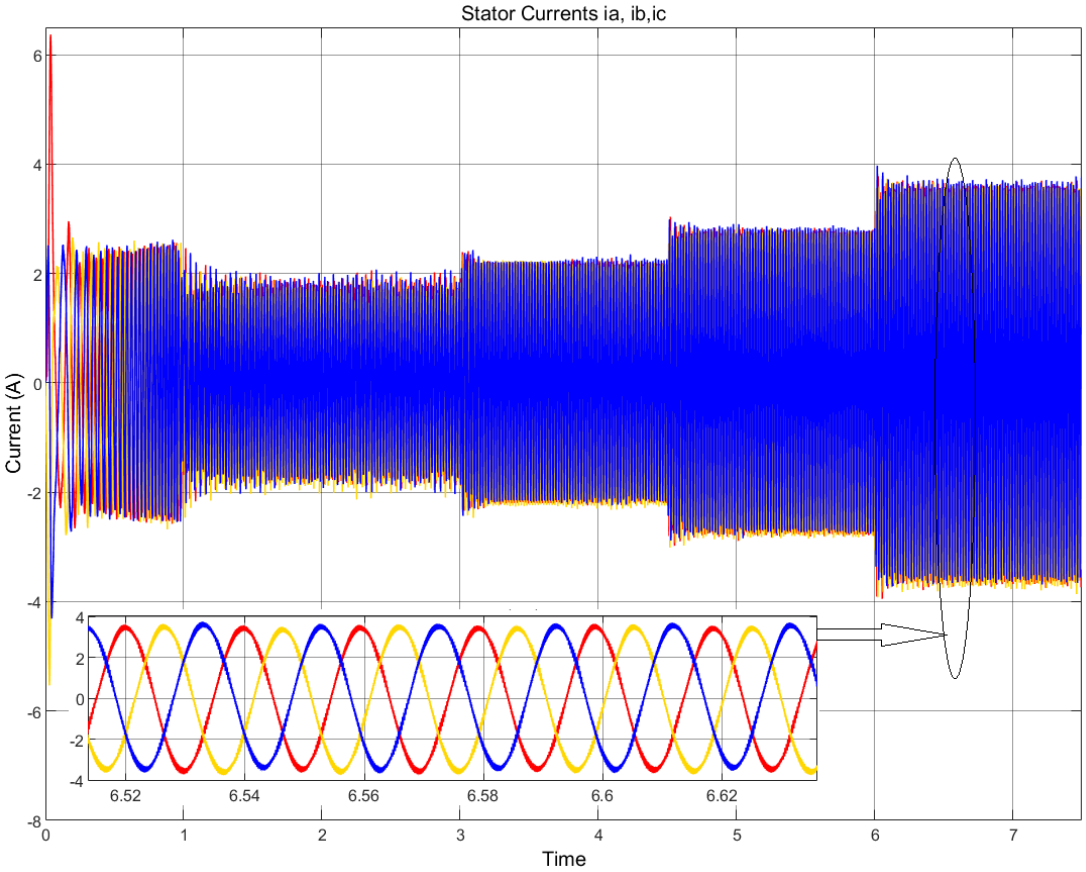

Fig.7.9 Stator current

Figure 7.9 is stator current waveform of induction motor. In this waveform change in current corresponding to change in mechanical torque shown in figure 7.8 can be observed. From table 7.1 and table 7.2, it can be observed that operating current is less when speed control is used as compared to induction motor operation without speed controller.

It can also be concluded that stator current required is less when control is applied as compared to without controller. The reason is that slip is not increasing when the mechanical torque load is increased and because there is very less change in slip, there is less increase in stator current.

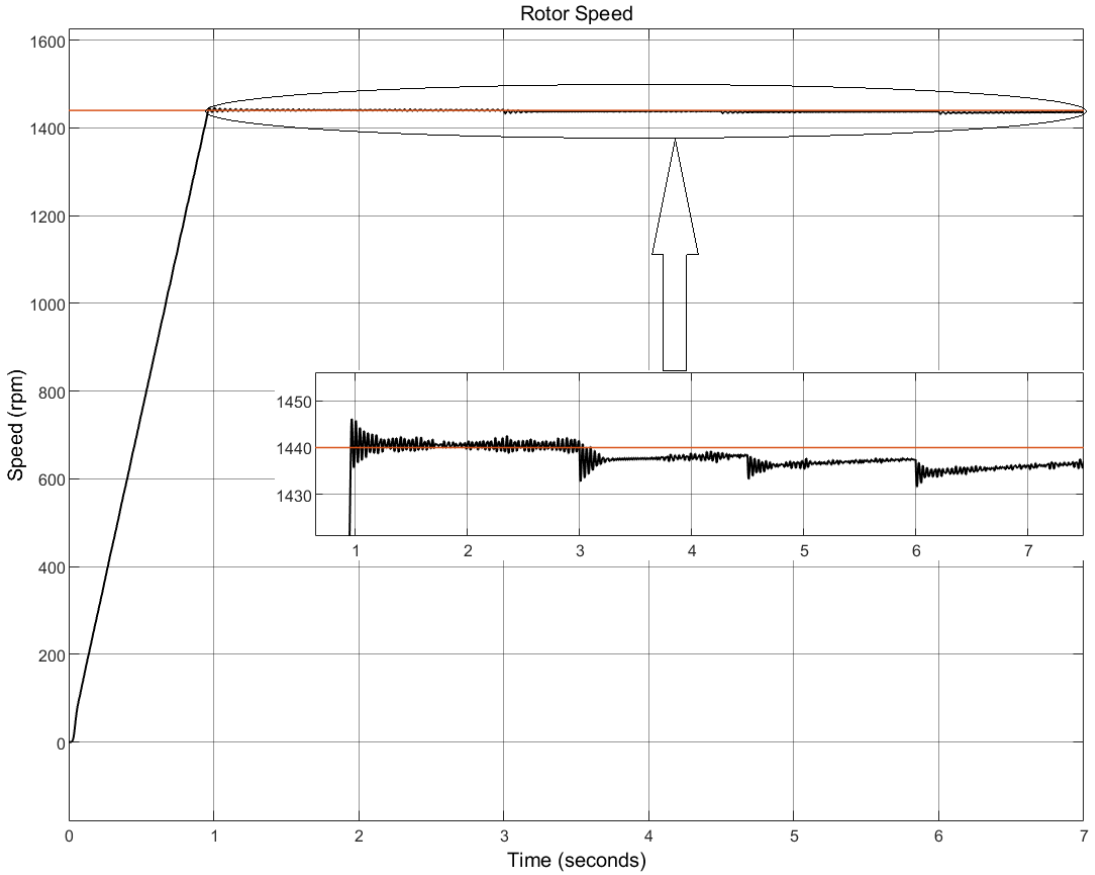

Fig.7.10 Speed

Figure 7.10 represents the speed of induction motor. In figure 7.10 shows that even with change in mechanical torque, there is almost no to very slight change in speed which even cannot be seen in speed waveform in fig.7.11, therefore to see the change in speed, an enlarged waveform is also shown in figure 7.10, in this figure it can be seen that there is variation of 1 to 4 rpm.

7.4 INDUCTION MOTOR OPERATION WITH ANN

The table 7.3 shows the variation in stator current (i_a) and speed with respect to change in mechanical torque. In this table also stator current is rms value of phase a. Rise time and settling time are obtained for different loads

Table-7.3 Induction Motor Operation with ANN

S. No.	Mechanical Torque (N-m)	Stator Current (A)	Speed (rpm)	Rise Time (sec)	Settling Time (sec)
1.	0	0.76	1431	1.376	3.4
2.	0.5	1	1440	0.55	1.4
3.	1	1.3	1440	0.374	0.9
4.	1.5	1.5	1440	0.252	0.8
5.	2	1.7	1440	0.2	0.7
6.	2.5	1.86	1440	0.16	0.55
7.	3	2	1440	0.142	0.45
8.	3.5	2.15	1440	0.135	0.37
9.	3.7	2.2	1440	0.124	0.32

Figure 7.11 shows the torque variation; the mechanical torque is changed three times at 3 sec, 4.5 sec and 6 sec from 0 N-m to 1.5 N-m, 2.5 N-m and 3.7 N-m respectively.

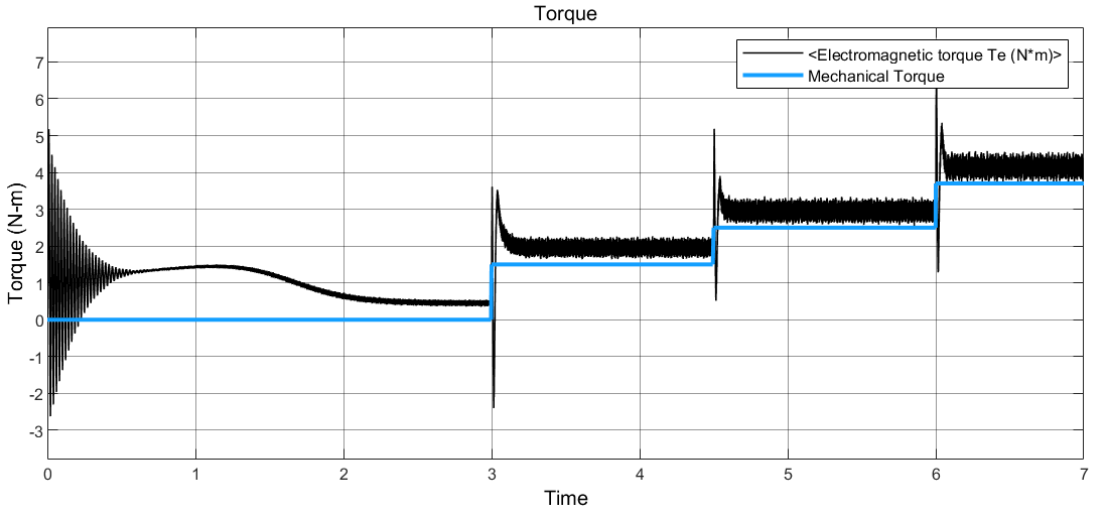

Fig.7.11 Mechanical and Electromagnetic Torque

Figure 7.12 shows the waveform of stator current with changes in mechanical torque. From table 7.3, the variation in current can be seen with respect to change in mechanical torque. Here it can also be seen that there is no variation in speed with load changes except in one case, the no load speed is not as expected. Induction motor is running at 1430 rpm in no load but for other loads, speed is as desired and there is almost no change in speed.

It can also be seen from figure 7.12 that stator currents are more balanced than PI controller used for speed control. These balanced currents can be seen more clearly in same figure with enlarged image.

Tables 7.1, 7.2 and 7.3, also shows that there is very slight difference in stator currents of ANN controlled induction motor and PI controlled induction motor.

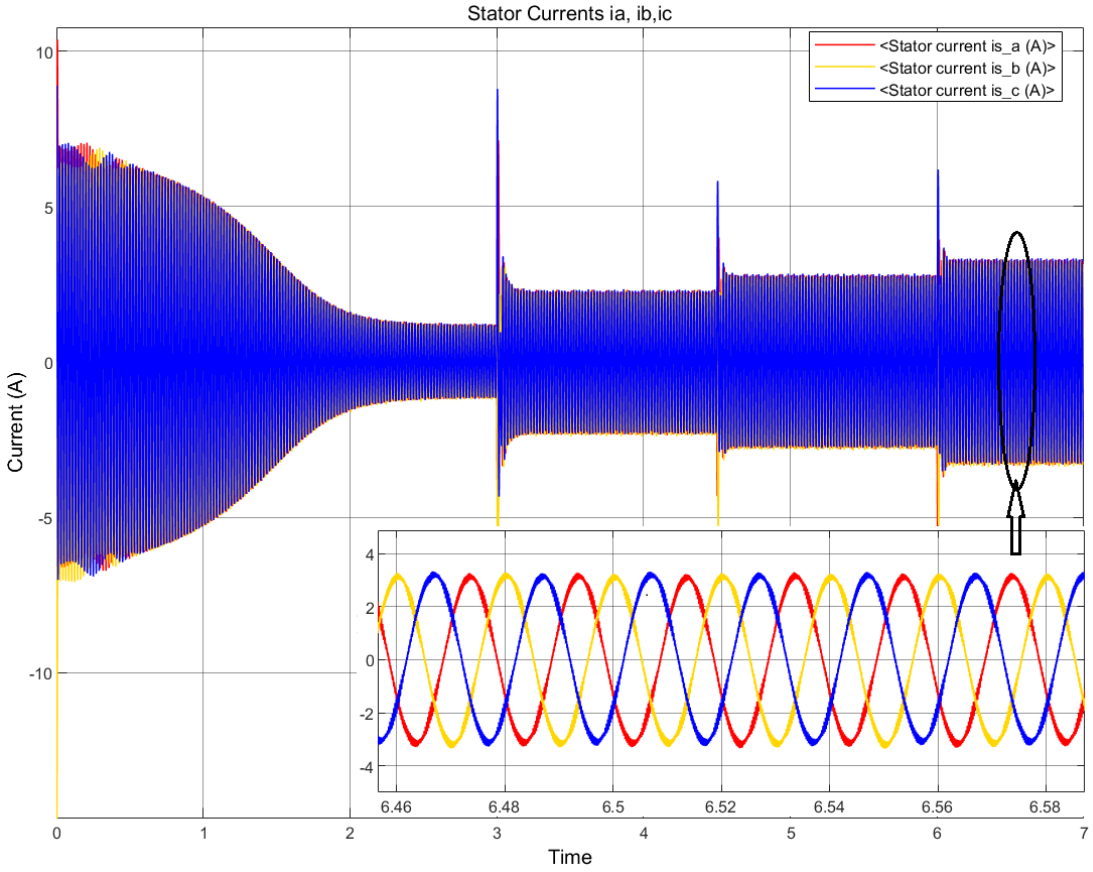

Fig.7.12 Stator Current

Figure 7.13 shows the waveform of speed. This figure shows that there is no variation in speed in steady state and rotor speed follows the reference speed. However, motor is

not running at desired speed at no load but it is running at slightly lesser speed of 1430 rpm and at other loads it is running at reference speed even on full load.

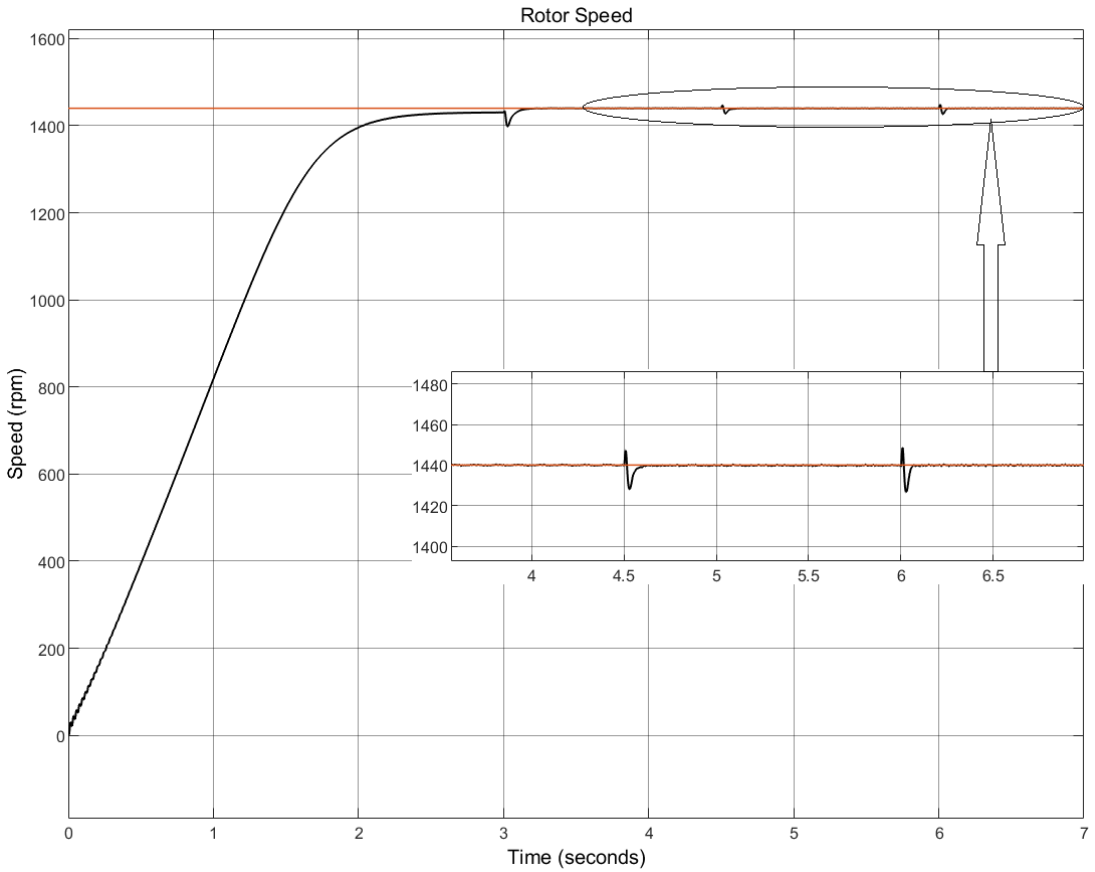

Fig.7.13 Speed

7.5 INDUCTION MOTOR OPERATION WITH ANFIS

The table below shows the variation in stator current (i_a) and speed with respect to change in mechanical torque. In this table stator current is the rms value of phase a current. Rise time and settling time are observed by starting induction motor at different loads. Here, the changes in speed with load change are almost none and motor operates as desired on all loads.

In this section the results of load changes in ANFIS controlled induction motor has been analysed. In figure 7.14, the load changes done to see the response of induction motor is shown. Figure 7.15 shows the corresponding stator current waveform of induction motor. The values of phase a current can be seen in table 7.4.

Table-7.4 Induction Motor Operation with ANFIS

S. No.	Mechanical Torque (N-m)	Stator Current (A)	Speed (rpm)	Rise Time (sec)	Settling Time (sec)
1.	0	0.73	1441	1.465	2.75
2.	0.5	1	1440	0.544	1.4
3.	1	1.31	1440	0.354	1
4.	1.5	1.52	1440	0.252	0.7
5.	2	1.67	1440	0.199	0.6
6.	2.5	1.86	1440	0.158	0.46
7.	3	2	1440	0.141	0.4
8.	3.5	2.15	1440	0.114	0.35
9.	3.7	2.2	1440	0.124	0.33

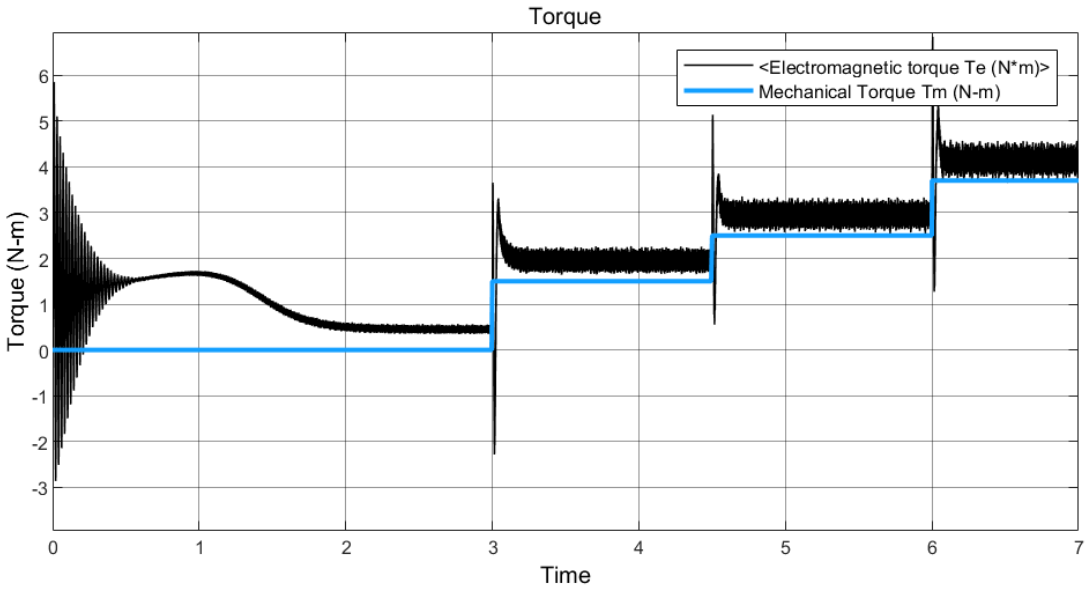

Fig.7.14 Mechanical and Electromagnetic Torque

In figure 7.15 the enlarged waveform of stator current can be seen when mechanical torque is 3.7 N-m, in this waveform it can be seen that stator currents are balanced. Waveform of the speed can be seen in figure 7.16. By looking at the speed waveform it can be concluded that time taken to regain the reference speed is least in ANFIS controller.

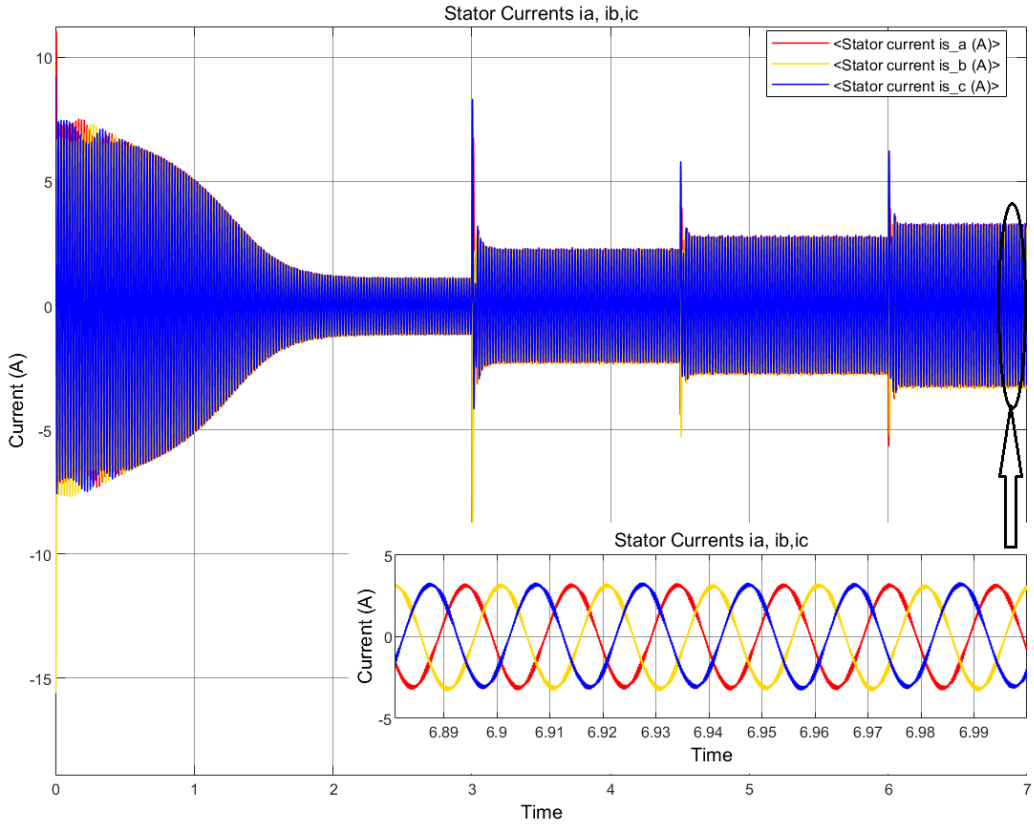

Fig.7.15 Stator Current

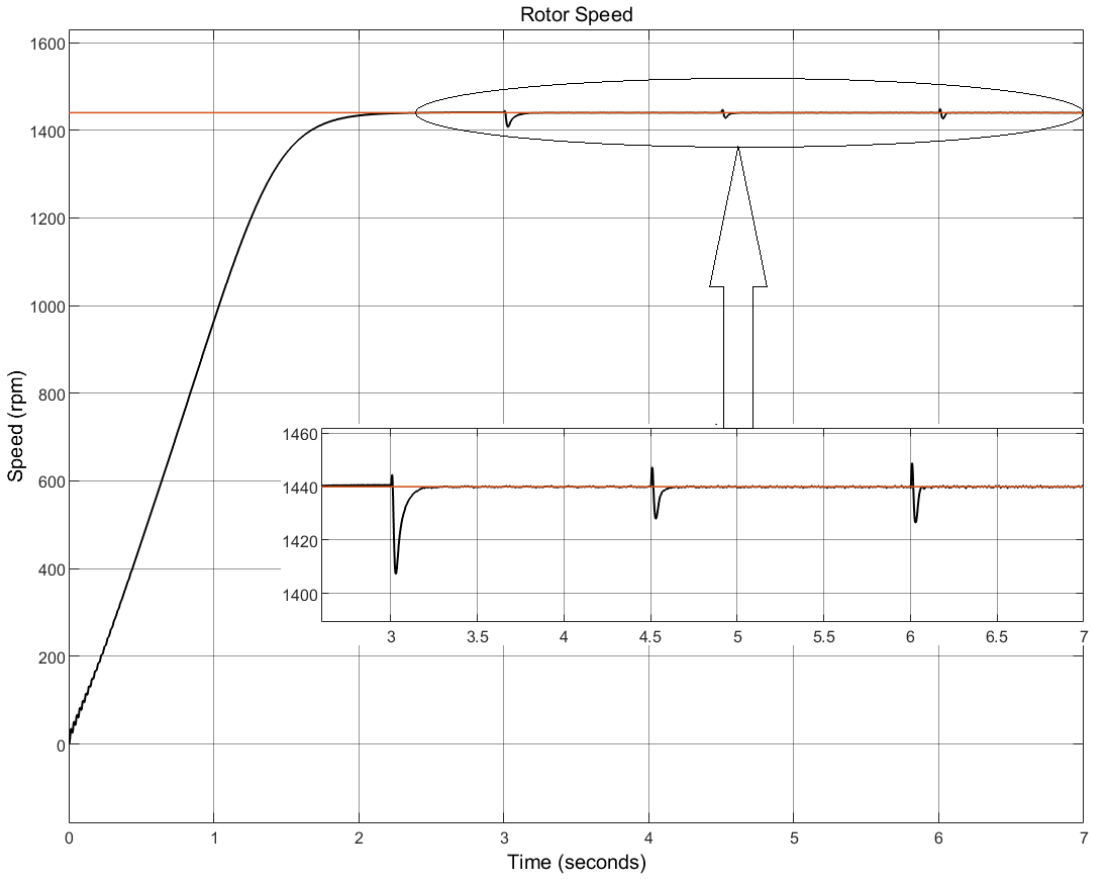

Fig.7.16 Speed

7.6 SPEED COMPARISON

The variation of speed can also be observed using graphs. From the data of table 7.5 shown, a graph in figure 7.17 is drawn.

Table-7.5 Induction Motor Speed Comparison

S. No.	Mechanical Torque (N-m)	Speed (rpm)			
		Without Controller	PI Controller	ANN Controller	ANFIS Controller
1.	0	1476	1441	1431	1441
2.	0.5	1451	1442	1440	1440
3.	1	1423	1439	1440	1440
4.	1.5	1392	1443	1440	1440
5.	2	1354	1438	1440	1440
6.	2.5	1308	1442	1440	1440
7.	3	1251	1437	1440	1440
8.	3.5	1163	1441	1440	1440
9.	3.7	1106	1442	1440	1440

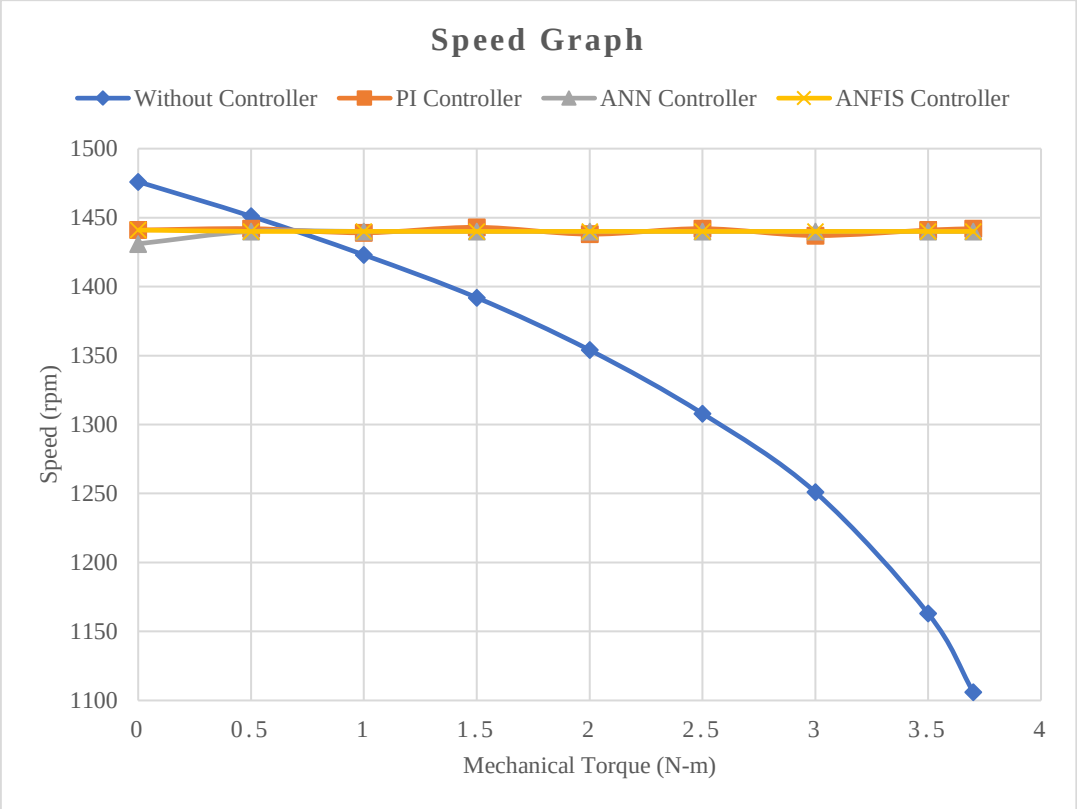

Fig.7.17 Speed Graphs

This graph only shows the speed when steady state is reached and therefore all the controllers are almost in one line and variation cannot be seen, however there is difference in time of reaching the steady state speed after the application of load change which can be seen in table-7.5.

7.7 CURRENT VARIATION

Table-7.6 shows the changes in stator current with load change. It is to mention that these currents are rms value of stator current of phase a.

Table-7.6 Stator Current Comparison

S. No.	Mechanical Torque (N-m)	Stator Current (A)			
		Without Controller	PI Controller	ANN Controller	ANFIS Controller
1.	0	0.77	1.1	0.76	0.73
2.	0.5	1	1.18	1	1
3.	1	1.39	1.29	1.3	1.31
4.	1.5	1.81	1.45	1.5	1.52
5.	2	2.27	1.6	1.7	1.67
6.	2.5	2.82	1.87	1.86	1.86
7.	3	3.44	2.1	2	2
8.	3.5	4.27	2.3	2.15	2.15
9.	3.7	4.71	2.4	2.2	2.2

The stator current noted in table-7.6 are rms value of phase-a current. Here, it can be observed that current of induction motor without any controller or in open loop is increasing with increase in load very sharply whereas in case of speed controllers, it is increasing but these increases are gradual and less.

Also, no load current can be observed to be very high in PI based V/f controller whereas it is low in ANN and ANFIS based controllers.

With this graph it can be conclude that for better speed regulation ANN and ANFIS based speed controllers are much better than PI controller as they will consume less power and therefore losses will also be less.

The graph of stator current variation is shown in figure 7.18. Both ANN and ANFIS controllers are showing approximately same stator current and hence in figure 7.18.

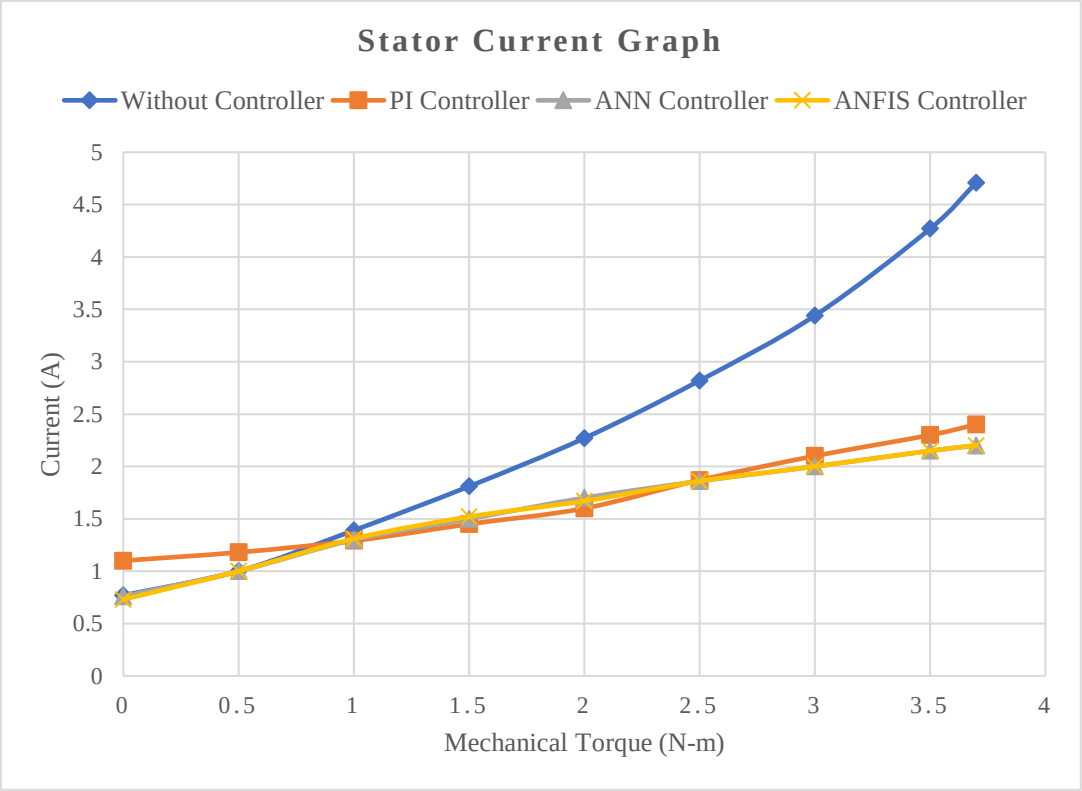

Fig.7.18 Stator Current Graph

7.8 RISE TIME VARIATION

Rise time is very important characteristic which tells how fast the induction motor gains the speed from 0 rpm to reference speed. Table-7.7 shows the rise time of speed with various controllers.

From table-7.7, it can be seen that in case of without controller, rise time is increasing with load and when motor is put on full load, it ran in opposite direction which indicating the pull-out of induction motor. When PI controller is used, rise time curve shows very peculiar behavior, it remained almost constant up to 2 N-m and then reduced and then decreased. With ANN and ANFIS controller rise time is very high at the starting and is gradually decreasing with increase in load, it is because that the ANN and ANFIS controllers are trained according to mechanical torque and speed of the induction motor.

Table-7.7 Rise Time Comparison

S. No.	Mechanical Torque (N-m)	Rise Time (sec)			
		Without Controller	PI Controller	ANN Controller	ANFIS Controller
1.	0	0.35	0.761	1.376	1.465
2.	0.5	0.43	0.762	0.55	0.544
3.	1	0.48	0.766	0.374	0.354
4.	1.5	0.6	0.768	0.252	0.252
5.	2	0.835	0.736	0.2	0.199
6.	2.5	1.13	0.476	0.16	0.158
7.	3	1.963	0.606	0.142	0.141
8.	3.5	-	0.498	0.135	0.114
9.	3.7	-	0.515	0.124	0.124

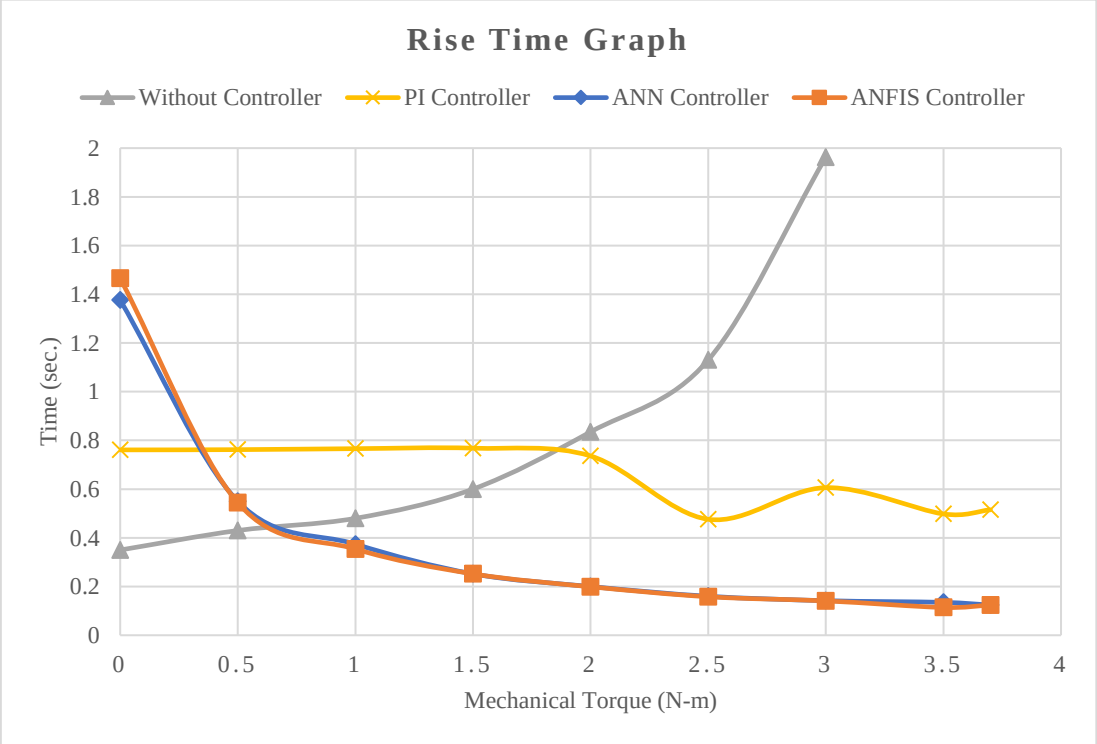

Fig.7.19 Rise Time Graph

In case of PI controller, control voltage of SVPWM increases gradually with increase in speed whereas ANN and ANFIS controllers are trained so that it gives specific SVPWM control voltage at specific mechanical torque.

7.9 SETTLING TIME VARIATION

Table 7.8 is the settling time of induction motor without and with various controllers and figure 7.20 is graph plotted with these data.

Table-7.8 Settling Time

S. No.	Mechanical Torque (N-m)	Settling Time (sec)			
		Without Controller	PI Controller	ANN Controller	ANFIS Controller
1.	0	0.95	1.2	3.4	2.75
2.	0.5	1.1	1.1	1.4	1.4
3.	1	1.2	1.3	0.9	1
4.	1.5	1.45	1.18	0.8	0.7
5.	2	1.9	1.15	0.7	0.6
6.	2.5	2.5	6	0.55	0.46
7.	3	4.1	7.3	0.45	0.4
8.	3.5	-	8	0.37	0.35
9.	3.7	-	9	0.32	0.33

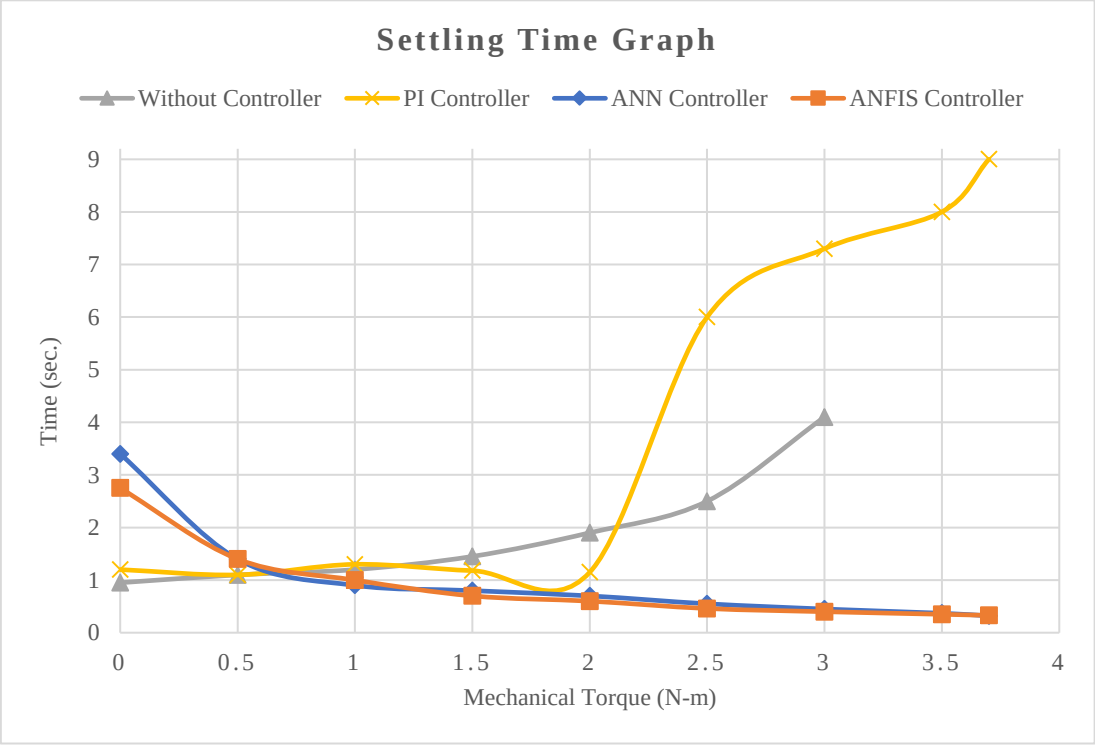

Fig.7.20 Settling Time Graph

Settling time is the time required for a pulse to reach its steady state value or within the limits of steady state value. The settling time increases as the load is increased in an induction motor if induction motor is operated without any controller as it can be seen in grey color line of figure 7.20. Similar to rise time, in settling time graph also PI controller is showing very peculiar pattern. Rise time was changing suddenly so is the settling time increasing suddenly at 2.5 N-m mechanical torque. With ANN controller, settling time with no load is highest but as the load is increased, settling time reduces and induction motor becomes faster and its controlling is also faster as compared to PI controller. In case of ANFIS controller also settling time waveform is normal and showing gradual decay.

CHAPTER 8

CONCLUSION AND FUTURE SCOPE

8.1 CONCLUSION

Simulation of SVPWM based control of induction motor drive using PI control, ANN control and ANFIS control method is done in MATLAB/Simulink. The simulation is made for without speed controller and with speed controllers and anticipated output is obtained. The speed of induction motor is controlled to reference speed with changes in load.

The variation of speed of induction motor is observed by varying load torque with and without speed controllers and results are noted in table. It is observed that overall performance of induction motor is good with ANFIS controller. Speed is found to be reference speed in all loading conditions, stator current is least in almost all the loads among all the controllers. Though rise time is high during no load but with increased load, ANFIS controller gives least rise time, also settling time is less with increase in load.

8.2 FUTURE SCOPE

Some workable recommendations for future work to the work carried out in this dissertation are given below:

- The experimental execution of induction motor drive can be carried out using dSpace.
- SVPWM technique can also be carried out for multilevel inverter in order to further reduce the harmonics.

APPENDIX

INDUCTION MOTOR

Induction motor is the load used in this project. It's a half hp double cage induction motor. Simulink block of double cage induction motor is shown in figure 6.12.

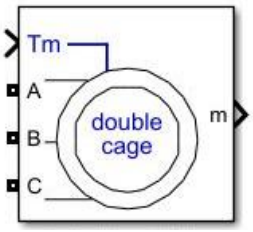

Fig.6.12 Induction Machine

Induction motor used for the load has the following parameters:

Nominal line to line rms voltage	:	400 V
Nominal frequency	:	50 Hz
Nominal (full load) line current (I_n)	:	2.33 A
Nominal (full load) mechanical torque (T_n)	:	3.69 N-m
Synchronous speed	:	1500 rpm
Starting current to nominal current ratio (I_{st}/I_n)	:	7
Starting torque to full load torque ratio (T_{st}/T_n)	:	2.2
Stator resistance (R_s)	:	13.08 Ω
Stator inductance (L_s)	:	6.32 mH
Cage 1 resistance (R_{r1}`)	:	10.39 Ω
Cage 1 inductance (L_{r1}`)	:	6.49 mH
Cage 2 resistance (R_{r2}`)	:	10.42 Ω
Cage 2 inductance (L_{r2}`)	:	6.32 mH
Mutual inductance (L_m)	:	0.4859 H
Pole pairs	:	2

REFERENCES

[1] A. Iqbal, "Analysis of space vector pulse width modulation for five phase voltage source inverter" IE (I)journal-EL, Volume 89 Issue 3, pp. 8-15, 2008.

[2] Mondal, S.K.; Bose, B.K.; Oleschuk, V.; Pinto, J.O.P, "Space vector pulse width modulation of three-level inverter extending operation into overmodulation region", IEEE Transactions on Power Electronics Volume 18, Issue 2, pp. 604 – 611, 2003.

[3] V. Blasko, "Analysis of a hybrid PWM based on modified space-vector and triangle-comparison methods," IEEE Transactions on Industry Applications, vol. 33, no. 3, pp. 756-764, 1997.

[4] S. R. Bowes and L. Yen-Shin, "The relationship between space-vector modulation and regular-sampled PWM," IEEE Transactions on Industrial Electronics, vol. 44, no. 5, pp. 670-679, 1997.

[5] W. Fei, "Sine-triangle versus space-vector modulation for three-level PWM voltage-source inverters," IEEE Transactions on Industry Applications, vol. 38, no. 2, pp. 500-506, 2002.

[6] Z. Keliang and W. Danwei, "Relationship between space-vector modulation and three-phase carrier-based PWM: a comprehensive analysis [three-phase inverters]," IEEE Transactions on Industrial Electronics, vol. 49, no. 1, pp. 186-196, 2002.

[7] W. Yao, H. Hu, and Z. Lu, "Comparisons of space-vector modulation and carrier-based modulation of multilevel inverter," IEEE Transactions on Power Electronics, vol. 23, no. 1, pp. 45-51, 2008.

[8] Syed Mahamood Ali, Dr. Mohammad Haseeb Khan, Dr. Arshia Azam, "Control Of Induction Motor Drive Using Space Vector PWM," International Journal Of Science, Engineering And Technology, vol. 3, no. 4, pp. 888-894, 2015.

[9] Vikramarajan Jambulingam, “SVPWM Based Speed Control of Induction Motor with Three Level Inverter Using Proportional Integral Controller,” International Journal of Engineering Development and Research, vol. 4, no. 1, pp. 271-280, 2016.

[10] R. Arulmozhiyal, K.Baskaran, R. Manikandan ", A Fuzzy Based PI Speed Controller For Indirect Vector Controlled Induction Motor Drive "IEEE, 2011 Sona College of Technology, Salem, Tamilnadu 636005, and India.

[11] Hanan Mikhael D. Habbi, Hussein Jalil Ajeel. Inaam Ibrahim Ali, “Speed Control of Induction Motor using PI and V/F Scalar Vector Controllers,” International Journal of Computer Applications, vol. 151, no. 7, pp. 36-43, 2016.

[12] Jia YingYing, Wang XuDong, Mao LiangLiang, Yang ShuCai, Zhang HaiXing, “Application and Simulation of SVPWM in three phase inverter,” IEEE The 6th International Forum on Strategic Technology, pp. 541-544, 2011.

[13] Qamar Muhammad Attique, Yongdong Li, and Kui Wang, “A Survey on Space-Vector Pulse Width Modulation for Multilevel Inverters,” CPSS Transactions On Power Electronics And Application, vol. 2, no. 3, pp. 226-236, 2017.

[14] Govinthasamy N.R., Arungopal R, Harudhran S., Rajashekar T., “IEEE International Conference on Innovations in Green Energy and Healthcare Technologies,” pp. 1-5, 2017.

[15] Waheed Ahmed, and Syed M Usman Ali, “Comparative study of SVPWM (space vector pulse width modulation) & SPWM (sinusoidal pulse width modulation) based three phase voltage source inverters for variable speed drive,” IOP Conference Series: Materials Science and Engineering, doi:10.1088/1757-899X/51/1/012027, 2013.

[16] G. Vivek, Jayanta Biswas, “Study On Hybrid SVPWM Sequences For Two Level VSIs,” IEEE, pp. 219-224, 2017.

[17] Subrata K. Mondal, Bimal K. Bose, Valentin Oleschuk, Joao 0. P. Pinto, “Space Vector Pulse Width Modulation Of Three-Level Inverter Extending Operation Into Overmodulation Region,” IEEE, pp. 497-502, 2002.

[18] M. A. Boost and P. D. Ziogas, “State-of-the-art carrier PWM techniques: a critical evaluation,” IEEE Transactions on Industry Applications, vol. 24, no. 2, pp. 271-280, 1988.

[19] V. Blasko, “Analysis of a hybrid PWM based on modified space-vector and triangle-comparison methods,” IEEE Transactions on Industry Applications, vol. 33, no. 3, pp. 756-764, 1997.

[20] N. Celanovic and D. Boroyevich, “A comprehensive study of neutral-point voltage balancing problem in three-level neutral-pointclamped voltage source PWM inverters,” IEEE Transactions on Power Electronics, vol. 15, no. 2, pp. 242-249, 2000.

[21] Rajesh Namdev, Mahendra Singh Bhadoria, Deshdeepak Shrivastava, “application of artificial neural network in electrical based power industry,” IJAREEIE, vol. 2, no. 10, pp. 4704-4711, 2013.

[22] Mishra and Choudhary P. (2012) Artificial Neural Network Based Controller for Speed Control of an Induction Motor Using Indirect Vector Method, International Journal of Power Electronics and Drive System (IJPEDS), Vol.2, pp. 402-408.

[23] G. Durgauskumar, M.K. Pathak, “Comparision of Adaptive Neuro-Fuzzy based space-vector modulation for two-level inverter,” Electrical Power and Energy Systems, doi:10.1016/j.ijepes.2011.10.017, 2011.

[24] Fábio Limaa, Walter Kaiserb, Ivan Nunes da Silvac, Azauri A.A. de “Open-loop neuro-fuzzy speed estimator applied to vector and scalar induction motor drive” 2014 Elsevier .

[25] Yuksel Oguz, Mehmet Dede “Speed estimation of vector controlled squirrel cage asynchronous motor with artificial neural networks”2014

[26] Czeslaw T. Kowalski, Teresa Orlowska-Kowalska “Neural networks application for induction motor faults diagnosis”

[27] Bogdan Pryymak, Juan M. Moreno-Eguilaz, Juan Peracaula 1 “Neural network flux optimization using a model of losses in Induction motor drives” 18 April 2006.

[28] M. A. Hannan, Jamal Abd Ali, Azah Mohamed and Mohammad Nasir Uddin, “A Random Forest Regression Based Space Vector PWM Inverter Controller for the Induction Motor Drive,” IEEE Transactions On Industrial Electronics vol. 64, no. 4, pp. 2689-2699, 2017.

[29] Subrata K. Mondal, João O. P. Pinto, Bimal K. Bose, “A Neural-Network-Based Space-Vector PWM Controller for a Three-Level Voltage-Fed Inverter Induction Motor Drive,” IEEE Transactions On Industry Applications, vol. 38, no. 4, pp. 660-669, 2002.

[30] Adel Gastli, Mohamed Magdy Ahmed, “ANN-Based Soft Starting of Voltage-Controlled-Fed IM Drive System,” IEEE Transactions On Energy Conversion, vol. 20, no. 3, pp. 497-503, 2005.

[31] W.W.L. Keerthipala, B.R. Duggal and Miao Hua Chun, “Torque And Speed Control Of Induction Motors Using Ann Observers,” IEEE, 1998.

[32] B. O. Omijeh, D.C.Idoniboyeobu and G. O. Ajabuego, “Artificial Neural Network Based Induction Motor Speed Controller,” International Journal of Electronics Communication and Computer Engineering, vol. 6, no. 1, ISSN (Print): 2278–4209, 2015.

[33] Aakanksha Tripathi, Naveen Asati, “Artificial Neural Network Controller for Induction Motor Drive,” International Journal of Science and Research (IJSR), vol. 4, no. 6, pp. 805-812, 2015.

[34] A.Muthuramalingam, D. Sivaranjani and S. Himavathi, “Space Vector Modulation of a Voltage fed Inverter Using Artificial Neural Networks,” IEEE Indicon 2005 Conference, pp. 487-491, 2005.

[35] Joao O. P. Pinto, Bimal K. Bose, Luiz Eduardo Borges da Silva and Marian P. Kazmierkowski, “A Neural-Network-Based Space-Vector PWM Controller for Voltage-Fed Inverter Induction Motor Drive,” IEEE transactions on industry applications, vol. 36, no. 6, pp 1628-1636, 2000.

[36] A. Bakhshai, J. Espinoza, G. Joos and H. Jin, “A combined artificial neural network and DSP approach to the implementation of space vector modulation techniques,” IEEE, doi. 0-7803-3544-9196, pp 934-940, 1996.

[37] S. Mitra, Y. Hayashi, S. Member, “Neuro Fuzzy Rule Generation : Survey in,” IEEE transactions on neural networks, Vol. 11, No. 3, pp. 748-768, 2000

[38] U. B. Malkhandale, Dr. N. G. Bawane, “Design & Simulation of an Adaptive Neuro-Fuzzy Inference System (ANFIS) for Current Control of AC Drive,” International Journal of Pure and Applied Mathematics, vol. 118, no. 9, pp 203-210, 2018.

[39] P. Tripura and Y. Srinivasa Kishore Babu, “Intelligent speed control of DC motor using ANFIS,” Journal of Intelligent & Fuzzy Systems, DOI:10.3233/IFS-120729, pp 223-227, 2014.

[40] Navneet Walia, Harsukhpreet Singh, Anurag Sharma, “ANFIS: Adaptive Neuro-Fuzzy Inference System- A Survey,” International Journal of Computer Applications, vol. 123, no. 13, pp 32-38, 2015.

[41] Anindita Das Bhattacharjee, Shibashis Mitra, Asiya Amreen Zaman, “Robust Prediction Capability of Feed Forward Back Propagation Network over Adaptive Neuro Fuzzy Inference System on Optical Characteristics of Ironbased Superconductor Glass materials,” IJCSN - International Journal of Computer Science and Network, vol. 7, no. 3, pp 166-181, June 2018.